

**The Impact of
Very Short-Lived Substances on the
Stratospheric Chemistry and
Interactions with the Climate**

Phoebe Graf

Deutsches Zentrum für Luft- und Raumfahrt
Institut für Physik der Atmosphäre
Oberpfaffenhofen

Dissertation
an der Fakultät für Physik
der Ludwig-Maximilians-Universität
München



Herausgeber Deutsches Zentrum
für Luft- und Raumfahrt e. V.
Bibliotheks- und
Informationswesen
D-51170 Köln
Porz-Wahnheide
Linder Höhe
D-51147 Köln

Telefon (0 22 03) 6 01 - 44 44
Telefax (0 22 03) 6 01 - 47 47

Als Manuskript gedruckt.
Abdruck oder sonstige Verwendung
nur nach Absprache mit dem DLR gestattet.

ISSN 1434-8454

Forschungsbericht 2017-15

The Impact of Very Short-Lived Substances on the Stratospheric Chemistry and Interactions with the Climate

Phoebe Graf

Deutsches Zentrum für Luft- und Raumfahrt
Institut für Physik der Atmosphäre
Oberpfaffenhofen

Dissertation
an der Fakultät für Physik
der Ludwig-Maximilians-Universität
München

123 Seiten
50 Bilder
13 Tabellen
137 Literaturstellen



DLR

Deutsches Zentrum
für Luft- und Raumfahrt

Erstgutachter: Prof. Dr. Martin Dameris
Zweitgutachter: Prof. Dr. Bernhard Mayer
Tag der mündlichen Prüfung: 08.02.2017
Tag der Einreichung: 08.12.2016

**The Impact of
Very Short-Lived Substances
on the
Stratospheric Chemistry
and
Interactions with the Climate**

Phoebe Graf

Dissertation
an der Fakultät für Physik
der Ludwig-Maximilians-Universität
München

vorgelegt von
Phoebe Graf
aus Starnberg

Kurzfassung

Bis Anfang der 2000er Jahre wurden sehr kurzlebige Halogenverbindungen, sogenannte Very Short-Lived Substances (VSLS), mit Lebenszeiten von weniger als sechs Monaten in Klima-Chemie-Studien, die die Stratosphäre betrafen, vernachlässigt. In dieser Studie wird gezeigt, dass ein signifikanter Anteil der VSLS die Stratosphäre erreicht und daher in zukünftigen Klima-Chemie-Studien berücksichtigt werden muss.

Die Stärke und Verteilung der überwiegend natürlichen VSLS Emissionen ist sehr unsicher, da sie sehr lokalisiert und variabel sind. Vier Emissionskataster wurden im Klima-Chemie Modell EMAC verwendet. Die Modellergebnisse wurden mit Boden- und Flugzeugmessdaten verglichen und evaluiert. Mit einem neueren Emissionskataster werden die VSLS in EMAC besser und realistischer dargestellt.

Eine Veränderung der VSLS Bodenemissionen führt zu signifikanten Änderungen im stratosphärischen Brom- und Ozongehalt. Bei Verwendung der neueren Emissionsdaten ist bis zu (30–60) % weniger stratosphärisches Brom vorhanden. Dies beeinflusst auch die Ozonwerte in der Stratosphäre, die bis zu 13 % höher sind als in der Referenzsimulation. Der Beitrag der VSLS zum stratosphärischen Brom beträgt 4.5 ± 0.8 pmol/mol, wobei sich der Unsicherheitsbereich aus den Unsicherheiten in den Bodenemissionen ergibt.

In einer freilaufenden Zeitscheiben-Simulation des Jahres 2000 führen die VSLS zu zusätzlichen 5.3 ± 0.1 pmol/mol stratosphärischen Brom. Trotz des beschleunigten vertikalen Transports im Jahr 2100 nimmt der Beitrag der VSLS zum stratosphärischen Brom durch Änderungen der Oxidationskapazität leicht ab und beträgt dann 5.0 ± 0.1 pmol/mol. Die Berücksichtigung des zusätzlichen Broms von VSLS führt global zu einem stratosphärischen Ozonverlust, der in der südpolaren unteren Stratosphäre während des südhemispherischen Frühlings am ausgeprägtesten ist. Gegenüber einer Simulation ohne VSLS ist 2000 etwa 14 % weniger Ozon vorhanden. Im Jahr 2100 werden etwa 4 % des stratosphärischen Ozons durch VSLS abgebaut. Dieser in der Zukunft reduzierte Einfluss der VSLS auf Ozon ist eine Folge der abnehmenden Chlormischungsverhältnisse, die eine effiziente Ozonerstörung über den gekoppelten BrO_x - ClO_x Zyklus limitieren.

Eine Verzehnfachung der VSLS Emissionen führt annähernd zu einem zehnfachen Eintrag von Brom in die Stratosphäre. Die durch VSLS verursachte Ozonerstörung nimmt auch zu, ist jedoch durch das vorhandene Chlor limitiert. Das stratosphärische Ozon ist 2000 um bis zu 70 % reduziert, 2100 um bis zu 40 %.

Abstract

Halogen containing very short-lived substances (VSLS) with lifetimes of less than six months were neglected until the early 2000's in studies on chemistry-climate interactions of the stratosphere. In this study it is shown that a significant amount of VSLS is able to reach the stratosphere and thus must be taken into account in future chemistry-climate studies.

The emission strength and distribution of VSLS is highly uncertain due to strongly localized and variable emissions predominantly from natural sources. Four recent emission inventories were applied to the chemistry-climate model EMAC. Compared to ground-based and air-borne observations the model results were evaluated. With a more recent emission inventory the representation of VSLS in EMAC is improved and more realistic.

A change of VSLS surface emissions significantly alters the stratospheric bromine (Br_y) and ozone burden. With respect to the reference simulation up to (30–60) % less Br_y is available in the stratosphere when using more recent VSLS surface emissions. The reduced stratospheric bromine content also affects the stratospheric ozone mixing ratios leading to an increase of ozone by up to 13 %. The contribution of VSLS to the stratospheric bromine content amounts to 4.5 ± 0.8 pmol/mol provided that the uncertainty range arises from uncertainties on the surface emissions.

In a free-running year 2000 time-slice simulation VSLS yield in 5.3 ± 0.1 pmol/mol additional stratospheric bromine. Despite an accelerated vertical transport in the year 2100 the contribution of VSLS to total stratospheric bromine decreases slightly to 5.0 ± 0.1 pmol/mol due to changes in the oxidation capacity. The consideration of the additional bromine from VSLS leads globally to a stratospheric ozone loss being most distinct in the south polar lower stratosphere during Southern hemisphere spring. In 2000, up to 14 % less ozone is available compared to a simulation with no VSLS emissions. In 2100, stratospheric ozone is reduced by up to 4 % due to VSLS. The decreased impact of VSLS on ozone in the future is a result of declining chlorine mixing ratios which limit the efficient ozone destruction via the coupled BrO_x - ClO_x cycle.

A tenfold increase of the VSLS emissions yields in approximately a tenfold injection of bromine from VSLS into the stratosphere. The ozone depletion due to VSLS also increases but is limited by the available chlorine. Stratospheric ozone is diminished by up to 70 % and 40 % due to VSLS in year 2000 and year 2100, respectively.

Contents

Kurzfassung	iii
Abstract	iv
1 Introduction	1
1.1 General Background	1
1.2 Motivation	2
1.3 Thesis Aims	4
2 Scientific Background	7
2.1 Stratospheric Ozone	7
2.1.1 Chemistry	7
2.1.2 Transport and Dynamics	14
2.2 Climate Change and Trends	15
2.2.1 Climate Change	15
2.2.2 The Ozone Hole	16
2.3 Halogenated Very Short-Lived Substances	19
2.3.1 Sources and Emissions	20
2.3.2 Troposphere-Stratosphere Transport	22
2.3.3 Stratospheric Bromine Loading	23
2.3.4 Influence on Ozone	24
2.3.5 Future Changes	24
3 Model Description and Set-ups	25
3.1 The Model System EMAC	25
3.2 A New Online Diagnostic: The Submodel TBUDGET	27
3.3 Model Set-ups and Simulations	29
3.3.1 Model Set-ups	29
3.3.2 Simulations	31
4 Modelling selected VSLs, Br_y and Ozone	39
4.1 General Model Validation	39
4.2 Evaluating VSLs representation in EMAC	44

4.2.1	EMAC versus Observations	44
4.2.2	Final Conclusion	65
4.3	Stratospheric Sensitivity to Changes in VSLs Surface Emissions	66
4.3.1	Bromine Loading	67
4.3.2	Ozone	70
4.4	Summary	72
5	The Impact of VSLs on Bromine and Ozone Loss	73
5.1	Bromine Loading	73
5.2	Ozone	75
5.3	Summary	78
6	The Impact of Climate Change on VSLs Transport and Chemistry	81
6.1	Future Changes in Bromine Loading	81
6.2	Impact of VSLs on Stratospheric Ozone	88
6.3	Climatic Impact of a Potential VSLs Emission Scenario	90
6.3.1	Bromine Loading	92
6.3.2	Impact on Ozone Loss	96
6.4	Implication of Changed VSLs Emissions on Radiative Forcing	99
6.5	Summary	101
7	Summary and Conclusions	103
	List of Figures	109
	List of Tables	110
	References	111

Chapter 1

Introduction

1.1 General Background

Ozone (O_3) is an important radiative gas in the Earth's atmosphere playing different roles depending on its occurrence. In the troposphere it is usually created in consequence of air pollution and injurious to the respiratory system. In the stratosphere O_3 absorbs most of the incoming ultra-violet (UV) radiation that is harmful to humans, animals and plants (Dameris et al., 2007).

The ozone layer (in about 20–30 km altitude) became famous when in 1984 for the first time a dramatic reduction of ozone in the Antarctic stratosphere - the so-called ozone hole - was observed by a team of scientists (Farman et al., 1985). Besides the pronounced seasonal Southern hemisphere polar ozone loss, depletion of stratospheric O_3 has been detected at all latitudes since the late 1970s. Many studies showed that the main reason for the stratospheric ozone decrease is the anthropogenic emission of ozone depleting substances (ODS), in particular chlorofluorocarbons (CFCs) and halons (e.g. Wofsy et al., 1975; Solomon et al., 1986). Due to their long tropospheric life times, the halogen source gases accumulate in the troposphere and are transported to the stratosphere. There, they are converted to reactive halogen-containing gases through photolysis and can effectively deplete ozone in catalytic reactions. Within the Montreal Protocol (1987) and amendments (e.g. London 1990, Vienna 1995) anthropogenic emissions of ODS were regulated and finally phased out. Due to the success of the Montreal Protocol the tropospheric halogen loading peaked in the second half of the 1990s and a few years later a reduction of stratospheric concentrations could be observed. Consequently, stratospheric halogens are expected to continuously decline over the next years (Montzka et al., 2003, Carpenter et al., 2014). As a result of descending atmospheric halogen concentrations chemistry-climate models (CCMs) predict a recovery of the ozone layer to 1980 values in the course of the second half of the 21st century in most regions of the atmosphere (WMO, 2011; Pawson et al., 2014; Dameris et al., 2014).

Even if the connection between anthropogenic emission of long-lived halogens is known, it is still challenging to predict future concentrations of atmospheric ozone as it is also affected by rising greenhouse gas (GHG) emissions through changes in temperature and transport patterns. Stratospheric cooling induced by increasing GHG concentrations leads on one hand to decelerated ozone depleting chemical gas-phase reactions in tropical and subtropical latitudes. On the other hand a colder stratosphere favours the formation of polar stratospheric clouds (PSCs) leading to more polar ozone depletion. Furthermore, climate models and chemistry-climate models suggest that climate change will lead to an acceleration of the Brewer-Dobson-Circulation (BDC). The BDC moves air masses from the tropics to higher latitudes and contributes crucially to the global distribution of trace gases (Shepherd, 2008).

Overall, to reliably predict the evolution of atmospheric ozone values it is necessary to consider changes in the chemical composition (e.g. halogens), temperature and dynamics (transport) and to increase our knowledge about chemistry-climate interactions.

1.2 Motivation

Until the early 2000's stratospheric bromine was thought to arise from emissions of long-lived ODS (e.g. halons) and methyl bromide (CH_3Br) only. Recent approaches to quantify the inorganic stratospheric inorganic bromine (Br_y) showed that long-lived halogen gases cannot be the only source for the observed stratospheric bromine. Changes in Br_y derived from balloon-borne and ground based observations of bromine monoxide (BrO) combined with calculations of a three-dimensional chemical transport model (CTM) (Figure 1.1: orange and black symbols) were compared to trends in measured tropospheric bromine (CH_3Br plus halons; purple line). While CH_3Br and halons make up the most of the observed stratospheric Br_y there remains a difference of about 2–8 pmol/mol. This additional Br_y is assumed to originate from the depletion of halogen-containing very short-lived species (VSLS) in the troposphere and stratosphere leading to the release of reactive bromine. VSLS are defined as halogen compounds with lifetimes of less than six months (Ko et al., 2003).

Bromine-containing VSLS are thought to predominantly arise from natural sources. Natural sources include marine phytoplankton, seaweeds in coastal areas and to a minor part terrestrial vegetation like rice paddies (Law et al., 2007; Leedham et al., 2013). Dibromomethane (CH_2Br_2) and bromoform (CHBr_3) constitute the biggest fraction of brominated VSLS. Sources of VSLS are strongly localised and emissions are highly variable in space and time. Observations of surface mixing ratios range from less than 1 pmol/mol up to occasional values of hundreds of pmol/mol (Quack and Wallace, 2003; Yokouchi et al., 2005; O'Brien et al., 2009; Pyle et al., 2011). This fact hampers the estimation of the global VSLS emission flux which is essential to realistically represent VSLS in chemistry-climate models.

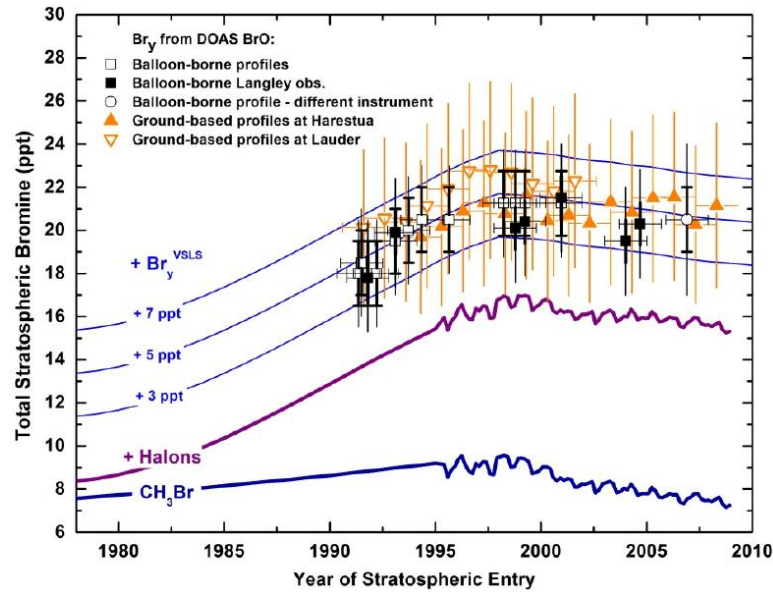


Figure 1.1: Stratospheric inorganic bromine (ppt) derived from balloon-borne/ground based measurements of BrO and photochemical modelling (open and filled squares/ rectangles). Lines show the expected contribution from methyl bromide (CH_3Br) (fat blue line), methyl bromide plus the halons (fat purple line), the sum of methyl bromide plus halons plus additional 3, 5, 7 pmol/mol from very short-lived substances is shown in thin blue lines. Figure 1-20 from Carpenter et al. (2014).

Very short-lived (VSL) source gases (SGs) or product gases (PGs) can probably enter the stratosphere when vertical transport is rapid, i.e. primarily in the tropics where deep convection occurs. Recent observational and model studies indicate, that brominated VSLs contribute currently about 25% to the total stratospheric inorganic bromine (e.g. Liang et al., 2010; Hossaini et al., 2013; Aschmann and Sinnhuber, 2013; Carpenter et al., 2014).

Moreover, it has been suggested that natural emissions of VSLs may vary under a future climate in consequence of changes in sea surface temperatures (SST), nutrient supply, salinity and surface wind speeds (Law et al., 2007). The farming of seaweed is likely to increase. Seaweed is cultivated for several applications in the food and cosmetics industries but also for energy generation and the production of bio fuels. In addition, altered dynamical processes, like a probably accelerated tropical upwelling in the future, might enhance the amount of halogens from VSLs reaching the stratosphere (Dessens et al., 2009; Hossaini et al., 2012a). Due to the phase out of long-lived halogens under the Montreal Protocol, the relative contribution of VSLs to stratospheric bromine will increase in the future.

Last but not least, several model studies showed that VSLs contribute to the stratospheric ozone depletion (e.g. Salawitch et al., 2005; Feng et al., 2007; Hossaini et al., 2015; Sinnhuber and Meul, 2015). As ozone is an important radiative gas a precise prediction of the future climate is only possible when ozone depleting processes are

quantified.

Even though longer-lived ozone depleting substances provide the majority of the halogen burden in the present stratosphere, naturally emitted very short-lived substances must be considered for several reasons:

- VSLS most probably contribute to the stratospheric halogen loading,
- a changing climate potentially alters emissions and pathways of VSLS,
- natural halogens might get more important with declining anthropogenic long-lived halogen abundances, and
- VSLS potentially affect the stratospheric ozone depletion.

A key problem in investigating the effects of VSLS in the atmosphere is the high degree of uncertainty over strengths, distributions and trends of surface emissions. Further research is needed to assess these uncertainties, to identify and quantify potential effects of VSLS on chemistry and climate, in order to realistically simulate future climate.

1.3 Thesis Aims

The primary aim of this research is to improve the current understanding of the chemistry and transport of brominated VSLS and their impact on stratospheric ozone. To achieve this, the chemistry-climate model EMAC is used in combination with observational data. This study should answer the following questions:

- How well are VSLS represented in the chemistry-climate model EMAC?
Data from several EMAC simulations with four different emission inventories will be compared to observations of VSLS. On this basis, one emission inventory will be determined for further simulations.
- How do emission inventories at the surface influence stratospheric halogen and ozone abundances?
Compared to other trace gases, emissions of VSLS are small and only a little fraction might reach higher altitudes. Therefore, it should be investigated if the signal of perturbed surface emissions can be detected in the stratosphere, in particular through altered halogen or ozone mixing ratios.
- How big is stratospheric ozone loss by VSLS?
Until the early 2000s VSLS were thought to have a negligible impact on the chemistry-climate system and were not taken into account for analysis concerning the stratospheric chemistry. Now it should be investigated to what extent VSLS contribute to the past and future stratospheric ozone depletion.

- What impact does climate change have on the chemistry and distribution of VSLs?

So far, it is highly uncertain if the emissions of predominantly natural VSLs will alter in consequence of a changed climate. Moreover, future dynamical changes might influence the transport of trace gases from the troposphere to the stratosphere.

Chapter 2

Scientific Background

This chapter contains a summary of the chemical and dynamic processes that control the stratospheric ozone abundance. In section 2.3 the very short-lived species (VSLs) are introduced.

2.1 Stratospheric Ozone

Ozone is one of the most important trace gases in the atmosphere. By absorbing incoming short-waved solar radiation it shields the Earth's surface and makes human life possible. To understand observed ozone values and predict future climate it is essential to know the partially interacting processes that affect stratospheric ozone.

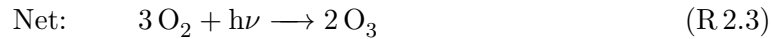
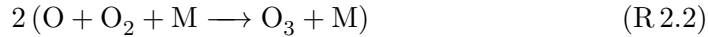
2.1.1 Chemistry

The atmospheric trace gas ozone was already discovered in 1839 by Christian Friedrich Schönbein in the laboratory. In 1858 André Houzeau verified that ozone is a component of natural air (Walker, 2007). But it was only in the late 20's century that the chemical processes involved in ozone production and depletion could be explained.

The Chapman Mechanism

In 1930, the British scientist Sydney Chapman proposed a chemical cycle which continually produces ozone in the stratosphere, the so called Chapman mechanism (Chapman, 1930). Ozone formation occurs in altitudes where solar ultraviolet (UV) radiation is very energetic and of wave lengths $\lambda < 242$ nm (above 30 km). Molecular oxygen (O_2) is dissociated to two reactive oxygen atoms (O, reaction R.2.1). The oxygen atoms then react with O_2 and a third body M (nitrogen (N_2) or O_2) to ozone (reaction R.2.2). Thereby $h\nu$ denotes the energy of a photon with h being the Planck constant and ν

the frequency.



The ozone molecule absorbs UV radiation and decomposes back to O and O₂ (reaction R 2.4). Only a small amount of the oxygen atoms produced from O₃ photolysis reacts with O₃ to form two oxygen molecules (reaction R 2.5). As O₃ and O rapidly interchange via reactions R 2.2 and R 2.4, the sum of O and O₃ is considered as an odd oxygen family O_x (Solomon, 1999).



The ozone abundance predicted by the Chapman reactions is about two times higher than the actual atmospheric amount (Seinfeld and Pandis, 2006). In the following 40 years after Chapman's famous paper, several additional ozone depleting cycles were identified.

Catalytic Cycles

By destroying ozone in a catalytic cycle even species with low atmospheric concentrations can alter the ozone abundance significantly. The general ozone-depleting catalytic cycle is given in reactions R 2.7 - R 2.9. Initially, a catalyst X (e.g. H, OH, Cl, NO) reacts with a ozone molecule to build XO and O₂ (reaction R 2.7). In a second reaction XO bonds with atomic oxygen which leads to the release of O₂ and X. Thus, the catalyst is regenerated and can loop through the catalytic cycle several 1000 times until it reacts to a deactivated reservoir gas (see below).

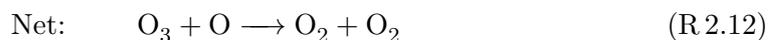
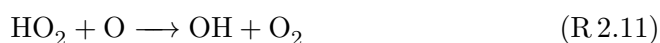
Catalytic Cycle



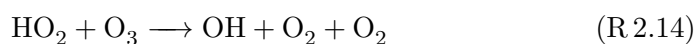
The HO_x Cycles

Bates and Nicolet (1950) were the first who identified ozone destroying catalytic cycles involving hydrogen, the so called HO_x cycles (HO_x = OH + HO₂). Reactions R 2.10 - R 2.15 show the HO_x cycles involving the hydroxyl OH and hydroperoxyl radical HO₂. Cycle 1 dominates in about 50 km altitude, cycle 2 in the lower stratosphere (i.e. 20 km). Stratospheric OH is mainly produced by reaction of O¹D from ozone photolysis (see R 2.1) with water vapour (H₂O) or methane (CH₄). Reaction of OH with O₃ yields in HO₂ and O₂ (R 2.10). Thus, the HO_x concentration is dependent on water vapour and methane concentrations and may change due to anthropogenic activity (Dlugokencky et al., 2011). The idea of the catalytic cycles involving hydrogen was a scientific breakthrough but it still did not explain the observed ozone concentrations.

HO_x Cycle 1



HO_x Cycle 2

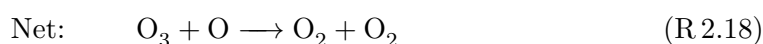


The NO_x Cycles

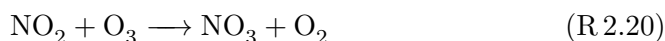
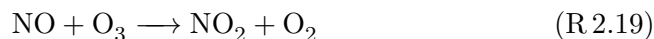
Crutzen (1970) and Johnston (1971) discovered the role of nitrogen oxides in the stratospheric ozone chemistry in the early 1970s. The NO_x family consists of NO and NO₂. The main source for stratospheric NO_x is photolysis of nitrous oxide (N₂O), a naturally occurring gas from soils. The two NO_x cycles are shown in reactions R 2.16 - R 2.22. Cycle 1 dominates in the upper stratosphere where the concentration of O atoms is highest. Cycle 2 requires no atomic oxygen and is most effective in the lower

stratosphere.

NO_x Cycle 1



NO_x Cycle 2



The Halogen Cycles

Only a few years after the identification of the NO_x cycles, Molina and Rowland realized the impact of the widely-used chlorofluorocarbons (CFCs) on ozone (Molina and Rowland, 1974; Rowland and Molina, 1975). CFCs are almost exclusively man-made and particularly long-lived. They have no tropospheric sink and can spread to high altitudes where short-waved UV radiation ($\lambda = 185$ to 210 nm) finally photolyzes them releasing reactive halogen atoms (e.g. reactions R 2.23, R 2.24; Seinfeld and Pandis, 2006).



Similar to NO_x, reactive chlorine (ClO_x = Cl + ClO) takes part in catalytic ozone-depleting cycles like shown in reactions R 2.25 - R 2.27 (Stolarski and Cicerone, 1974). However, at stratospheric temperatures the ClO_x cycle is considerably faster than the

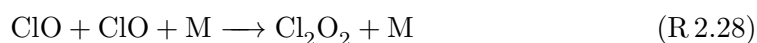
NO_x cycle and thus more efficient in depleting ozone (Molina and Rowland, 1974).

ClO_x cycle 1



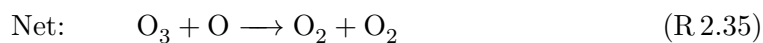
Very low temperatures in the polar regions during winter favour the self reaction of chlorine monoxide (ClO) to chlorine peroxide (Cl_2O_2) which is decomposed to chlorine radicals upon photolysis (R 2.28 - R 2.32).

ClO_x cycle 2



Ozone depletion by bromine happens in a analogous catalytic fashion as the reactions involving chlorine (see R 2.33 - R 2.35).

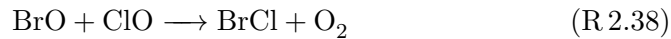
BrO_x cycle



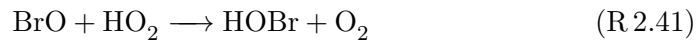
There are also catalytic cycles coupling the BrO_x and ClO_x and the BrO_x and HO_x families (e.g. reactions R 2.36 - R 2.40 and R 2.41 - R 2.45) and being quite effective in destroying O_3 in the lower stratosphere (Wofsy et al., 1975; Yung et al., 1980; Lary

et al., 1996; Salawitch et al., 2005).

BrO_x–ClO_x cycle



BrO–HO₂ cycle



The catalytic cycles described above would go on forever if the reactive catalyst would not convert to a more stable reservoir gas. One chlorine atom, for instance, can destroy 100 000 molecules of ozone before it is removed and the catalytic cycle interrupted (Seinfeld and Pandis, 2006). Chlorine atoms react for example with CH₄ to form HCl and ClO is tied to the relatively stable form ClONO₂ by reaction with NO₂. The latter reaction couples the ClO_x and NO_x families (Solomon, 1999). The total inorganic chlorine budget (Cl_y = Cl + ClO + HOCl + ClONO₂ + HCl) consists of reactive chlorine and chlorine tied up in reservoir forms (Seinfeld and Pandis, 2006). Reactive bromine is also temporarily removed by conversion to more stable forms. The bromine reservoirs hydrogen bromide (HBr) and bromine nitrate (BrONO₂) are less stable than their chlorinated counterparts and are rapidly photolyzed. Thus, active bromine (BrO_x) makes up the biggest part of the total inorganic bromine budget (Br_y = Br + BrO + HOBr + BrONO₂). Due to the relatively unstable brominated reservoirs, bromine is as effective in destroying ozone as chlorine despite its lower atmospheric abundance. One bromine radical is about 50 times more effective in depleting O₃ than a chlorine atom (Seinfeld and Pandis, 2006). In the troposphere, soluble Cl_y

and Br_y such as HCl and HBr can be washed out by precipitation. Fluorine and iodine-containing substances are thought to be of minor importance for stratospheric ozone. The fluorine reservoir hydrogen fluoride (HF) is extremely stable and thus non-reactive towards O_3 . Iodine-containing compounds generally have short atmospheric lifetimes and only small fractions (< 0.15 ppt) are able to enter the stratosphere (Butz et al., 2009; Carpenter et al., 2014). Figure 2.1 shows the fractional contribution of the different catalytic cycles to ozone depletion in a function of altitude. It can clearly be seen that at different altitudes not only one cycle is important but several cycles interact and have to be considered.

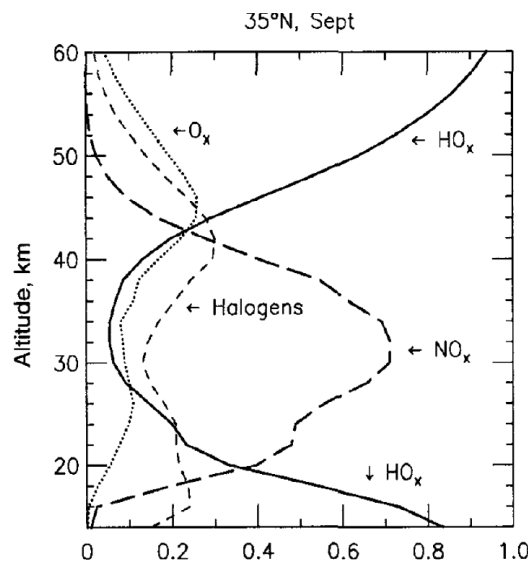


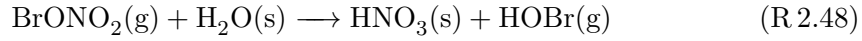
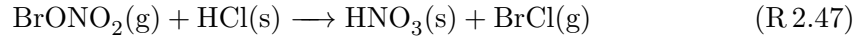
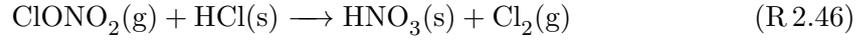
Figure 2.1: Vertical distribution of the relative contributions by different catalytic cycles to ozone loss rate in September at 35°N . Figure taken from Seinfeld and Pandis (2006).

Heterogeneous Chemistry

All the gas-phase reactions mentioned so far could not describe an stratospheric phenomena observed in the 1980s over Antarctica. Farman et al. (1985) noticed an enormous decrease in ozone concentrations during the polar spring (September to October), the so called ozone hole, which will be discussed in detail in section 2.2.

Condition for the extraordinary high ozone destruction in the polar regions is the formation of polar stratospheric clouds (PSCs; e.g McCormick et al., 1982) which occur at very low temperatures (< 195 K) and in altitudes of 15 to 26 km. The cloud particles are made up of is nitric acid trihydrate (NAT) particles ($\text{HNO}_3 \cdot 3\text{H}_2\text{O}$; Peter, 1996). On the surface of the solid (s) PSC particles relatively fast heterogeneous reactions can occur, which release photolytically active gaseous (g) halogens from reservoir gases

(e.g. reactions R 2.46 - R 2.48; Toon and Tolbert, 1995; Solomon, 1999).



An important effect of the heterogeneous reactions R 2.46 - R 2.48 is that nitric acid (HNO_3) remains on the PSC surface. If the PSC particles are sufficiently large they fall out and thereby permanently remove nitrogen from the stratosphere. This process, called denitrification, can enhance ozone destruction as less nitrogen is available to reform reservoirs like ClONO_2 .

Due to orography, a more stable polar vortex and lower temperatures, PSCs occur more often and for longer periods in the Southern polar regions compared to the Northern hemisphere. Therefore, ozone depletion over Antarctica is more distinct than over the Arctic. For more details about the atmospheric differences of the hemispheres see the following sections 2.1.2 and 2.2.2.

2.1.2 Transport and Dynamics

As mentioned before, ozone is exclusively formed by photochemical processes. As the incoming solar radiation is highest in the tropics, most of the ozone is formed there. In contrast, maximum O_3 concentrations can be found in middle to high latitudes (see Figure 2.2), which leads to the conclusion that air must be transported poleward from low to high latitudes. To explain the observed values of water vapour and ozone, Brewer

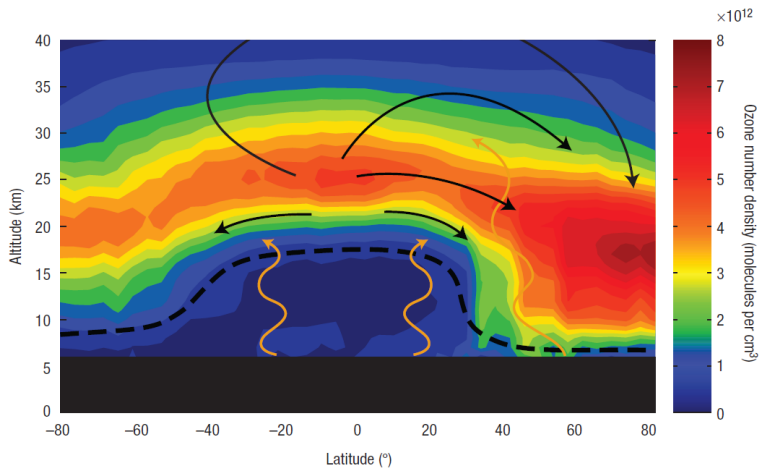


Figure 2.2: Brewer-Dobson circulation and ozone distribution. Ozone distribution measured by the OSIRIS satellite instrument in March 2004. Orange arrows denote wave propagation, black arrows sketch the stratospheric meridional circulation. Dashed black line represents the tropopause. Figure taken from Shaw and Shepherd (2008).

(1949) and Dobson (1956) proposed the existence of a mean meridional circulation in the stratosphere. The so called Brewer-Dobson circulation (BDC) involves upward motion in the tropics, meridional transport from the tropics poleward and downward motion in the extra tropics. The drivers of this circulation are atmospheric waves which are mainly triggered in the troposphere, for instance by topography or land-sea differences in diabatic heating (see orange arrows in Figure 2.2). These waves can propagate vertically into the stratosphere until they are damped or break. Charney and Drazin (1961) showed that vertical propagation is possible if the zonal wind is positive (west wind) and smaller than a certain critical velocity. The critical velocity is proportional to the wavelength, so that large scale waves can propagate vertically at higher zonal wind speeds than waves with shorter wave lengths. If the background wind field equals the critical velocity for a wave of a certain phase speed, wave breaking occurs, and a momentum from the wave is transferred to the zonal mean flow. Vertical wave propagation is more distinct in the particular winter hemisphere as there are west-winds in the stratosphere. In general, more waves are excited in the Northern hemisphere due to the orography and land-sea distribution. Therefore, the northward branch of the BDC is more pronounced than its Southern counterpart.

In conclusion, the meridional distribution of the transported trace gases is strongly dependent on season. Total ozone shows a maximum at high latitudes during spring (Figure 2.2) because the transport from its source region is highest during winter (WMO, 2011).

2.2 Climate Change and Trends

2.2.1 Climate Change

Due to anthropogenic activity the chemical composition of the atmosphere has significantly changed over the last 150 years. Long-lived greenhouse gases (GHG) like carbon dioxide (CO_2), methane (CH_4) or nitrous oxide (N_2O) absorb longwave radiation emitted by the Earth's surface and lead to changes in the atmospheric radiation budget. The natural greenhouse effect increases the mean surface temperature by 33 K to about 288 K. Additional emission of GHGs through industrialization enhanced the greenhouse effect and changed atmospheric physics, dynamics and chemistry substantially. Over the last 150 years a warming in the troposphere and a cooling in the stratosphere has been identified and ascribed to the anthropogenic greenhouse effect or climate change (e.g. IPCC, 2007; Randel et al., 2009). The changes in atmospheric and sea surface temperatures (SSTs) are also expected to affect the atmospheric circulations. Several modelling studies found, that the BDC, and in particular, the tropical upwelling, is strengthening in a changing climate (e.g. Butchart et al., 2006; Garcia and Randel, 2008; Deckert and Dameris, 2008; McLandress and Shepherd, 2009). This also influences the transport and distribution of trace gases and the exchange between

troposphere and stratosphere.

2.2.2 The Ozone Hole

As early as 1974 Molina and Rowland pointed out that anthropogenic long-lived chlorofluorocarbons (CFCs) may considerably destroy atmospheric ozone. Farman et al. (1985) described an incredible ozone decrease in the Antarctic stratosphere that was measured with ozone sondes in several years in October. Even though ozone was also measured via satellite since 1978, only then it was recognized that to date the dramatically low values were automatically sorted out as assumed measurement errors.

The reasons for the unusual high ozone loss, the so called ozone hole (by definition values < 220 DU), in the polar regions are now well understood. Halogenated gases like CFCs with lifetimes of the order of decades can reach the stratosphere where they are finally photochemically destructed into chemically more active forms (e.g. reaction R.2.23). As a result of the very stable southern polar vortex during the winter, air mass exchange with tropical air is disabled and very low temperatures occur over Antarctica leading to the formation of PSCs. As mentioned in section 2.1.1, PSCs enable the fast reactivation of inactive halogens (see reactions R.2.46 - R.2.48). Through sedimentation of PSC particles, nitrogen is removed from the stratosphere and the formation of reservoirs like BrONO_2 and ClONO_2 is prevented so that active halogens, particularly ClO, can accumulate. When sun rises in spring, the activated forms of halogens like Cl_2 or Br_2 are photolysed to radicals which then pass through the particular catalytic cycle several thousand times. The ClO_x cycle 2 (R.2.28-R.2.32) and the ClO_x - BrO_x cycle (R.2.36 - R.2.40) are responsible for 55 % to 70 % of the ozone loss observed in the Antarctic stratosphere (WMO, 2011). The catalytic ozone destruction goes on until the PSCs disappear in consequence of the increasing solar radiation. Nitrogen is released from the PSC particles and bounds active halogens to reservoir gases. Finally, after the break-down of the polar vortex, mixing with ozone-rich air from lower latitudes is possible and the ozone concentration regularises.

A summary of the discussed processes and chemical conditions that lead to the formation of the Antarctic ozone hole can be found in Figure 2.3. The top panel shows the 'normal' chemical conditions in the Antarctic stratosphere during fall. Relatively high ozone values come along with moderate temperatures, relatively high values of HCl and HNO_3 and low values of ClO. In the bottom panel the conditions during late winter are shown. Temperatures are significantly lower because of a stable polar vortex and isolation from lower latitudes. Severe O_3 depletion takes place through activation of halogens from reservoir gases at the surface of PSC particles. Sedimentation of PSC particles leads to denitrification and a reduction of HNO_3 values. HCl has been converted to ClO.

The anthropogenic emission of ozone-depleting substances (ODS) such as CFCs and halons were proven to be the main reason for the stratospheric ozone depletion

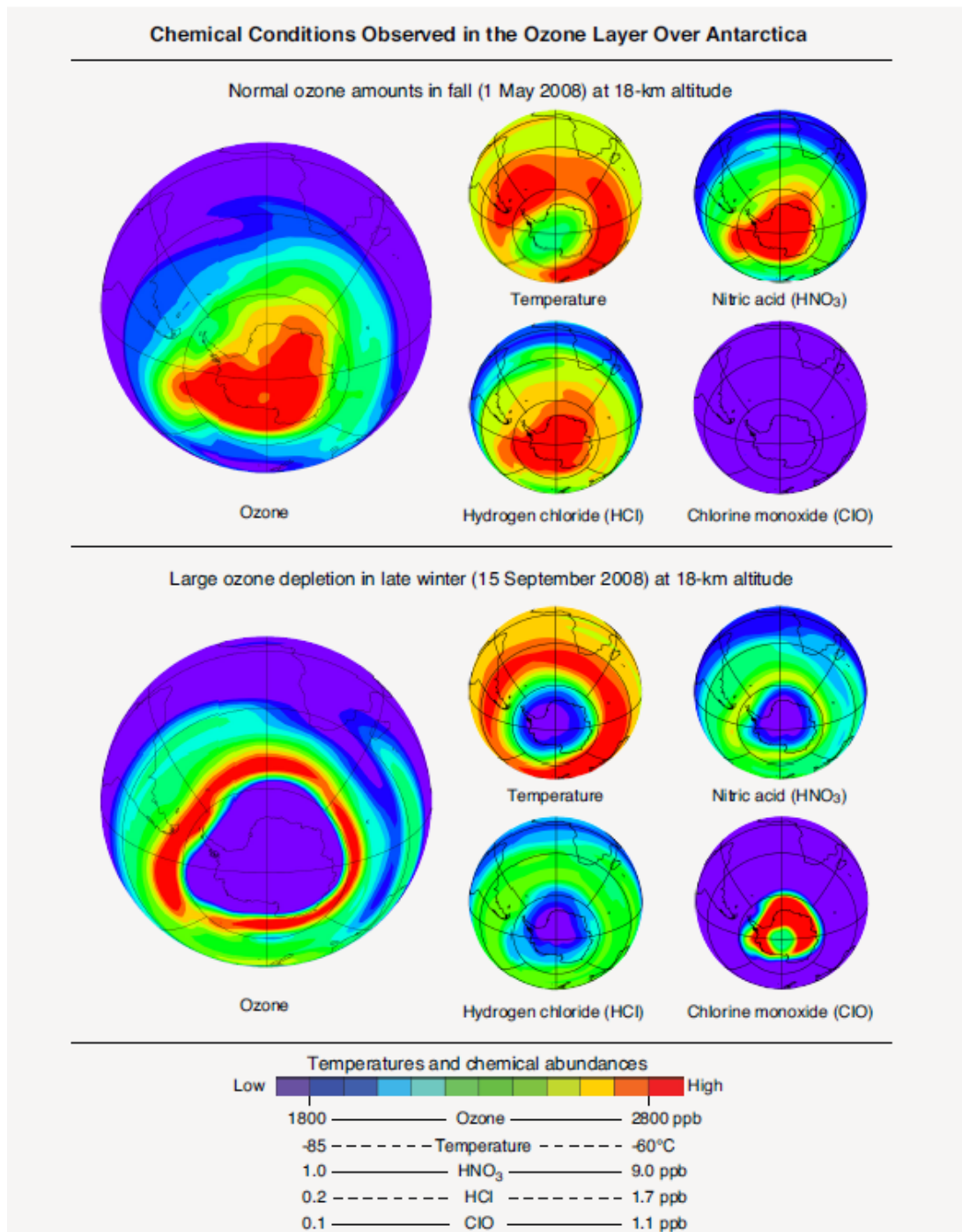


Figure 2.3: Chemical conditions observed in the ozone layer over Antarctica for May 2008 (upper panel) representing fall and September 2008 (lower panel) representing late winter. Figure taken from WMO (2011).

(e.g. Molina and Rowland, 1974, Solomon et al., 1986). As a consequence in 1987 the *Montreal Protocol on Substances That Deplete the Ozone Layer* was concluded. Therein and in following amendments most of the anthropogenic ODS were strongly constricted and eventually prohibited. Due to the success of the Montreal Protocol the atmospheric burden of ODS has been declining. Since the late 1990's a decrease of the tropospheric ODS concentrations can be found. The stratospheric halogen loading is expected to decline over the coming years (top panel Figure 2.4; WMO, 2011). A common measure to illustrate the stratospheric halogen abundance, is the so called Equivalent Effective Stratospheric Chlorine (EESC). EESC can be calculated from (measured or predicted) surface abundances of ODS and natural halogenated gases. It includes chlorine and bromine gases, considers the higher per-atom effectiveness of bromine and estimates the amount of all halogens available in the stratosphere to deplete ozone (Daniel et al., 1995, Newman et al., 2007).

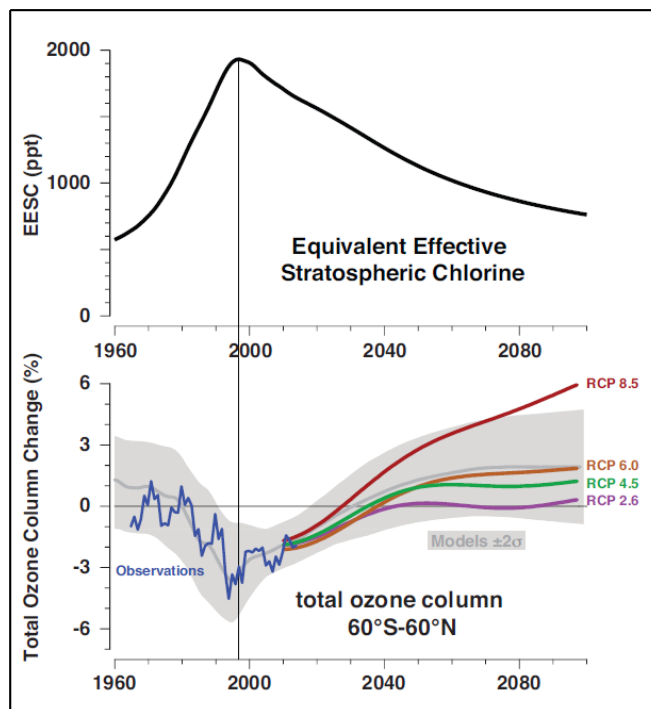


Figure 2.4: Top panel: Variation in Equivalent Effective Stratospheric Chlorine in mid latitudes; Bottom panel: Observed and modeled average total column ozone changes with four possible future scenarios. Figure taken from Carpenter et al. (2014).

In consequence of the reduced stratospheric halogen abundance, several modelling studies predict a recovery of the ozone layer to 1980 values in most regions of the atmosphere in the first half of the 21st century with regional and hemispheric differences (Eyring et al., 2010, Austin et al., 2010a, WMO, 2011). Ozone values in middle latitudes are expected to recover around 2020 (NH) and 2035 (SH). In high latitudes the ozone recovery to 1980 values is predicted to be approximately in 2030 (NH) and 2060

(SH). The differences occur predominantly due to a larger variability in the Northern hemisphere. However, in the tropics, ozone recovery is not projected during the 21st century (Austin et al., 2010a; Eyring et al., 2013a; WMO, 2014; Meul et al., 2016).

In general, the prediction of future ozone values is challenging because the ozone layer is also influenced by increasing concentrations of GHGs, i.e. climate change (Austin et al., 2010b; WMO, 2007, 2011, 2014). Stratospheric cooling, induced by rising GHG concentrations, affects the rate of chemical reactions (Haigh and Pyle, 1979). Ozone depleting reactions are decelerated by lower temperatures and ozone concentrations are expected to increase in a cooler stratosphere (e.g. Rosenfield et al., 2002). However, in polar regions lower temperatures might favour the formation of PSCs which leads to a higher O_3 loss. Moreover, the greenhouse gases N_2O and CH_4 affect the stratospheric chemistry by degrading into reactive hydrogen and nitrogen compounds (Ravishankara et al., 2009; WMO, 2011). Hydrogen compounds from methane rather increase ozone values by bonding active chlorine. Reactive nitrogen, on the contrary, lead to enhanced ozone depletion. Furthermore, the changes of the BDC due to climate change are expected to affect the ozone concentrations by changes in transport (e.g. Oman et al., 2010).

Thus, to predict future stratospheric ozone values several factors have to be taken into account: changes in stratospheric temperatures, altered concentrations of GHGs and ODS and modified transport patterns. Using different possible projections for the greenhouse gases CO_2 , CH_4 and N_2O , related to different radiative forcing values by the year 2100 (IPCC, 2007), shows that the recovery of the ozone layer varies strongly depending on the climate scenario (see Figure 2.4).

Another factor that is suggested to have a significant effect on the ozone layer, is the emission of very short-lived halogens, which are introduced in the following section.

2.3 Halogenated Very Short-Lived Substances

Very short-lived substances (VSLs) are defined as trace gases whose local tropospheric lifetime is less or of the order of tropospheric transport time scales (i.e. 6 months). Because of their relatively short lifetimes their tropospheric distribution is non-uniform, in contrast to the long-lived gases that were discussed before (WMO, 2007). In this study the term VSLs refers to halogenated VSLs, i.e. gases that contain bromine, chlorine or iodine. VSLs include very short-lived (VSL) source gases (SGs) and inorganic product gases (PGs) which mainly originate from SG degradation. Recently, halogen-containing VSLs are thought to provide a significant amount to the stratospheric halogen loading and ozone depletion (WMO, 2007, 2011, 2014). With regard to the mainly natural sources of VSLs and the decreasing anthropogenic long-lived halogens, it is important to quantify the contribution of VSLs to the natural background halogen loading in the stratosphere in order to determine their impact on ozone. Moreover, the emission and

atmospheric distribution of natural halogens might vary in a changing climate.

2.3.1 Sources and Emissions

The majority of chlorine-containing VSLS such as dichloromethane (CH_2Cl_2), trichloromethane (CHCl_3), tetrachloroethene (C_2Cl_4) is from anthropogenic sources. The emissions are mainly related to industrial processes (e.g. Miller et al., 2012; Xue et al., 2011). A minor part of chlorinated VSLS is provided by natural sources like biomass burning, phytoplankton production or soils (e.g. Simpson et al., 2007; Simmonds et al., 2010; Ooki and Yokouchi, 2011). The contribution of chlorinated VSLS to the total stratospheric chlorine loading appears to be small. About 95 (50–145) pmol/mol chlorine of very short-lived source and product gases is able to enter the stratosphere in comparison to about 3300 pmol/mol from long-lived source gases (Carpenter et al., 2014).

Brominated VSLS like bromoform (CHBr_3), dibromomethane (CH_2Br_2), bromodichloromethane (CHBrCl_2) and dibromochloromethane (CHBr_2Cl) are predominately of natural origin. About 90 to 95 % of the global flux of brominated VSLS is thought to be from oceanic sources (WMO, 2007). A small anthropogenic source is provided by drinking water and cooling water chlorination (Worton et al., 2006).

Emissions of iodated VSLS (e.g. methyl iodide (CH_3I)) are also dominated by natural oceanic emissions with small contributions from terrestrial sources (e.g. rice paddies and wet lands; Bell et al., 2002; Lee-Taylor and Redeker, 2005; Youn et al., 2010).

Photolysis or reaction with hydroxide (OH) leads to atmospheric removal of VSLS. Chlorine-containing VSLS are predominantly removed in the troposphere through reaction with OH . Iodated VSLS are almost entirely removed by photolysis. Brominated VSLS are dissipated by a combination of UV photolysis and reaction with hydroxide, where with higher halogen substitution the importance of photolysis increases. The local lifetime of a very short-lived substance is therefore a combined lifetime with respect to oxidation with OH and to photolysis. Regional variations in OH concentration and solar flux can lead to deviating lifetimes.

In the following emphasis is placed on the three VSL substances that origin almost exclusively from natural sources and are therefore not controlled under the Montreal Protocol.

The most abundant bromine-containing VSLS are bromoform (CHBr_3) and dibromomethane (CH_2Br_2), with estimated local lifetimes of 24 and 123 days respectively (Carpenter et al., 2014). They are mainly emitted by marine organisms such as micro-algae (phytoplankton) and macro-algae (seaweed) probably as a defence mechanism (Carpenter and Liss, 2000; Quack et al., 2004; Leedham et al., 2013). Thereby the emission rates strongly depend on algae species and environmental stresses such as salinity and nutrient supply (e.g. Laturmus et al., 1996; Bondu et al., 2008; Mata et al.,

2012). Elevated atmospheric mixing ratios of CHBr_3 and CH_2Br_2 are found in coastal areas, around islands, at oceanic fronts and upwelling areas (e.g. Quack and Wallace, 2003; Carpenter et al., 2003; Chuck et al., 2005; Yokouchi et al., 2005). In general, emissions in the tropics and particular in the West Pacific area seem to be elevated due to high biological productivity.

Methyl iodide (CH_3I) has only an estimated local lifetime of 7 days (Carpenter et al., 2014) but is nevertheless an important carrier of iodine from the surface to the free troposphere or possibly even to the stratosphere (Carpenter, 2003; Tegtmeier et al., 2013). Similar to CH_2Br_2 and CHBr_3 , emissions of methyl iodide are mainly from oceanic sources and associated with enhanced algae occurrence (Ziska et al., 2013).

Observed mixing ratios of VSLs source gases in different altitudes are given in Table 2.1. Background values of CHBr_3 , CH_2Br_2 and CH_3I in the marine boundary layer lie in the range of 0.4–4.0 pmol/mol, 0.6–1.7 pmol/mol and 0.3–2.1 pmol/mol, respectively (Carpenter et al., 2014). However, several studies illustrated the high temporal and spatial variability of VSLs emissions. O’Brien et al. (2009) found elevated atmospheric mixing ratios in the marine boundary layer around the Cape Verde Islands with a mean (range) for CHBr_3 of 8 (2.0–43.7) pmol/mol, for CH_2Br_2 of 2 (0.7–8.8) pmol/mol and for CH_3I of 3 (0.5–31.4) pmol/mol. Above the Mauritanian upwelling increased CHBr_3 mixing ratios of 6.2 (3.1–11.8) pmol/mol were measured. CH_2Br_2 showed similar patterns with atmospheric mixing ratios of 2.4 (1.8–3.4) pmol/mol (Quack et al., 2007). Yokouchi et al. (2005) measured up to 40 pmol/mol of CHBr_3 at the coasts of tropical islands in the Pacific Ocean. Pyle et al. (2011) highlighted the large variability of CHBr_3 mixing ratios due to localized emission hot-spots. Within their study, land-based measurements in Borneo showed background values of 2–5 pmol/mol but occasional values of many 10s of pmol/mol.

Table 2.1: Observations of selected VSLs source gases in the marine boundary layer (MBL) and tropical tropopause layer (TTL). All table entries are mole fractions with units of pmol/mol. Adapted from Table 1-7 of Carpenter et al. (2014).

	MBL	Lower TTL	Upper TTL
CHBr_3	0.4-4.0	0.2-1.1	0.01-0.29
CH_2Br_2	0.6-1.7	0.6-1.2	0.43-0.83
CH_3I	0.3-2.1	0.00-0.38	0.00-0.01
Total Br	2.8-18.0	2.2-6.7	1.1-3.2
Total I	0.3-2.1	0.00-0.38	0.00-0.01
Total Cl	76-125	36-103	38-89
Anthrop. Cl	55-115	22-96	24-68

Thus, atmospheric mixing ratios of VSLs exhibit a high and temporal variability. Elevated mixing ratios occur close to coastal areas, oceanic fronts and in the tropics

and subtropics. Localised sources and short life times lead to diverse mixing ratios and make it hard to estimate the total global oceanic flux into the atmosphere. Because of their almost exclusively marine origin inter hemispheric differences are small. Due to deviating lifetimes with respect to photolysis, CH_2Br_2 and CHBr_3 mixing ratios peak around the equator, whereas CH_3I mixing ratios peak at high tropical and subtropical latitudes (Blake et al., 2003; Butler et al., 2007).

Mixing ratios of these very short-lived compounds maximize during winter as destruction by photolysis and reaction with OH is limited (Yokouchi et al., 1996; Liang et al., 2010).

There is only few knowledge about long term trends of VSLS from natural sources. Firm air measurements showed that CHBr_3 mixing ratios in the Northern hemisphere increased by $16 \pm 6\%$ from 1950 to 1990. The increase was ascribed to anthropogenic water chlorination. For CH_2Br_2 no significant trend was found as it is entirely of natural origin (Worton et al., 2006). In the Southern hemisphere firm air measurements conducted by Sturges et al. (2001) showed no significant trends for CHBr_3 since 1950. However, it is possible the emission strength of VSLS will increase in the future. It seems likely that anthropogenic emissions will increase. Changes in regional land use, such as seaweed farming, or utilisation of short-lived halogens as substitute for the restricted long-lived ODS might enhance VSLS emissions. Additionally, the natural emission of VSLS might change in consequence of altered environmental conditions such as sea surface temperatures, nutrient supply or wind stress (Leedham et al., 2013). Ziska (2014) found an increase of VSLS emissions from 1986 to 2100 due to increasing sea surface temperatures and wind that are related to climate change.

The picture of brominated VSLS emissions involves high uncertainties. Observation-based studies can only supply a snapshot of a highly variable and heterogeneous system. Often differences between calibration scales and methods of estimating emission fluxes lead to further discrepancies between the studies (Butler et al., 2010). Uncertainties related to the VSLS emission fluxes remain in emission inventories that are used to simulate VSLS in chemistry-climate models. Therefore, it is essential to increase our knowledge on seasonal and regional variations of VSLS emissions to reliably examine their potential impact on the atmosphere.

2.3.2 Troposphere-Stratosphere Transport

VSL source gases (SGs) can be transported into the stratosphere via two pathways. Source gas injection (SGI) occurs when SGs are transported rapidly vertically and release their halogen content directly in the stratosphere. The tropospheric degradation of SGs forms inorganic and organic product gases (PGs). These PGs may also reach the stratosphere - called product gas injection (PGI). Both pathways lead to a contribution of VSLS to the stratospheric halogen loading. The efficiency of SGI and PGI depends on chemical and dynamical conditions: chemical destruction via photolysis and reaction

with OH, removal via wash-out of PGs and vertical transport time scales.

Generally, strong convective uplift allows VSLS to reach the tropical tropopause layer (TTL), the transition layer between troposphere and stratosphere (Fueglistaler et al., 2009). Once in the TTL, the probability of wash-out is small and the VSLS potentially can enter the stratosphere.

SGI of VSLS is thought to be large when high emissions occur in convective source regions, e.g. in the tropical oceans and in particular in the tropical Western Pacific (Aschmann et al., 2009). The efficiency of the transport to the TTL varies with season and has a maximum in Northern hemisphere (NH) winter (Aschmann et al., 2009; Gettelman et al., 2009). In contrary, PGI may be reduced under high convective conditions as inorganic PGs are highly soluble and can be removed from the troposphere in convective precipitation (Liang et al., 2014). Global model studies suggest that about 50 % of the total bromine reaching the stratosphere from CHBr_3 and about 90 % from CH_2Br_2 are delivered via SGI (Aschmann et al., 2011; Hossaini et al., 2012b).

VSLS transport into the stratosphere is probably also related to phases of the El Niño-Southern Oscillation (ENSO) (Aschmann et al., 2011; Ashfold et al., 2012). A strong El Niño event allows more SGs to reach the stratosphere but may reduce PGI through wash-out of PGs.

Thus, Liang et al. (2014) conclude the net transport of bromine from VSLS into the stratosphere to be largest under low convective conditions as the minor reduction in SGI may be exceeded by a distinct increase of PGI.

2.3.3 Stratospheric Bromine Loading

Quantifying the VSLS contribution to the stratospheric bromine content $\text{Br}_y^{\text{VSLS}}$ has been the subject of many studies in the last years. Several uncertainties hamper the quantification of the total (SGI + PGI) bromine input from VSLS.

Observations of SGs in the tropopause region are due to the highly variable values quite challenging but provide information about the magnitude of SGI. However, observational evidence for PGs is sparse and around the limit of detection (~ 1 pmol/mol).

Estimates for $\text{Br}_y^{\text{VSLS}}$ are usually derived by measurements of BrO, combined with model estimates of the BrO/Br_y ratio to determine the total stratospheric Br_y and then subtract the contribution of long-lived SGs. Another approach is the measurement of SGs in the TTL - as transport from there into the stratosphere is likely - and an estimated contribution of PGs from global modeling studies. Moreover, the consideration of VSLS in global chemistry-climate-models facilitates the quantification of $\text{Br}_y^{\text{VSLS}}$. This procedure also includes uncertainties as it is sensitive to assumptions concerning the convection parametrization, the partitioning of Br_y or the wet deposition of soluble inorganic bromine species. Furthermore, Hossaini et al. (2013) showed that the model contribution of VSLS to the stratospheric bromine burden is dependent on the chosen emission inventory.

Recent observations and model studies suggest that SGs provide (0.7–3.4) pmol/mol and PGs (1.1–4.3) pmol/mol to the stratospheric bromine content. The total contribution of brominated VSLS to the inorganic stratospheric bromine is thus estimated to be about 5 (2–8) pmol/mol (Carpenter et al., 2014).

2.3.4 Influence on Ozone

Several modelling studies have shown that inclusion of stratospheric bromine from VSLS enhances the agreement between modeled and observed ozone trends (e. g. Salawitch et al., 2005; Feng et al., 2007; Sinnhuber and Meul, 2015). Using a CTM, Feng et al. (2007) found a 10 DU decrease in the mid latitude ozone column compared to a simulation not considering VSLS. Braesicke et al. (2013) found up to 20 % less ozone in the lower stratosphere in the polar regions between a CCM simulation with and without $\text{Br}_y^{\text{VSLS}}$. Bromine from VSLS is suggested to enhance the coupled $\text{BrO}_x\text{--ClO}_x$ cycle (see previously discussed reactions R.2.36-R.2.40) that is most effective in destroying ozone in the lower stratosphere (Salawitch et al., 2005). This influence on ozone seems to be largest following large volcanic eruptions. In these periods stratospheric aerosol values are elevated and heterogeneous halogen activation is enhanced relative to volcanic quiescent years (Salawitch et al., 2005; Feng et al., 2007; Sinnhuber et al., 2009; Yang et al., 2014). Moreover, Salawitch et al. (2005) found evidence that additional $\text{Br}_y^{\text{VSLS}}$ increases the BrO--HO_2 cycle (reactions R.2.41-R.2.45) which then competes with the HO_x cycle 2 (reactions R.2.13-R.2.15) below 14 km altitude. However, this effect is independent from volcanic aerosol.

2.3.5 Future Changes

As previously mentioned it is highly uncertain if VSLS emissions will alter in consequence of a changed climate. More certain is the further decline of long-lived halogens from anthropogenic sources due to the success of the Montreal Protocol. This may influence the impact of $\text{Br}_y^{\text{VSLS}}$ on ozone as less available chlorine reduces the effectiveness of the $\text{BrO}_x\text{--ClO}_x$ ozone loss cycle (Braesicke et al., 2013; Yang et al., 2014). Furthermore, model studies suggest an accelerated troposphere-stratosphere transport of VSLS due to dynamical changes in a future climate resulting in more bromine from short-lived halogens reaching the stratosphere (e.g. Dessens et al., 2009; Hossaini et al., 2012b). In addition, it cannot be ruled out that VSLS emissions change due to altered environmental conditions (e.g. SSTs, wind stress, nutrient supply) or increased anthropogenic utilisation (e.g. seaweed farming, water chlorination, substitution of long-lived halogens). For instance, Ziska (2014) found in CMIP5 climate model simulations from 2006 to 2100 an increase of natural VSLS emissions as a result of increased SSTs and zonal wind fields.

Chapter 3

Model Description and Set-ups

To analyse chemical and dynamical processes and their interactions in the atmosphere it is a convenient method to use numerical models. In the context of climate science there are arbitrarily complex models available simulating processes in the Earth's atmosphere. For this study the chemistry-climate model (CCM) ECHAM5/MESSy Atmospheric Chemistry (EMAC) is used. In the following sections the components of the model system are shortly presented. Afterwards a description of the conducted simulations and associated model set-up and the used measurement data is given.

3.1 The Model System EMAC

An approach in the evolution of Earth System Modeling is to link several models for specific domains (e.g. ocean, atmosphere, land) with a coupler organizing the communication and data exchange between the domain models (Jöckel et al., 2005, 2016). However, those kind of models get very complex and hard to control. So, another approach to Earth System Modeling is to split chemical, physical and biological processes from the base model and implement them as submodels.

MESSy

The **Modular Earth Model System (MESSy)** (<http://www.messy-interface.org>, Jöckel et al., 2005, 2016) was developed to handle data exchange and communication between several submodels and a base model (see Figure 3.1). The submodels can be easily switched on and off depending on the scientific focus and available resources like computational power, data storage and computing time. Via namelists model parameters can be changed without recompiling the model code.

EMAC

The model system **ECHAM5/MESSy Atmospheric Chemistry (EMAC)**, (Jöckel et al., 2005, 2006, 2010, 2016) is composed of the fifth generation European Centre HAMBurg

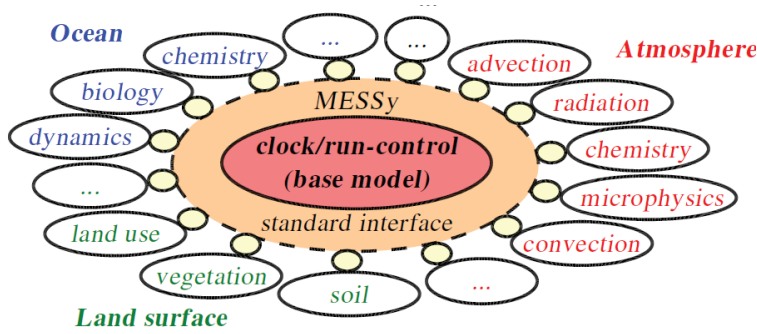


Figure 3.1: The MESSy architecture: the interface MESSy couples separated processes/submodels to a base model (Figure 2 from Jöckel et al., 2005).

general circulation model ECHAM5 (Roeckner et al., 2003, 2006) as base model and the interface MESSy coupling several submodels to it.

ECHAM5 integrates the prognostic dynamical equations. It is a spectral model and in different horizontal resolutions available. In this work the model is used in resolution T42 which is associated with a Gaussian grid of approximately $2.8^\circ \times 2.8^\circ$ in zonal and meridional direction. The vertical resolution of the modelled atmosphere is described with hybrid σ -p-coordinates. Close to the surface the model layers are adjusted to the orography (σ -coordinates) and transform with increasing height to pressure coordinates. The here applied EMAC middle atmosphere (MA) version T42L90MA L90 consists of 90 model layers distributed from ground to 0.01 hPa (about 80 km). The time step length is 720 s.

In order to get a chemistry-climate model the atmospheric chemistry module MECCA (Module Efficiently Calculating the Chemistry of the Atmosphere; Sander et al., 2005) is linked to the base model ECHAM5. MECCA includes the basic O_3 (ozone), CH_4 (methane), HO_x (hydrogen oxide radicals) and NO_x (nitrogen oxide radicals) chemistry, non-methane-hydrocarbon (NMHC) chemistry, halogen and sulfur chemistry. The module considers gas-phase, aqueous-phase and heterogeneous reactions and can be used for both, tropospheric and stratospheric chemistry calculations. According to requirements the user can select a custom-made chemical mechanism, e.g. tropospheric reactions only. The chemical mechanism of this study contains 155 gas phase species and 310 reactions including heterogeneous reactions on particles. Due to very different lifetimes of atmospheric species it is necessary to use a robust numerical solver for the differential equations. For MECCA the kinetic preprocessor (KPP) software (Damian et al., 2002; Sandu and Sander, 2006) is used to translate the chemical equations into Fortran95 code (Sander et al., 2005). KPP includes different solvers to integrate the chemical differential equations. In this study the Rosenbrock solver of 3rd order (Sandu et al., 1997) is applied as Sander et al. (2005) comment in their study, that it is the most appropriate solver for very stiff differential equations which is the case for multiphase chemistry.

MESSy submodels

As mentioned above MESSy couples processes or submodels to a base model. In EMAC there are some processes taken from the base model ECHAM5 and reimplemented as submodels. In addition, several new submodels have been developed and linked to the base model. An overview of the submodels used in this study is given in Table 3.1. As mentioned above, atmospheric chemistry is calculated by the module MECCA. Radiation is computed within the submodel RAD, which is based on the original ECHAM5 radiation code. RAD calculates atmospheric radiative transfer considering the atmospheric chemical composition. Radiatively active chemical substances (e.g. O₃, CH₄ and H₂O) are handed over by the chemistry submodel MECCA to RAD and affect the radiative budget. Changes in the radiative budget in turn feedback on the dynamics (Jöckel et al., 2006; Deckert et al., 2011). The convection processes are described with the Tiedtke scheme (Tiedtke, 1989). More details about the submodels can be found in Jöckel et al. (2006, 2010, 2016), the references in Table 3.1 and on the MESSy project homepage (www.messy-interface.org).

3.2 A New Online Diagnostic: The Submodel TBUDGET

In the framework of this study the submodel TBUDGET was developed. It is a diagnostic tool that depicts the contribution of different production cycles (e.g. associated with different source gases) to a tracer (family). The code is generic but the submodel was originally designed and will be described here exemplarily in the context of VLS analysis.

As mentioned before, VLS are known to contribute significantly to the total inorganic bromine budget Br_y (see Section 2.1.1) but uncertainties to what extent are high. To quantify the amount of Br_y originating from VLS, the total tracer Br_y is splitted into two summands: a tracer Br_L which is defined as active forms of bromine coming from long-lived (> 6 months) source gases and a tracer Br_S containing active bromine from short-lived (≤ 6 months) source gases (see Figure 3.2). The temporal change of each tracer can be described by its production and loss rate, with Br_y = Br_L + Br_S:

$$\frac{d}{dt}Br_L = ProdBr_L - LossBr_y \cdot \frac{Br_L}{Br_y} \quad (3.1)$$

$$\frac{d}{dt}Br_S = ProdBr_S - LossBr_y \cdot \frac{Br_S}{Br_y} \quad (3.2)$$

$$\text{Net: } \frac{d}{dt}Br_y = ProdBr_y - LossBr_y \quad (3.3)$$

By integrating the equations the amount of inorganic bromine originating from long- and short-lived bromine source gases can be specified and the contribution of bromi-

Table 3.1: MESSy submodels used in this study

submodel	description	reference
AEROPT	aerosol optical properties	http://www.messy-interface.org
AIRSEA	air-sea exchange of tracers	Pozzer et al. (2006)
CLOUD	ECHAM5 cloud scheme	Roeckner et al. (2006); Jöckel et al. (2006)
CLOUDOPT	optical properties of clouds	Dietmüller et al. (2016)
CONVECT	convection parametrisations	Tost et al. (2006a), Tiedtke (1989)
CVTRANS	convective tracer transport	Tost (2006)
CH4	CH ₄ oxidation	Eichinger et al. (2015)
DRADON	²²² Rn as diagnostic tracer	Jöckel et al. (2010)
DDEP	dry deposition	Kerkweg et al. (2006a)
GWAVE	non-orographic gravity wave	Hines (1997a,b); Manzini and McFarlane (1998)
H2O	stratospheric water vapour	Jöckel et al. (2006); Lelieveld et al. (2007)
JVAL	photolysis rate coefficients	Landgraf and Crutzen (1998); Jöckel et al. (2006)
LNOX	lightning NO _x production	Grewe et al. (2001), Tost et al. (2007), Jöckel et al. (2010)
MECCA	tropospheric and stratospheric chemistry	Sander et al. (2005)
MSBM	multi-phase stratospheric box model	Jöckel et al. (2010)
O3ORIG	ozone origin diagnostics	Grewe (2006)
OFFEMIS	offline emissions	Kerkweg et al. (2006b)
ONEMIS	online emissions	Kerkweg et al. (2006b)
ORBIT	Earth's orbit around the Sun	Roeckner et al. (2003)
PTRAC	additional tracers beyond the chemical mechanism	Jöckel et al. (2008)
QBO	assimilation of the Quasi-biennial oscillation	Jöckel et al. (2006)
RAD	radiation scheme	Roeckner et al. (2006); Jöckel et al. (2006); Dietmüller et al. (2016)
S4D	Sampling in 4 dimensions	Jöckel et al. (2010)
SCALC	simple algebraic calculations	Kern (2013)
SCAV	scavenging and wet deposition of aerosol and trace gases	Tost et al. (2006b)
SCOUT	stationary column output	Jöckel et al. (2010)
SEDI	sedimentation of aerosol particles	Kerkweg et al. (2006a)
SORBIT	sampling along sun-synchronous satellite orbits	Jöckel et al. (2010)
SURFACE	surface temperatures	http://www.messy-interface.org
TBUDGET	contribution of different production cycles to a tracer family	this study, see Section 3.2
TNUDGE	Newtonian relaxation of tracers	Kerkweg et al. (2006b)
TROPOP	tropopause definitions	Jöckel et al. (2006)
VISO	iso-surfaces and maps	Jöckel et al. (2010)

nated VSLs to Br_y quantified. A numerical correction of Br_y is applied to guarantee that the sum of all summands equals the total tracer. Technically, the production terms ProdBr_L and ProdBr_S are diagnostic tracers which are defined in the MECCA chemical mechanism of the model. All reactions describing the degradation of source gases lead to a release/production of active bromine. Depending on the lifetime of the source gas either the diagnostic tracer Br_L (lifetimes > 6 months) or the tracer Br_S (lifetimes ≤ 6 months) is produced. The tracer family, thus the total tracer Br_y is defined in the namelist of the submodel TRACER as the sum of inorganic reactive brominated species ($\text{Br}_y = \text{Br} + \text{BrO} + \text{HOBr} + \text{BrNO}_2 + \text{BrNO}_3 + \text{HBr} + \text{Br}_2$). The loss rate LossBr , also specified via namelist entries, is obtained by summing the scavenging tendencies of water-soluble brominated species calculated by the submodel SCAV with SCALC (Kern, 2013). In the framework of this study the diagnostic submodel TBUDGET is applied in all simulations for the above described bromine budgets but also in an equivalent form for chlorine-containing species. With the aid of further already implemented diagnostic tracers describing ozone depletion rates through different tracer families (i.e. ozone loss through bromine (LossO3Br) or chlorine (LossO3Cl)) the contribution of short-lived halogens to ozone loss can be specified without extra computational efforts.¹ A schematic overview of the submodel TBUDGET is given in Figure 3.2.

All reactions of MECCA including the here defined diagnostic tracers are listed in the supplement of the paper by Jöckel et al. (2016).

3.3 Model Set-ups and Simulations

A common practice to analyse chemical feedback mechanisms in the atmosphere with a chemistry-climate model is to perform sensitivity studies. Generally, a reference simulation is compared to a sensitivity simulation which is identical except for certain model parameters. In the following section the used model set-up is described. Afterwards, Section 3.3.2 contains an overview of the simulations performed within this study.

3.3.1 Model Set-ups

QCTM mode

Any chemical perturbation (i.e. changed surface emissions) in the chemistry-climate model will lead to a response in the climate system which is the result of radiative, chemical and dynamic feedbacks. Natural variability makes it difficult to extract the effect of small perturbations. Therefore, Deckert et al. (2011) developed the so-called quasi chemistry-transport model (QCTM) mode. In this mode any on-line impact from the

¹Addendum: During the analyses an error in the definition of the variable LossO3Br was detected which makes a quantitative comparison to LossO3Cl not possible.

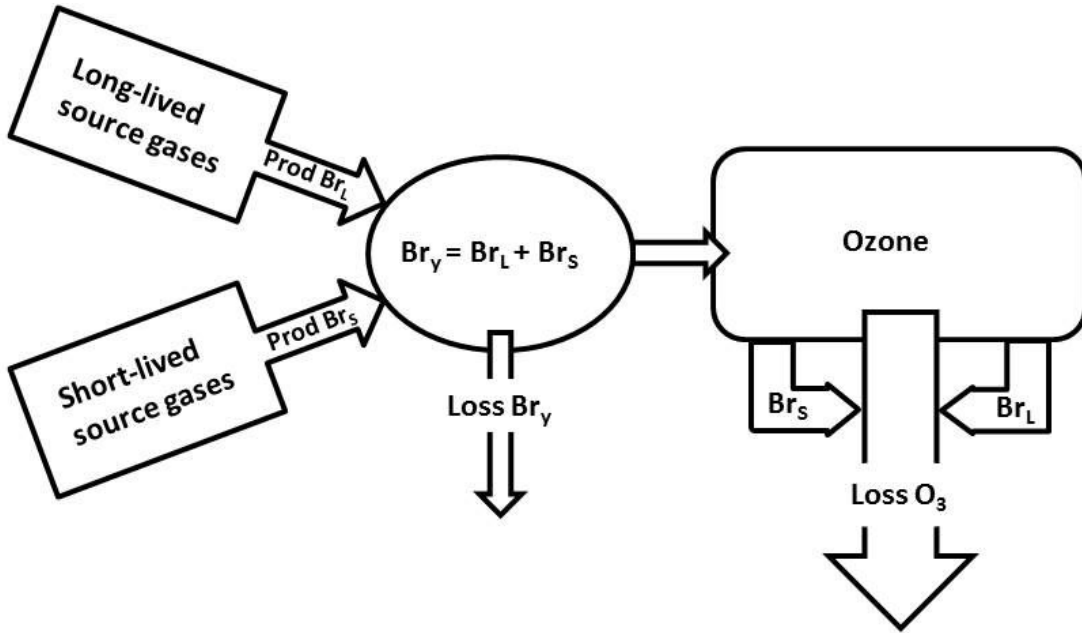


Figure 3.2: Schematic of the MESSy submodel TBUDGET applied for detecting the contribution of brominated VSLs to ozone loss.

chemistry on dynamics is disabled, so that the meteorological situation is in all sensitivity simulations equal and atmospheric differences only arise from chemical differences between the simulations. With this method the noise by feedbacks is suppressed and even signals of small chemical perturbations can be identified using shorter simulation times. The QCTM mode, more precisely the decoupling of chemistry and dynamics, is achieved by the following approach: At first a preparatory simulation is performed with fully coupled chemistry and dynamics to get monthly mean mixing ratios of the radiatively active chemical species and total nitric acid (HNO_3) for radiative effects of polar stratospheric clouds. After that, the QCTM simulations can be performed where mixing ratios of the radiatively active species are prescribed with the offline climatology of the preparatory simulation. The oxidation of methane to water vapour is described via the submodel CH4 using an offline climatology of CH_4 to ensure the same dynamics in all QCTM simulations. To allow the chemical processes on PSCs but suppress the impact on radiation and dynamics after a chemical perturbation, both an offline climatology of HNO_3 and an interactive HNO_3 are applied. It must be pointed out that the model chemistry still supplies mixing ratios of all radiatively active species, but these are not used by the radiation submodel RAD.

Transient and time-slice experiments

There are two types of simulations to be distinguished in this study: Transient and time-slice simulations. In transient simulations greenhouse gas forcings, emissions and

sea surface temperatures alter continuously to represent the devolution of the actual climate. Thus, trends of atmospheric parameters can be determined. In contrary, the boundary conditions in time-slice experiments are repeated perpetually every year to represent the atmospheric condition of one year, for instance the year 2000 for a “year-2000 time-slice”. The cyclic recurrence of one year provides a comparatively large sample for statistical analyses.

Nudged and free-running mode

It is particularly useful to run the model in nudged mode, when the model data is to be compared directly to chemical observations. In this mode, Newtonian relaxation of four prognostic model variables (temperature, divergence, vorticity and the logarithm of surface pressure) to observed values is applied to reproduce the real meteorology as accurately as possible. However, for the validation of the model in “hindcast” simulations depicting the past climate and for the analysis of future climate scenarios the model simulations are performed in the free-running mode.

3.3.2 Simulations

The emission strength and distribution of halogenated very short-lived substances (VSLs) are relatively uncertain. However, the inclusion of realistic emissions in chemistry-climate models is essential to simulate a realistic chemistry in both, troposphere and stratosphere as VSLs contribute significantly to the inorganic bromine (Br_y) loading. In the stratosphere Br_y is a major sink for ozone and in the troposphere bromine chemistry can perturb oxidation capacity (Lary and Toumi, 1997).

Generally, model version and set-up are the same as for the recent EMAC simulations that were conducted by the MESSy Consortium within the “Earth System Chemistry Integrated Modelling (ESCiMo)” initiative (Jöckel et al., 2016) for the upcoming WMO ozone assessments and IPCC reports. The design of the ESCiMo simulations was recommended by the SPARC (Stratosphere-troposphere Processes And their Role in Climate) Chemistry-Climate-Initiative (CCMI) in favour of a chemistry-climate model evaluation. The CCMI also provided references for forcings and boundary conditions (Eyring et al., 2013b) which were applied for both, the ESCiMo simulations and the simulations conducted especially for the VSLs analysis in this study. Within the ESCiMo initiative the most recent model developments, emissions and boundary conditions were aggregated to provide a large set of state-of-the-art chemistry-climate simulations that are well described in Jöckel et al. (2016). Therefore, the simulations performed in the framework of this study are conducted with the same EMAC version 2.52, emissions and boundary conditions.

In order to extract only the effects of changed VSLs emissions, the model was run in the QCTM mode (see Section 3.3.1). Initially a fully coupled preparatory simulation is computed to obtain monthly mean fields of radiatively active species for the QCTM

runs. The sensitivity simulations then only differ in the prescribed VLSL emissions. Using the QCTM approach enables a concordant dynamic in all QCTM simulations so that differences only arise from chemical perturbations, thus, in this case from changes in the VLSL surface emissions.

In the following a description of the conducted simulations and applied VLSL emissions is given. An overview of all simulations can be found in Table 3.3.

Transient Simulations

In this study, the first set of simulations is designed to assess the uncertainties of VLSL emissions and the representation of selected VLSL in EMAC. Four emission inventories for the major brominated VLSL bromoform (CHBr_3) and dibromomethane (CH_2Br_2) and two emission inventories for methyl iodide (CH_3I) are applied

- to identify the most suitable emission inventory for a realistic representation of VLSL mixing ratios and associated quantities in EMAC and
- to determine how sensitive stratospheric parameters respond to varied emission inventories at the surface.

The transient simulations are nudged by Newtonian relaxation towards ERA-Interim reanalysis data. Sea surface temperatures (SSTs) and sea ice concentrations (SICs) in the nudged simulations were consistently used from ERA-Interim (Dee et al., 2011). Further boundary conditions are prescribed via the submodel TNUDGE: surface mixing ratios of species with uncertain emission fluxes are relaxed by Newtonian relaxation in the lowest model layer to observed mixing ratios from the Advanced Global Atmospheric Gases Experiment (AGAGE: <http://agage.eas.gatech.edu>) and the National Oceanic and Atmospheric Administration/Earth System Research Laboratory (NOAA/ESRL: <http://www.esrl.noaa.gov>). Species that are prescribed are the greenhouse gases CO_2 , N_2O and CH_4 , several ozone depleting substances, H_2 and SF_6 .

At first the fully coupled preparatory simulation *base* was performed for the period 2005 to 2012 to obtain the monthly mean fields that are required for the QCTM set-up (see Section 3.3.1). After that the QCTM runs *ref*, *zis*, *ord* and *lia* were conducted for the same time period only differing from each other through the applied emission inventory for the VSL substances CHBr_3 , CH_2Br_2 and CH_3I . The first year of the simulations is taken as spin-up and only the years 2006 to 2012 are taken for the analyses.

The QCTM simulations *ref*, *lia* and *ord* used emission fluxes derived from top-down emission estimates from Warwick et al. (2006), Liang et al. (2010) and Ordóñez et al. (2012), respectively (hereafter "Warwick2006", "Liang2010" and "Ordóñez2012"). Run *zis* used the bottom-up estimate from Ziska et al. (2013) (hereafter "Ziska2013"). The top-down inventories rely on aircraft observations and assumed atmospheric loss rates to estimate surface fluxes with global models. Uncertainties in this approach are

mainly due to relatively few number of measurements and the lack of knowledge about the geographical distribution. Coarse horizontal resolutions of the models may add further uncertainties as local emission "hot spots" may be underrepresented.

Description of Surface Emissions

The Warwick2006 surface emissions for bromoform and dibromomethane are derived from aircraft observations collected during the National Aeronautics and Space Administration (NASA) Pacific Exploratory Mission (PEM) Tropics B in 1999. These emissions have been used as a "standard" emission inventory in past EMAC simulations and therefore the simulation using this inventory in this study is called *ref* for "reference emissions".

The Liang2010 inventory for CH_2Br_2 and CHBr_3 , also a top-down estimate, is derived using airborne measurements in the Pacific and North American troposphere and lower stratosphere obtained during NASA aircraft campaigns that took place between 1996 and 2006 (Liang et al., 2010).

Ordóñez et al. (2012) also used a compilation of measurements from several aircraft campaigns between the years 1996 and 2006 and observations in the marine boundary layer. The Ordóñez2012 inventory is the only emission data set with seasonal variations. Tropical ($20^\circ\text{N} - 20^\circ\text{S}$) emissions of the short-lived bromocarbons are correlated to chlorophyll-a which is probably a proxy for biological activity. Over coastal areas the emission fluxes are considered higher than over the open ocean by a factor of 2.5.

Finally, emissions by Ziska et al. (2013) are calculated sea-to-air flux estimates from surface observations within the HalOcAt (Halocarbons in the Ocean and Atmosphere) database (<https://halocat.geomar.de>). The data are classified into regions considering physical and biogeochemical characteristics, for instance open ocean or coastal regions, and the interpolated on a $1^\circ \times 1^\circ$ grid. Missing values are extrapolated using an ordinary least squares method. Ziska et al. (2013) provide not only emission data sets for bromoform and dibromomethane but also one for methyl iodide which is applied in the EMAC simulation *zis*. The simulations *ref*, *ord* and *lia*, with Warwick2006, Ordóñez2012 and Liang2010 emissions for CHBr_3 and CH_2Br_2 , use emissions for CH_3I from Bell et al. (2002) as no further CH_3I data sets were available. The global CH_3I source strength in *zis* is smaller (206 Gg/year) than in the other three simulations (241 Gg/year).

The total source strength of CHBr_3 and CH_2Br_2 under the emission inventories is specified in Table 3.2. For both substances the reference emissions from Warwick et al. (2006) are clearly larger than in the other inventories. Generally, for CH_2Br_2 the source strength in the inventories is more constraint than for CHBr_3 . The bottom-up estimate from Ziska et al. (2013) provides the smallest CHBr_3 emissions ($\sim 36\%$ of *ref*) but larger CH_2Br_2 emissions ($\sim 77\%$ of *ref*) than *ord* ($\sim 59\%$) and *lia* ($\sim 55\%$). CHBr_3 emissions in *ord* and *lia* amount to $\sim 89\%$ and 76% of the reference emissions.

Table 3.2: Global source strength (Gg source gas per year) of CHBr_3 and CH_2Br_2 in the EMAC simulations

Simulation	Emissions	CHBr_3	CH_2Br_2
ref	Warwick2006	595	113
zis	Ziska2013	215	87
ord	Ordóñez2012	529	67
lia	Liang2010	450	62

Figures 3.3 and 3.4 show the zonally averaged emission field of CHBr_3 and CH_2Br_2 for each inventory. The inventories differ significantly, especially in the tropical West Pacific region, where transport of VSLs into the stratosphere is thought to be large (Aschmann et al., 2009). The distribution of the CHBr_3 and CH_2Br_2 emissions in

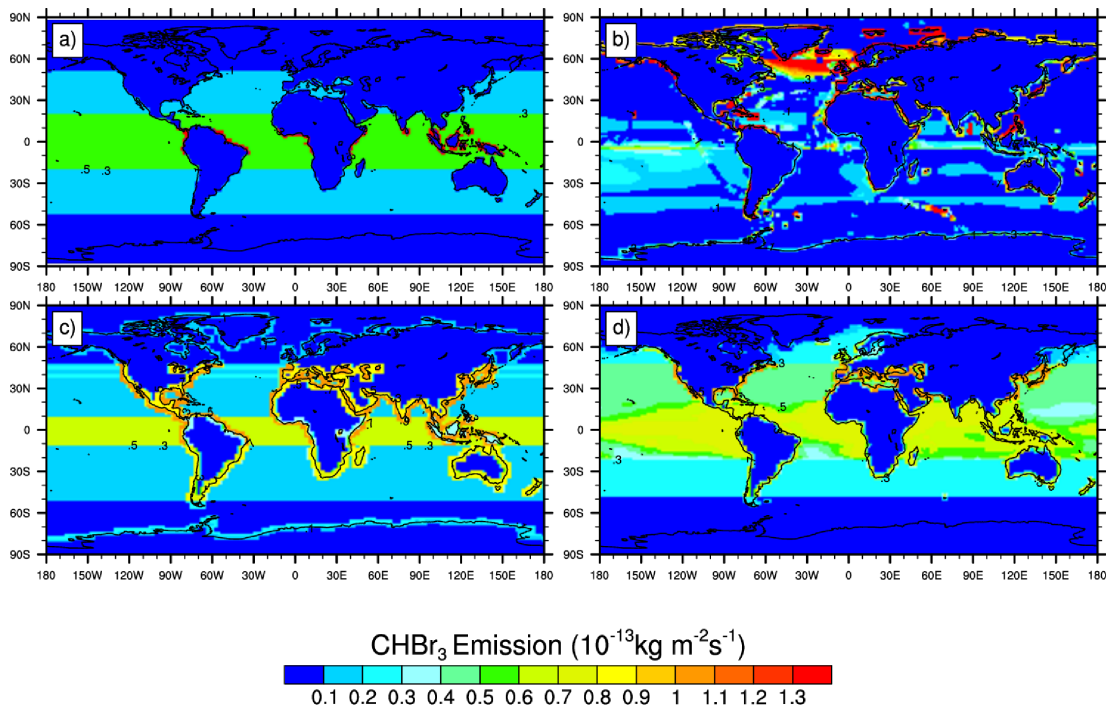


Figure 3.3: Annual mean of input CHBr_3 emission (in $10^{-13} \text{kg m}^{-2} \text{s}^{-1}$) from (a) Warwick et al., 2006, (b) Ziska et al., 2013, (c) Liang et al., 2010, and (d) Ordóñez et al., 2012.

dependence of latitude shows significant differences, on the one hand between the previous EMAC "standard" inventory Warwick2006 and the others, and on the other hand between the top-down derived estimates (Warwick2006, Liang2010 and Ordóñez2012) and the bottom-up estimate (Ziska2013). In particular, in high latitudes the Ziska2013 emissions are noticeably larger (Figures 3.5(a) and 3.5(b)). For CH_3I only the data sets from Bell et al. (2002) and Ziska et al. (2013) were available. Thus, in *ref*, *ord* and *lia* CH_3I emissions are equally prescribed and lines of these simulations lie on top of each other. Both inventories show elevated values in the mid latitudes. Compared to *ref* the source strength in *zis* is larger in the Southern polar region (Figure 3.5(c)).

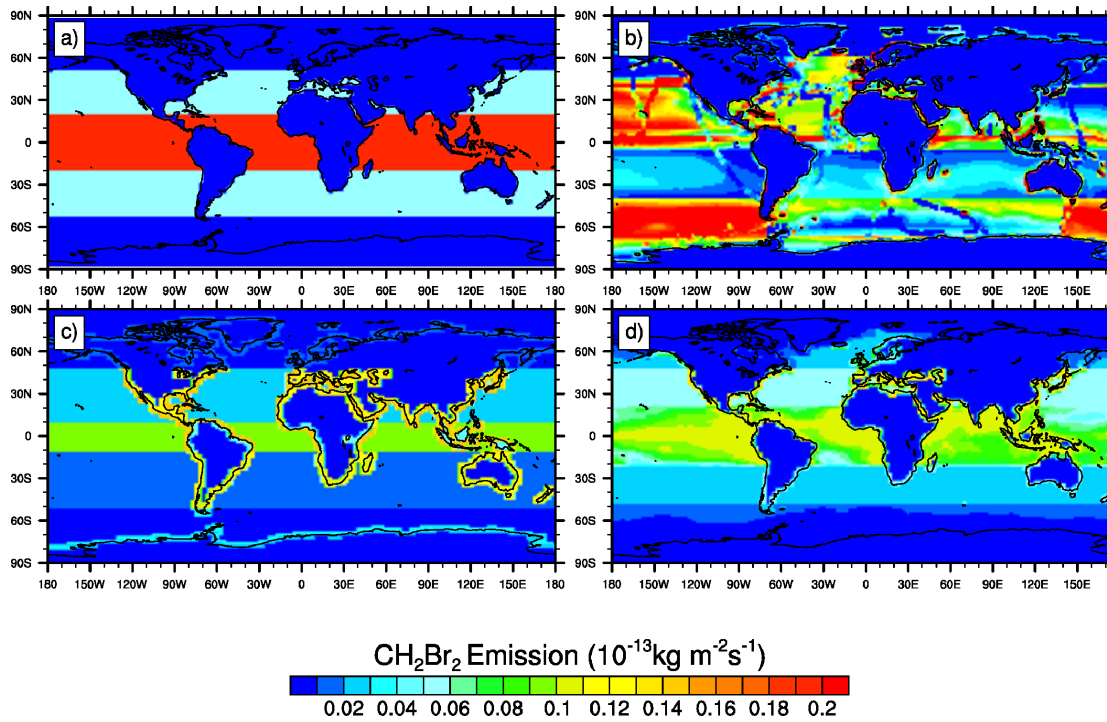


Figure 3.4: Annual mean of input CH₂Br₂ emission (in $10^{-13}\text{kgm}^{-3}\text{s}^{-1}$) from (a) Warwick et al., 2006, (b) Ziska et al., 2013, (c) Liang et al., 2010, and (d) Ordóñez et al., 2012.

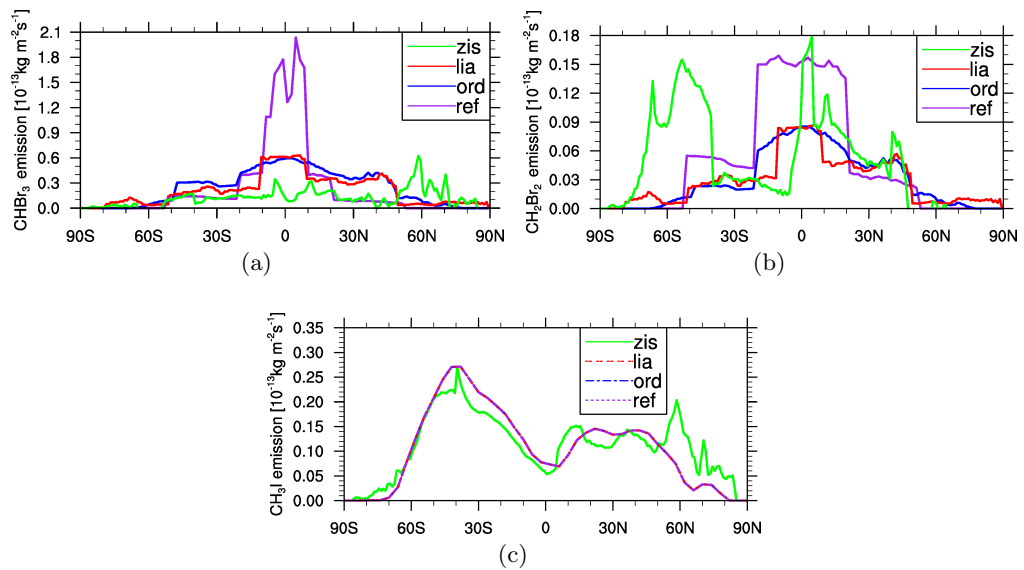


Figure 3.5: Zonally averaged global emission source strength (in $10^{-13}\text{kgm}^{-3}\text{s}^{-1}$) for (a) CHBr₃, (b) CH₂Br₂ and (c) CH₃I.

Note that emissions of the minor very short-lived bromocarbons CH_2ClBr , CHCl_2Br and CHClBr_2 remain the same for all simulations and are taken from Warwick et al. (2006) as no updated inventories for these substances were available.

Time-Slice Experiments

As the future development of VSLs emissions is highly uncertain the second set of simulations is targeted at investigating three VSLs scenarios under present/recent past and future climate conditions.

For this purpose, time-slice experiments representing the recent past (year 2000) and the future (year 2100) climate are carried out. Three VSLs emission scenarios for all brominated VSLs and methyl iodide are used for both, the year-2000 and the year-2100 time-slice experiments: a reference emission scenario (i.e. 1 x reference VSLs emissions), a No-VSLs scenario (0 x reference VSLs emissions and last but not least a 10xVSLs scenario (10 x reference VSLs emissions). There is no reliable data on the future development of VSLs emissions. The tenfold multiplied surface emissions enable to assess the impact of potentially increased surface emissions.

This set-up of experiments allows

- to specify the contribution of VSLs to past stratospheric ozone depletion,
- to analyse the effect of climate change on VSLs chemistry and transport with constant VSLs emissions,
- to investigate the impact of increased VSLs emissions particularly on stratospheric ozone with decreasing long-lived halogen concentrations, and
- to assess the sensitivity of stratospheric ozone and bromine to changes in VSLs emissions at the surface.

The time-slice simulations are free-running, i.e. no relaxation to meteorological reference data is applied. Here, SSTs and SICs are taken from the climate model HadGEM2 (Collins et al., 2011; Martin et al., 2011). Analogous to the transient simulations, species with uncertain emission fluxes are relaxed to prescribed mixing ratios by the submodel TNUDGE. The prescribed mixing ratios were taken from Meinshausen et al. (2011) using the RCP6.0 scenario as recommended by Eyring et al. (2013b).

Again, after preparatory simulations named *TS2000* and *TS2100*, correspondingly, the model is run in QCTM mode using the dynamics of the preparatory simulations. The QCTM simulations were carried out for 21 years, repeating the boundary conditions and emissions of the year 2000 and 2100. To ensure a sufficient spin-up of the free-running time-slice simulations only the last ten years of each run will be taken for the analyses. Due to the QCTM mode, differences between the year-2000 experiments only occur through changes in VSLs surface emissions. The same is true for the year-2100 experiments.

For this set of simulations the "reference VSLs emission scenario" is differently defined as for the previous transient simulations. *TS2000lia* and *TS2100lia* contain a combination of three VSLs inventories: CHBr_3 and CH_2Br_2 are used from Liang et al. (2010), minor brominated VSLs from Warwick et al. (2006) and CH_3I from Bell et al. (2002). Reasons for the combination of VSLs inventories will be discussed in Chapter 4. To avoid confusion with the previously transient reference simulation *ref*, the time-slice simulations with the newly defined reference VSLs scenario are labeled with suffix 'lia'.

For the 10xVSLs simulations *TS2000ten* and *TS2100ten* the new reference VSLs emissions were multiplied with a factor of 10. For the No-VSLs scenario emissions of all brominated VSLs were set to 0. The corresponding simulations are called *TS2000zero* and *TS2100zero*.

ESCiMo simulations

As previously mentioned, the reference simulations performed within this study are equivalent to the simulations within the ESCiMo initiative. The simulation *base* corresponds to the ESCiMo simulation *RC1SD-base-10*, a transient, nudged (SD for **S**pecified **D**ynamics) reference run from 1979 to 2013. The set-up of the transient free-running simulation *RC1-base-07* from 1950 to 2011 corresponds to the time-slice experiment *TS2000*.

A detailed description of the model version, submodels and boundary conditions can be found in Jöckel et al. (2016). An overview of the simulations carried out and used in this study is given in Table 3.3.

Table 3.3: Overview of conducted EMAC simulations.

name	run-mode	years	VSLs emissions
base	transient, nudged, coupled	2005-2012	CHBr ₃ , CH ₂ Br ₂ from Warwick et al. (2006), CH ₃ I from Bell et al. (2002)
ref	transient, nudged, QCTM	2005-2012	CHBr ₃ , CH ₂ Br ₂ from Warwick et al. (2006), CH ₃ I from Bell et al. (2002)
zis	transient, nudged, QCTM	2005-2012	CHBr ₃ , CH ₂ Br ₂ , CH ₃ I from Ziska et al. (2013)
ord	transient, nudged, QCTM	2005-2012	CHBr ₃ , CH ₂ Br ₂ from Ordóñez et al. (2012), CH ₃ I from Bell et al. (2002)
lia	transient, nudged, QCTM	2005-2012	CHBr ₃ , CH ₂ Br ₂ from Liang et al. (2010), CH ₃ I from Bell et al. (2002)
TS2000	time-slice, free-running, coupled	21 years	CHBr ₃ , CH ₂ Br ₂ from Liang et al. (2010), CH ₃ I from Bell et al. (2002)
TS2000ref	time-slice, free-running, QCTM	21 years	CHBr ₃ , CH ₂ Br ₂ from Liang et al. (2010), CH ₃ I from Bell et al. (2002)
TS2000ten	time-slice, free-running, QCTM	21 years	10 x CHBr ₃ , 10 x CH ₂ Br ₂ from Liang et al. (2010), 10 x CH ₃ I from Bell et al. (2002)
TS2000zero	time-slice, free-running, QCTM	21 years	no VSLs emissions
TS2100	time-slice, free-running, coupled	21 years	CHBr ₃ , CH ₂ Br ₂ from Liang et al. (2010), CH ₃ I from Bell et al. (2002)
TS2100ref	time-slice, free-running, QCTM	21 years	CHBr ₃ , CH ₂ Br ₂ from Liang et al. (2010), CH ₃ I from Bell et al. (2002)
TS2100ten	time-slice, free-running, QCTM	21 years	10 x CHBr ₃ , 10 x CH ₂ Br ₂ from Liang et al. (2010), 10 x CH ₃ I from Bell et al. (2002)
TS2100zero	time-slice, free-running, QCTM	21 years	no VSLs emissions
RC1-base-07	transient, free-running, coupled	1950-2011	CHBr ₃ , CH ₂ Br ₂ from Warwick et al. (2006), CH ₃ I from Bell et al. (2002)
RC1SD-base-10	transient, nudged, coupled	1979-2013	CHBr ₃ , CH ₂ Br ₂ from Warwick et al. (2006), CH ₃ I from Bell et al. (2002)

Chapter 4

Modelling selected VSLs, Br_y and Ozone

The chemistry-climate model EMAC has already been used in many investigations, showing in several studies to provide reliable results (e.g. Jöckel et al., 2006; Kerkweg et al., 2008; Righi et al., 2015; Jöckel et al., 2016; Löffler et al., 2016; Brinkop et al., 2016). Nevertheless, a short general model validation is conducted in the following section showing the general climate quantities in comparison to reanalysis and observational data. Section 4.2 then will focus on the representation of selected VSLs in EMAC when using four different emission inventories. In the last section of this chapter it will be investigated if the signal of changed VSLs surface emissions can be detected in the stratosphere.

4.1 General Model Validation

This section aims to illustrate the agreement of EMAC simulation results with ERA-Interim reanalysis or observational data and the general differences occurring through differing run modes, thus nudged vs. free running (i.e. *RC1SD-base-10* vs. *RC1-base-07*).

Results of the nudged simulation *RC1SD-base-10* conducted recently by Jöckel et al. (2016) and the corresponding simulation *base* of this study are statistically equal due to the same model configuration and boundary conditions. The same is true for the year 2000 of the free-running simulation *RC1-base-07* and the free-running time-slice simulation *TS2000*. Also statistically equal are the transient preparatory coupled simulations *base* and *TS2000* to their decoupled QCTM counterparts *ref* and *TS2000lia*. Uncertainties made by using the QCTM approach (see Section 3.3.1) can therefore be neglected. As there are no significant differences between the aforementioned simulations (not shown) results from the nudged ESCiMo simulation *RC1SD-base-10* are also valid for *ref* and results from the free-running ESCiMo simulation *RC1-base-07* are

valid for *TS2000lia*.

EMAC is known to have a cold bias in the extratropical lowermost stratosphere which is probably induced by an overestimation of water vapour concentrations. In free-running simulations a warm bias can be seen in the Southern hemisphere (SH) polar stratosphere which is related to a too weak polar vortex and an underestimation of the ozone hole (Righi et al., 2015; Jöckel et al., 2016). A comparison of the free-running (*RC1-base-07*) and nudged (*RC1SD-base-10*) EMAC simulations with ERA-Interim re-analysis data (Dee et al., 2011) for the years 2000 to 2009 shows the temperature biases (see Figure 4.1). Smaller discrepancies occur when nudging the model by Newtonian relaxation (simulation *RC1SD-base-10*). Jöckel et al. (2016) illustrated, that the smallest differences to ERA-I data are achieved when not only the temperature pattern is nudged but also the global mean temperature. However, the nudging of the global mean temperature was not applied for the simulations in this study as this improvement only became clear when the simulations of this study were already running.

Observational data for the total ozone column are taken from the GOME-type total ozone – essential climate variable (GTO-ECV) data set that combines data from the satellite sensors GOME, SCIAMACHY and GOME-2 (Loyola et al., 2009; Loyola and Coldewey-Egbers, 2012). EMAC reproduces the seasonal pattern of the observation qualitatively well (see Figure 4.2): low ozone values in the tropics, maximum values during Northern hemisphere (NH) spring and minimum ozone values over Antarctica known as the ozone hole. Though, as previously mentioned, the ozone hole is significantly underestimated by ~ 100 DU in both, the free-running and the nudged simulation. In the SH mid latitudes, ozone values are larger than the observations (by ~ 25 DU). Righi et al. (2015) however pointed out that partly relatively large discrepancies between satellite born data sets exist.

In Figure 4.3 the EMAC simulations *RC1-base-07* and *RC1SD-base-10* are compared to the zonally averaged ozone profile from the SWOOSH (Stratospheric Water and OzOne Satellite Homogenized data set) data set (Davis et al., 2016). Measurements from several limb sounding and solar occultation satellites with various instruments were merged and homogenized by applying corrections to obtain a long-term and consistent data set. Note that the SWOOSH data is only available for heights above ~ 300 hPa but allows a comparison of the vertical distribution in the stratosphere. The free-running and the nudged simulation show in comparison to the SWOOSH O_3 values similar results: both simulations significantly overestimate the observations in the stratosphere over Antarctica by ~ 0.8 $\mu\text{mol/mol}$. This corresponds to $\sim 40\%$ in 50 hPa and $\sim 60\%$ in 100 hPa. Relative differences in ~ 10 hPa over Antarctica amount to $\sim 10\%$. Apart from these differences the model reproduces stratospheric ozone values relative well ($\leq 10\%$).

More comparisons of the EMAC simulations to observations can be found in Jöckel et al. (2016). A systematic validation of selected climate variables with EMAC simu-

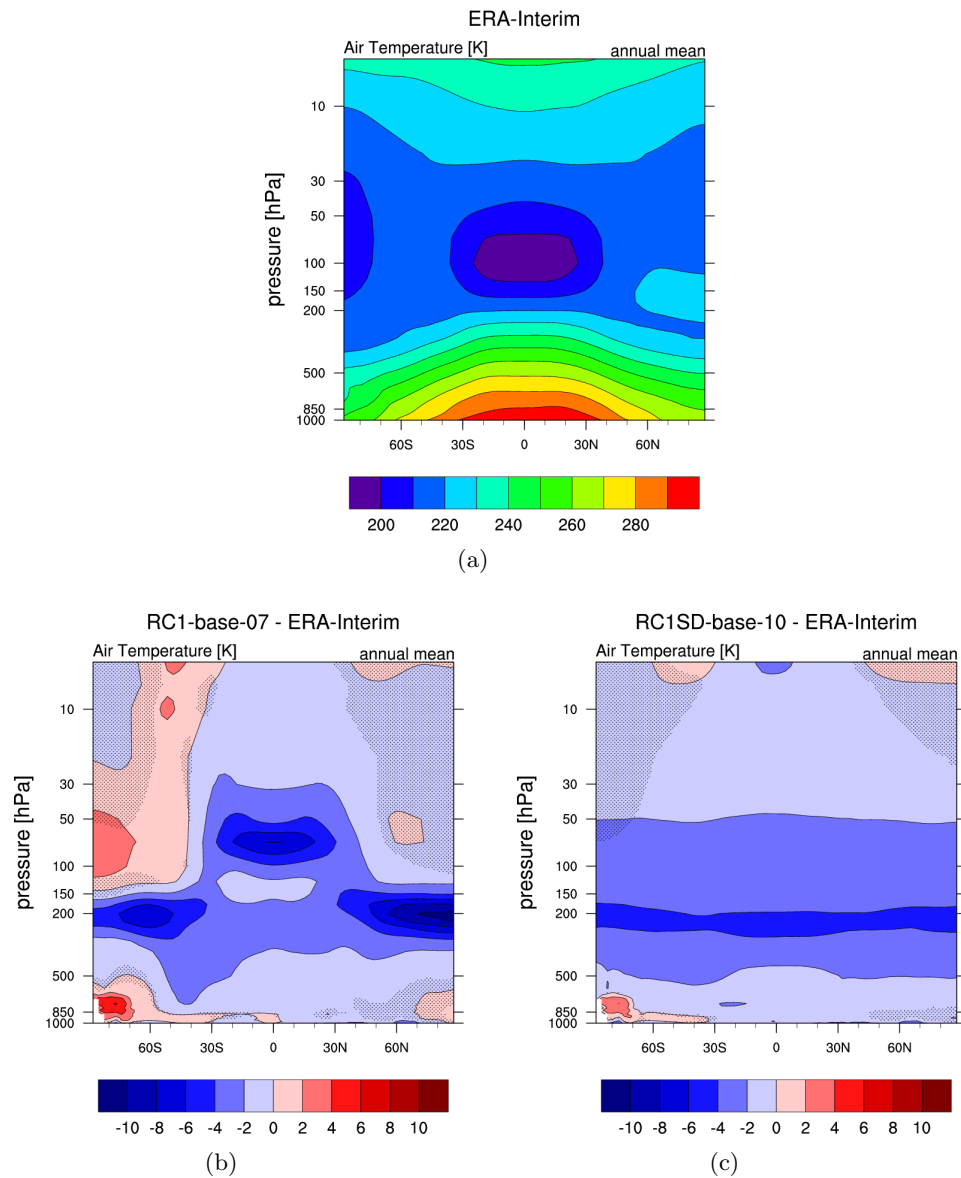


Figure 4.1: Annual mean (2000-2009) of zonally averaged temperature profile (in K) of a) ERA-Interim reanalysis data, b) differences between ERA-I and RC1-base-07 and c) differences between ERA-I and RC1SD-base-10. Differences that are not significant according to a t-test (95% confidence level) are shaded.

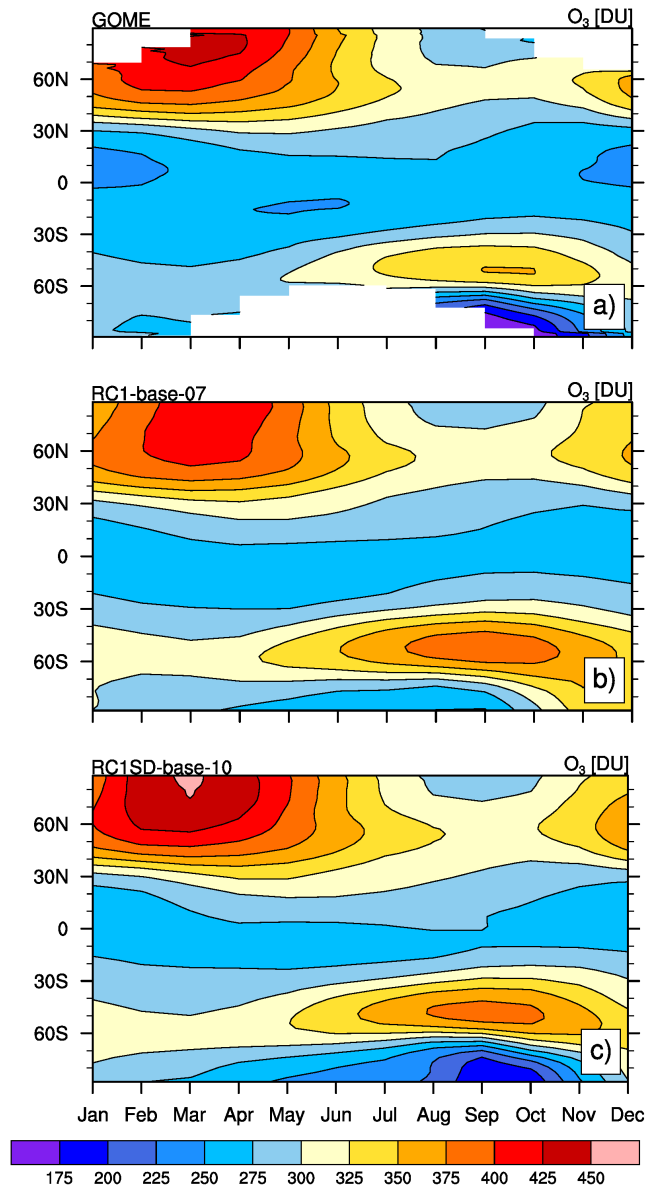


Figure 4.2: Climatology of the total ozone column (in DU) for the years 2000-2009. a) GOME observations b) EMAC simulation RC1-base-07 c) EMAC simulation RC1SD-base-10.

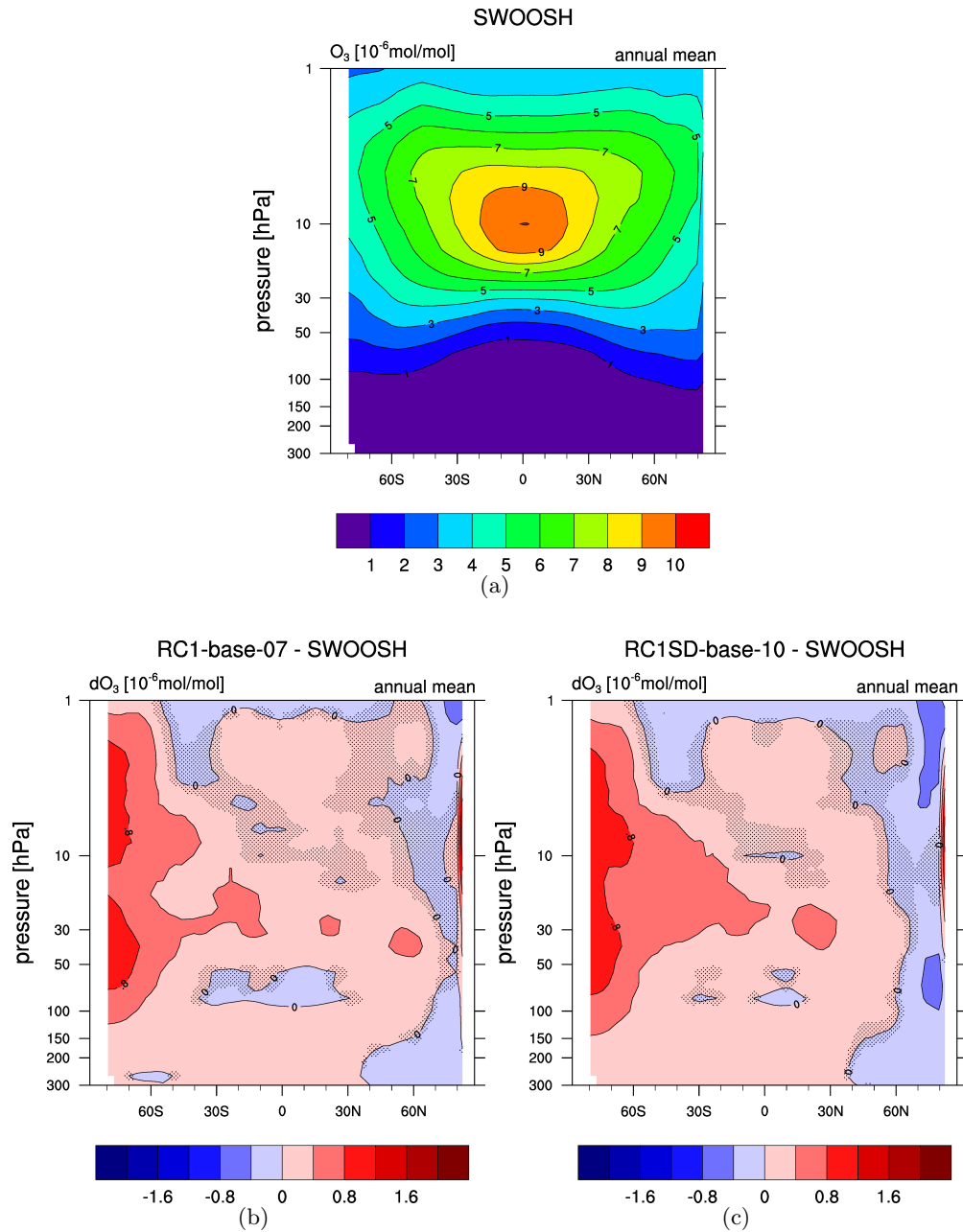


Figure 4.3: Annual mean (2000-2009) of zonally averaged ozone profile (in 10^{-6} mol/mol) of a) SWOOSH satellite data, b) differences between SWOOSH and RC1-base-07 and c) differences between SWOOSH and RC1SD-base-10. Differences that are not significant according to a t-test (95% confidence level) are shaded. Note, the limited pressure axis from 300 hPa to 1 hPa.

lations of various set-ups (i.e. free-running, nudged, QCTM) was conducted by Righi et al. (2015). The authors found only small differences that could be related to different set-ups. Therefore, the authors suggested the possibility to evaluate the overall model with shorter nudged simulations to avoid high temporal and computational effort related to free-running simulations. This approach is made in the following section for the evaluation of VSLS representation in EMAC.

4.2 Evaluating VSLS representation in EMAC

VSLS are characterised by generally low mixing ratios and strong local sources associated with strong oceanic activity (Carpenter and Liss, 2000; Quack and Wallace, 2003; Yokouchi et al., 2005; Leedham et al., 2013). To date there are only few measurements. Short lifetimes and the spatial variability make it hard to determine the global emission strength and distribution (Ziska et al., 2013). It is essential to apply realistic VSLS emissions to a chemistry-climate model to display realistic mixing ratios of atmospheric halogens that directly affect the radiatively active gas ozone. High uncertainties in global VSLS emissions lead to continuing uncertainties in the simulation of VSLS in global chemistry-climate models (Warwick et al., 2006; Liang et al., 2010; Pyle et al., 2011; Ordóñez et al., 2012; Ziska et al., 2013; Hossaini et al., 2013). To assess uncertainties related to prescribed surface emissions, four different VSLS emission inventories are applied to a set of four EMAC simulations (see Section 3.3.2). By comparing the results to observations and other model studies, it will be investigated how well EMAC is able to simulate the VSLS CHBr_3 , CH_2Br_2 , and CH_3I and related quantities like Br_y and O_3 . The emission inventory that leads to the best results in comparison to measurements will be selected for further simulations. Furthermore, it will be investigated if a modification of surface emissions, through an exchanged emission inventory, is detectable in stratospheric ozone or bromine mixing ratios.

4.2.1 EMAC versus Observations

In this section the four EMAC simulations with differing VSLS surface emissions will be compared to observations in order to determine i) how well VSLS are represented in EMAC, ii) which emission inventory is the most suitable in comparison to measurements and iii) if there are significant differences in stratospheric quantities when using different surface emissions. Note that Hossaini et al. (2013) also compared four VSLS emission inventories applied in a chemistry transport model (CTM). They also used the Liang2010, Ordóñez2012 and Ziska2013 emissions but an updated version of the Warwick2006 emissions. The comparison of EMAC model results with observations is similar to the study by Hossaini et al. (2013) who used a CTM.

Ground-based observations of VSLs

The ongoing global monitoring program of the National Oceanic and Atmospheric Administration's Earth System Research Laboratory (NOAA/ESRL) provides multi-annual surface observations of CHBr₃, CH₂Br₂ and CH₃I at globally distributed sites (<http://www.esrl.noaa.gov/gmd>; Montzka et al., 2003). Whole air samples were collected approximately weekly and analysed by gas chromatography/mass spectrometry (GC-MS) (Montzka et al., 2003). The model output of the four simulations with different VSLs input emissions was compared to NOAA/ESRL measurements at the sites shown in Table 4.1. Note, that site MLO on Hawaii is located at 3397m above sea level. The geographic distribution of the sites can be seen in Figure 4.4.

Table 4.1: NOAA/ESRL sampling sites.

Acronym	Name	lat	lon
ALT	Alert, Northwest Territories, Canada, USA	82.45°N	62.52°W
BRW	Barrow, Alaska, USA	71.32°N	156.60°W
MHD	Mace Head, County Galway, Ireland	53.33°N	9.90°W
LEF	Park Falls, Wisconsin, USA	45.93°N	90.27°W
NWR	Niwot Ridge, Colorado, USA	40.05°N	105.63°W
KUM	Cape Kumukahi, Hawaii, USA	19.52°N	154.82°W
MLO	Mauna Loa, Hawaii, USA	19.53°N	155.58°W
SMO	Tutuila, American Samoa	14.25°S	170.57°W
CGO	Cape Grim, Tasmania, Australia	40.68°S	144.68°E
PSA	Palmer Station, Antarctica	64.92°S	64.00°W
SPO	South Pole	89.98°S	24.80°W

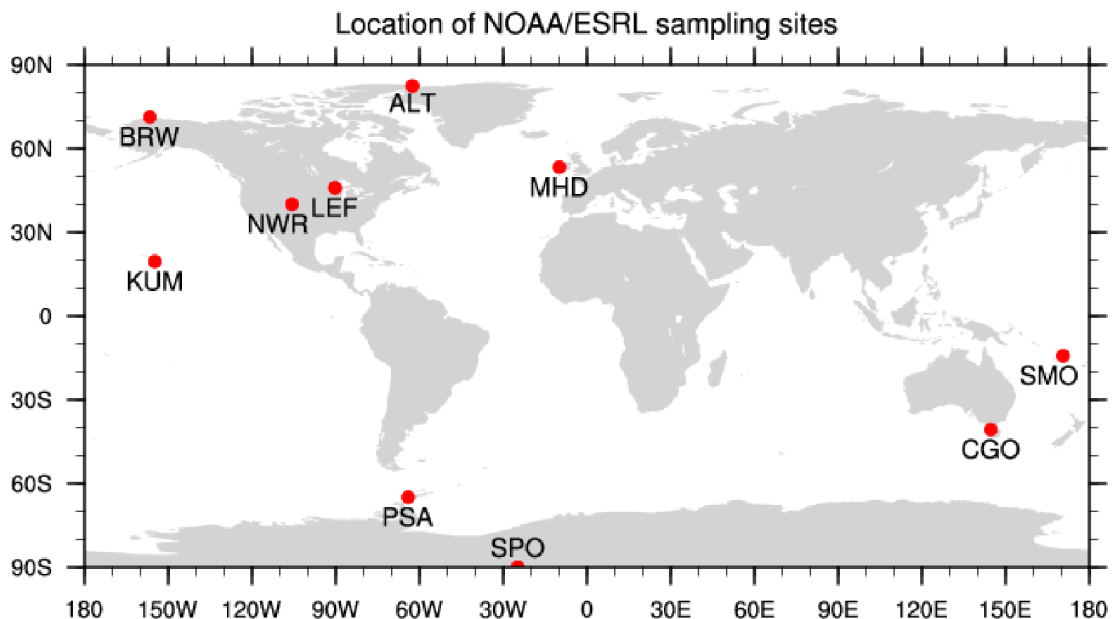


Figure 4.4: Location of the NOAA/ESRL ground-based sampling sites. Site MLO is omitted for clarity.

CHBr₃

Figure 4.5 shows a climatology of the modelled (coloured lines) and observed (black dots) CHBr₃ mixing ratio at 11 NOAA/ESRL sites, sorted from North to South. With the submodel s4d the EMAC data is sampled at the geographic location of each measurement site with a time resolution of 12 minutes. For each data set, model output and observations, the climatology is calculated over the years 2006 to 2011. This approach allows the determination of seasonal variations. Table 4.2 shows for each simulation the correlation coefficient (CO), the mean bias (MB) and the mean absolute percentage error (PE) to observations for selected zonal means. At the polar sites of the Northern hemisphere (ALT, BRW) the observations show a distinct seasonal cycle with elevated mixing ratios during NH winter (DJF) and lower values during the summer months (JJA). This seasonality is likely due to increased photochemical loss during NH summer and has also been observed by Yokouchi et al. (1996) at ALT. EMAC is generally able to reproduce the seasonal pattern at these sites, although only the Ordóñez2012 emissions prescribe a seasonality. The correlation coefficients (CO) between model and observation are ≥ 0.8 except for the simulation *zis* (see Table 4.2). Runs *ref*, *ord* and *lia* on average underestimate the observed values (mean bias -1.85, -1.02 and -0.6 pmol/mol, respectively) whereas *zis* significantly overestimates observed CHBr₃ particularly at ALT, leading to a MB of 1.14 pmol/mol. It was previously shown that Ziska2013 CHBr₃ emissions are larger at high Northern latitudes (Figure 3.5(a)). The relatively high standard deviation of *zis* indicates a higher year-to-year variability of CHBr₃ surface mixing ratios which may be caused by variable transport from the North Atlantic, a region with high emissions in the Ziska2013 inventory (see Figure 3.3). Run *lia* produces the smallest PE with 23%.

At NH midlatitude sites LEF and NWR the seasonal cycle in the observations is well reproduced by all simulations. However, the elevated summer values at MHD cannot be seen in *ref*, *ord* and *lia*, most probably in *zis*. Carpenter et al. (2005) showed that strong local biological sources at MHD overcompensate photochemical loss of CHBr₃ leading to a maximum in summer and minimum in winter. The localised sources are not captured by the emission inventories Warwick2006, Ordóñez2012 and Liang2010. Again, the Ziska2013 inventory prescribes comparatively high emissions in the North Atlantic region, in particular in coastal areas and therefore reproduces the seasonal cycle nearest. Averaged over the NH midlatitude sites LEF, NWR and MHD, the correlation is mainly due to the discrepancies at MHD for all simulations negative (≤ -0.5). Differences at MHD also lead to negative MBs for all simulations, though the magnitude at LEF and NWR is captured relatively well by the simulations. The smallest PE in this latitude range is achieved with the Ziska2013 emissions (23%).

At tropical sites (KUM, MLO, SMO) the seasonal cycle is less pronounced but correlation between observed and modelled CHBr₃ is relatively high (≥ 0.8) for all simulations. The absolute agreement between model and observation is dependent on

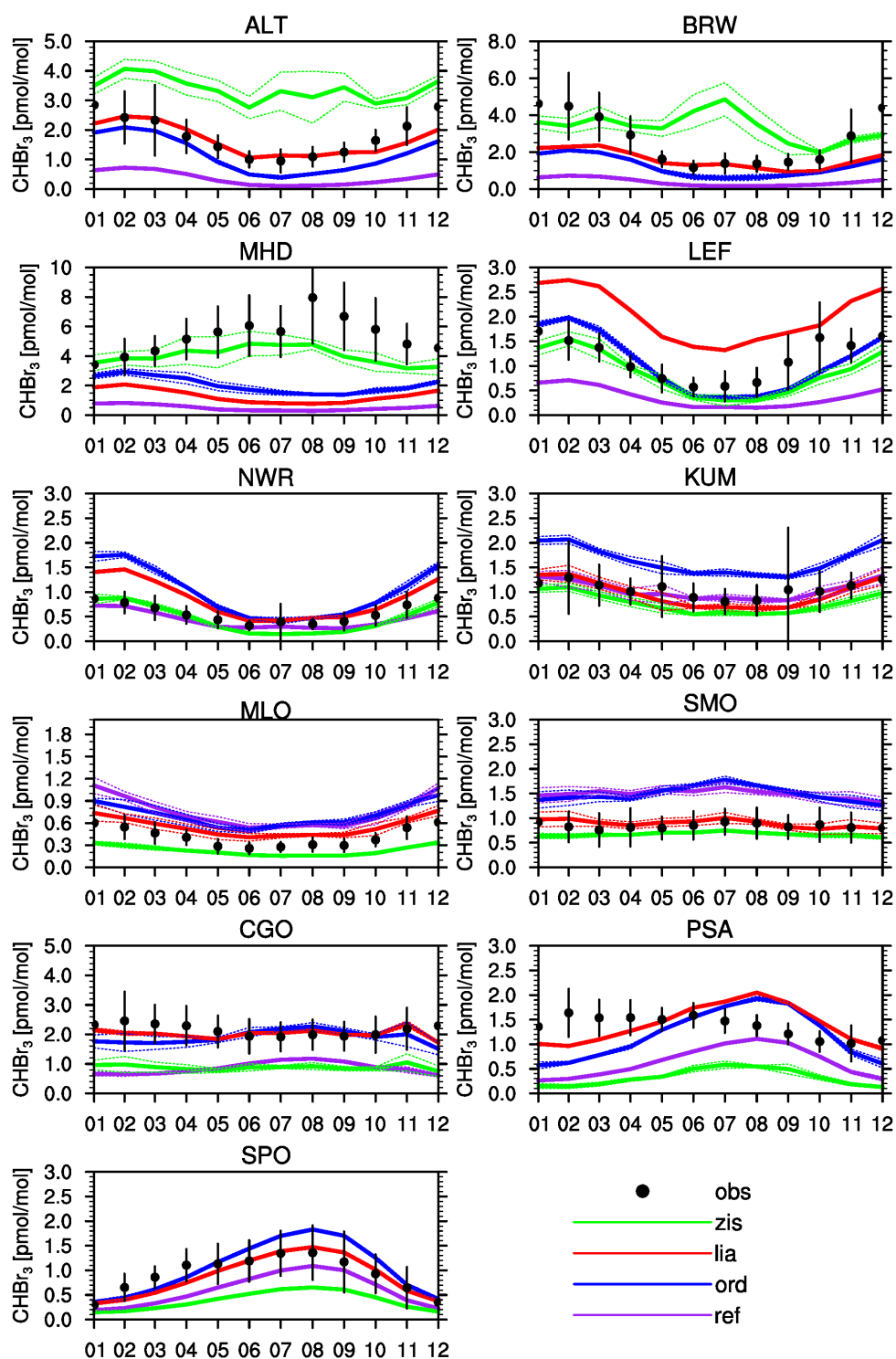


Figure 4.5: Climatology (2006-2011) of monthly mean CHBr_3 mixing ratios in pmol/mol observed at 11 NOAA/ESRL ground stations (black dots) in comparison to EMAC sensitivity simulations with different input emission inventories (coloured lines). Vertical bars and dashed lines denote \pm standard deviation.

the applied emission inventory: the highest mean bias (0.51 pmol/mol) for these stations is obtained in run *ord* that overestimates measured values at all sites. Simulation *ref* overestimates the observations with a MB of 0.32 pmol/mol. Run *zis* has a negative MB (−0.21 pmol/mol) and a PE of 28 %. *lia* performs relatively well with a small MB of 0.03 pmol/mol and a PE of 7 %.

Observations at the Southern hemisphere are sparse, for the midlatitudes only one site (CGO) is available. Here, all simulations underestimate observed values, particularly *ref* and *zis* (MB −1.29 pmol/mol and −1.26 pmol/mol, respectively). At this site mixing ratios of *ord* and *lia* agree reasonably (MB −0.25 pmol/mol and −0.13 pmol/mol).

At high SH latitudes observations from two sites (PSA, SPO) are available. Again, *ord* and *lia* produce the lowest discrepancies with MBs of ≤ 0.03 pmol/mol. At SPO the seasonal cycle can clearly be seen, with elevated mixing ratios during SH winter months (JJA). This seasonality is relatively well reproduced by all simulations.

On global average a better agreement between observed and modelled CHBr_3 values is definitely obtained with the Ordóñez2012 and Liang2010 emissions instead of the standard emissions by Warwick et al. (2006), when taking the here calculated metrics correlation, mean bias and mean absolute percentage error into account.

Averaged over all latitudes, observed values are significantly underestimated in *ref* (MB −0.98 pmol/mol). Simulation *zis* also underestimates measurements (MB −0.27 pmol/mol) and provides only a small correlation of 0.22. *ord* and *lia* show high correlation values (> 0.8) and a negative MB (−0.34 pmol/mol and −0.37 pmol/mol, respectively).

Considering the individual latitude bands, all simulations show deficits in reproducing the seasonal cycle at mid latitude sites leading to low or negative correlation values. It is possible, that regional sources are not resolved by the emission inventories leading to shifted patterns in the simulations.

ref underestimates measurements in the extratropics and overestimates the measurements in the tropics. Except for the NH polar region *zis* underestimates the observations at all latitude bands. Runs *ord* and *lia* also tend to underestimate the observations in the extratropics but to a smaller extent. In the tropics, which is suggested to be the most important region for the convective upward transport of VSLs into the stratosphere, run *lia* shows only small discrepancies to measured values. Therefore, the Liang2010 inventory is considered in this study as the most appropriate for the simulation of CHBr_3 based on these ground based measurements.

CH_2Br_2

Analogous to CHBr_3 , observations of CH_2Br_2 are compared to the four EMAC simulations at 11 NOAA/ESRL sites. Again, a 12-months-climatology was calculated from the time period 2006 to 2011 for each site (Figure 4.6). Differences between the inven-

Table 4.2: Calculated correlation (CO), mean bias (MB) and mean absolute percentage error (PE) between NOAA/ESRL observed surface CHBr₃ and analogous fields from EMAC runs *ref*, *zis*, *ord* and *lia*. 12-months-climatology from the time period 2006-2011.

lat	ref			zis			ord			lia		
	CO	MB	PE									
60N-90N	0.85	-1.85	84	0.20	1.14	87	0.87	-1.02	46	0.83	-0.6	23
60N-30N	-0.63	-1.91	80	-0.58	-0.57	23	-0.64	-0.98	41	-0.57	-0.95	39
30N-30S	0.86	0.32	42	0.86	-0.21	28	0.84	0.51	67	0.86	0.03	7
30S-60S	-0.84	-1.29	59	0.19	-1.26	59	-0.75	-0.25	17	-0.04	-0.13	10
60S-90S	0.61	-0.53	48	0.66	-0.79	70	0.62	-0.03	30	0.65	-0.01	20
global	0.75	-0.98	59	0.22	-0.27	17	0.82	-0.34	21	0.82	-0.37	23

tories are for CH₂Br₂ less distinct compared to CHBr₃ emissions (see Table 3.2). The global source strength of the Warwick2006 inventory is significantly larger compared to the other three inventories. While Liang2010 and Ordóñez2012 emissions are similarly distributed over the latitudes, Warwick2006 emissions are clearly higher in the tropics and Ziska2013 emissions are particularly elevated in SH mid and high latitudes (see Figure 3.5(b)). CH₂Br₂ has a lifetime of ~ 120 days at the surface and is less variable in space compared to CHBr₃ with a lifetime of only ~ 26 days (Law et al., 2007). The observations show mixing ratios of ~ 1 pmol/mol. At NH polar sites ALT and BRW all simulation show a seasonal cycle with correlation coefficients of ≥ 0.86 . All simulations underestimate the measured mixing ratios which is consistent with very small surface emissions in the Northern polar latitudes (see Figure 3.5(b)). The lowest discrepancies are achieved in *ref* and *lia* with a MB of -0.21 pmol/mol and -0.26 pmol/mol, respectively and PEs of $< 30\%$. With emissions from Ziska et al. (2013) the difference to the observations is at these sites the most distinct (MB 0.61 pmol/mol, PE $< 60\%$).

As for CHBr₃, elevated mixing ratios during NH summer months at MHD are not reproduced by the model probably due to strong local sources that are not resolved in the inventories. At the other two NH midlatitude sites MHD and LEF, model and observation are in good agreement considering the seasonal cycle. Averaged over these sites, CO is > 0.8 except for *zis* with a CO of 0.72 . Again, the model underestimates the observed values with *ref* and *zis* showing the smallest discrepancies (MB -0.24 pmol/mol and MB -0.29 pmol/mol, respectively). Simulations *ord* and *lia* provide similar results due to a similar source strength (see Figure 3.5(b) with a MB of -0.37 pmol/mol and -0.39 pmol/mol, respectively).

At tropical sites KUM, MLO and SMO the seasonal cycle is not very pronounced. *ref*, *ord* and *lia* show high correlation values of ≥ 0.88 whereas *zis* seems to be out of phase with a CO of 0.02 . Moreover, *zis* and *ref* overestimate observed mixing ratios (MB 0.66 pmol/mol and 0.28 pmol/mol). *ord* and *lia* provide good agreement with the measurements (MB 0.02 pmol/mol and -0.13 pmol/mol). This is consistent with the applied input emissions that are in *zis* and *ref* significantly larger in this latitude range

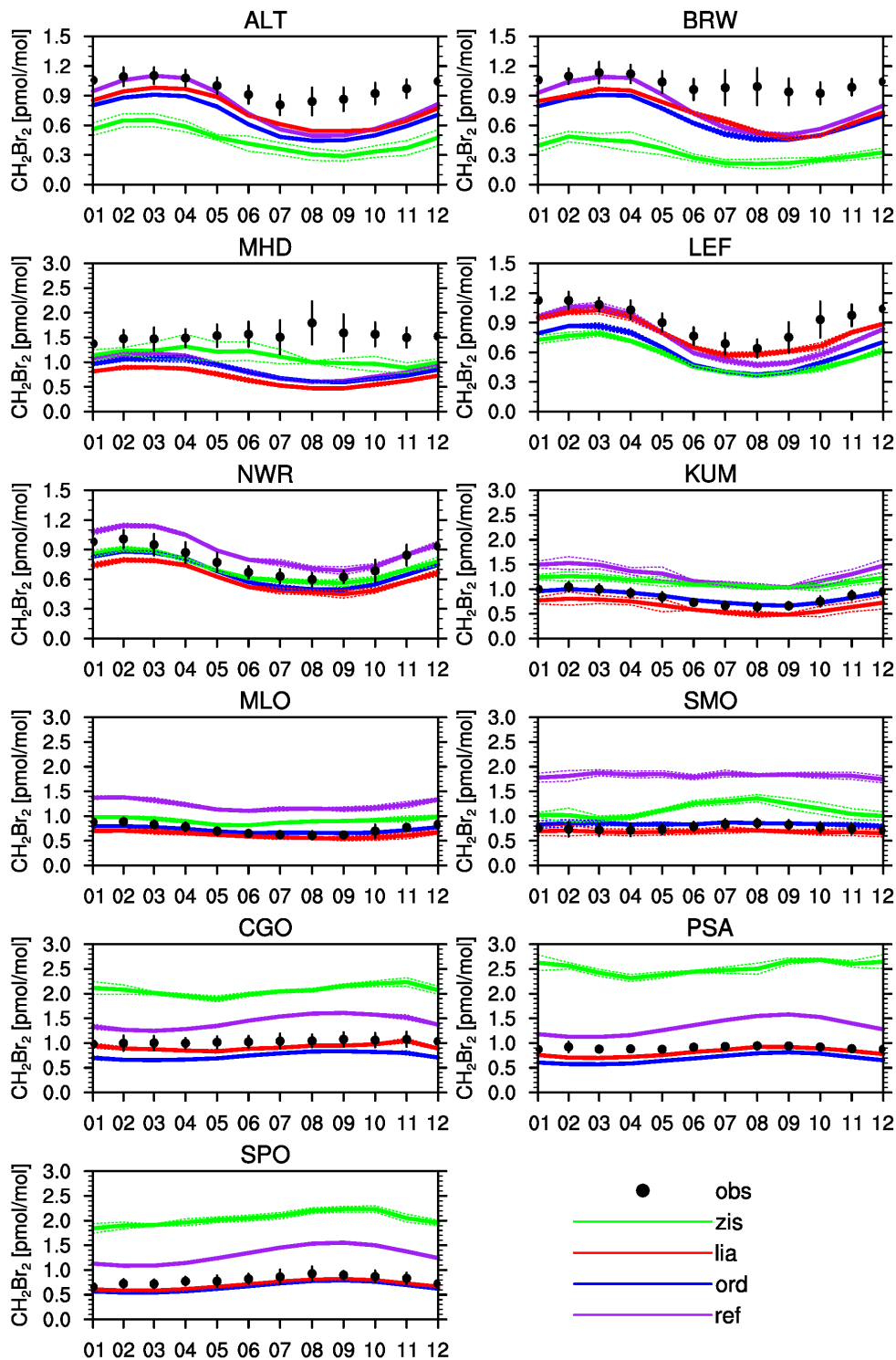


Figure 4.6: Climatology (2006-2011) of monthly mean CH_2Br_2 mixing ratios in pmol/mol observed at 11 NOAA/ESRL ground stations (black dots) in comparison to EMAC sensitivity simulations with different input emission inventories (coloured lines). Vertical bars and dashed lines denote \pm standard deviation.

than in *ord* and *lia* (Figure 3.5(b)).

The same pattern can be seen for the SH midlatitude site CGO: *ref* and particularly *zis* overestimate measured CH₂Br₂ values with a MB of 0.40 pmol/mol and 1.04 pmol/mol, respectively. However, *ord* and *lia* underestimate the measurements (MB -0.29 pmol/mol and -0.11 pmol/mol). Here, too, the source strength is in the Warwick2006 (*ref*) and Ziska2013 inventory notably larger than for the other two inventories (see Figure 3.5(b)). *lia* shows here small absolute differences (PE 11 %) to the observations but the pattern of the small seasonal variation seems not to be captured by the model (CO 0.58).

At the SH polar sites PSA and SPO similar results are obtained. The seasonal variation is reproduced in *ref*, *ord* and *lia* relatively well (CO \geq 0.84). *zis* shows a smaller correlation of 0.64. *ref* and especially *zis* overestimate measured CH₂Br₂ values significantly (MB 0.47 pmol/mol and 1.43 pmol/mol), *zis* has a PE of 169 %. *ord* and *lia* slightly underestimate the measurements (MB -0.18 pmol/mol and -0.10 pmol/mol) with PEs of \leq 22 %.

On global average all simulations show high correlation values (\geq 0.84) and relatively small absolute differences (PE \leq 26 %). However, taking the individual performance at the latitude bands into account *ref* and *zis* showed partly large discrepancies to the observations. Though *ref* provides at all latitude ranges high correlation values, the absolute values are often not well reproduced and especially in the tropics and in the Southern hemisphere overestimated. *zis* is at most sites not able to reproduce the pattern of the seasonal cycle and shows lower correlation values than the other simulations. Measured values at SH latitudes are significantly overestimated. *ord* and *lia* provide similar results due to similar emissions in the inventories (see Figure 3.5(b)). With both inventories EMAC is able to simulate the seasonal cycle relatively well with high correlation values of \sim 0.8 although only a seasonality was prescribed in the Ordonez2012 emissions. Both simulations tend to underestimate the measurements. However, in the tropics, an important region for upward transport of VSLs, *ord* and *lia* show only small discrepancies to the observations. In the Southern hemisphere, *lia* achieves slightly better results than *ord* when considering MB and PE, therefore the Liang2010 CH₂Br₂ emissions are depicted as the most suitable emissions.

CH₃I

For CH₃I only two inventories were available: the emissions by Ziska et al. (2013) and Bell et al. (2002). In *ref*, *ord* and *lia* the EMAC "standard" CH₃I emissions by Bell et al. (2002) are applied. *zis* uses the more recent CH₃I emissions by Ziska et al. (2013). Analogous to CHBr₃ and CH₂Br₂, the EMAC simulations with the two available emission inventories are compared to NOAA/ESRL observations (Figure 4.7). The corresponding correlation coefficients and error metrics can be seen in Table 4.4. Note, that only results of *ref* and *zis* are shown as *ord* and *lia* yield to equal results

Table 4.3: Calculated correlation (CO), mean bias (MB) and mean absolute percentage error (PE) between NOAA/ESRL observed surface CH_2Br_2 and analogous fields from EMAC runs *ref*, *zis*, *ord* and *lia*. 12-months-climatology from the time period 2006-2011.

lat	ref			zis			ord			lia		
	CO	MB	PE	CO	MB	PE	CO	MB	PE	CO	MB	PE
60N-90N	0.89	-0.21	23	0.89	-0.61	61	0.89	-0.33	34	0.86	-0.26	27
60N-30N	0.81	-0.24	23	0.72	-0.29	27	0.81	-0.37	35	0.83	-0.39	36
30N-30S	0.90	0.66	85	0.44	0.36	46	0.88	0.02	3	0.88	-0.13	17
30S-60S	0.80	0.40	39	0.54	1.04	101	0.80	-0.29	28	0.58	-0.11	11
60S-90S	0.84	0.47	55	0.64	1.43	169	0.83	-0.18	22	0.83	-0.10	12
global	0.86	0.20	21	0.84	0.24	26	0.84	-0.22	23	0.84	-0.22	23

as *ref* due to the same CH_3I surface emissions. Observed mixing ratios of CH_3I are

Table 4.4: Calculated correlation (CO), mean bias (MB) and mean absolute percentage error (PE) between NOAA/ESRL observed surface CH_3I and analogous fields from EMAC runs *ref* and *zis*. 12-months-climatology from the time period 2006-2011.

lat	ref/ord/lia			zis		
	CO	MB	PE	CO	MB	PE
60N-90N	0.15	0.17	63	0.50	1.38	470
30N-60N	0.35	0.09	34	0.38	0.97	230
30N-30S	0.67	-0.16	26	0.32	-0.2	33
30S-60S	-0.00	0.78	161	0.19	0.49	101
60S-90S	0.05	0.30	169	0.77	0.69	267
global	0.75	0.14	31	0.65	0.63	143

generally ≤ 1 pmol/mol. Due to a very short lifetime of only several days atmospheric abundances vary significantly in space and time. A clear seasonal cycle is not obvious from the measured data.

In the NH polar region (ALT, BRW) both simulations are not able to simulate the seasonal pattern. *ref* shows only a CO of 0.15 and *zis* a CO of 0.50. Simulation *zis* overestimates measured mixing ratios significantly (MB 1.38 pmol/mol, PE 470 %). Results from *ref* agree better with a MB of 0.16 pmol/mol (PE 63 %). These results are consistent as the CH_3I input emissions of the Ziska2013 inventory are significantly larger than the Bell2002 emissions in this latitude range (see Figure 3.5(c)).

At the NH midlatitude sites (MDH, LEF, NWR), *zis* shows a positive MB of 0.97 pmol/mol and a PE of 230 %. Too high mixing ratios are particularly at MHD obvious. The discrepancies between observations and *ref* are clearly smaller (MB 0.09 pmol/mol, PE 34 %). Correlation coefficients are for both simulations relatively small (≤ 0.38).

Considering the absolute values at the tropical sites (KUM, MLO, SMO) the simulations produce similar results with PEs of ≤ 33 %. The correlation of 0.67 is in *ref* clearly higher than in *zis* with a CO of 0.32.

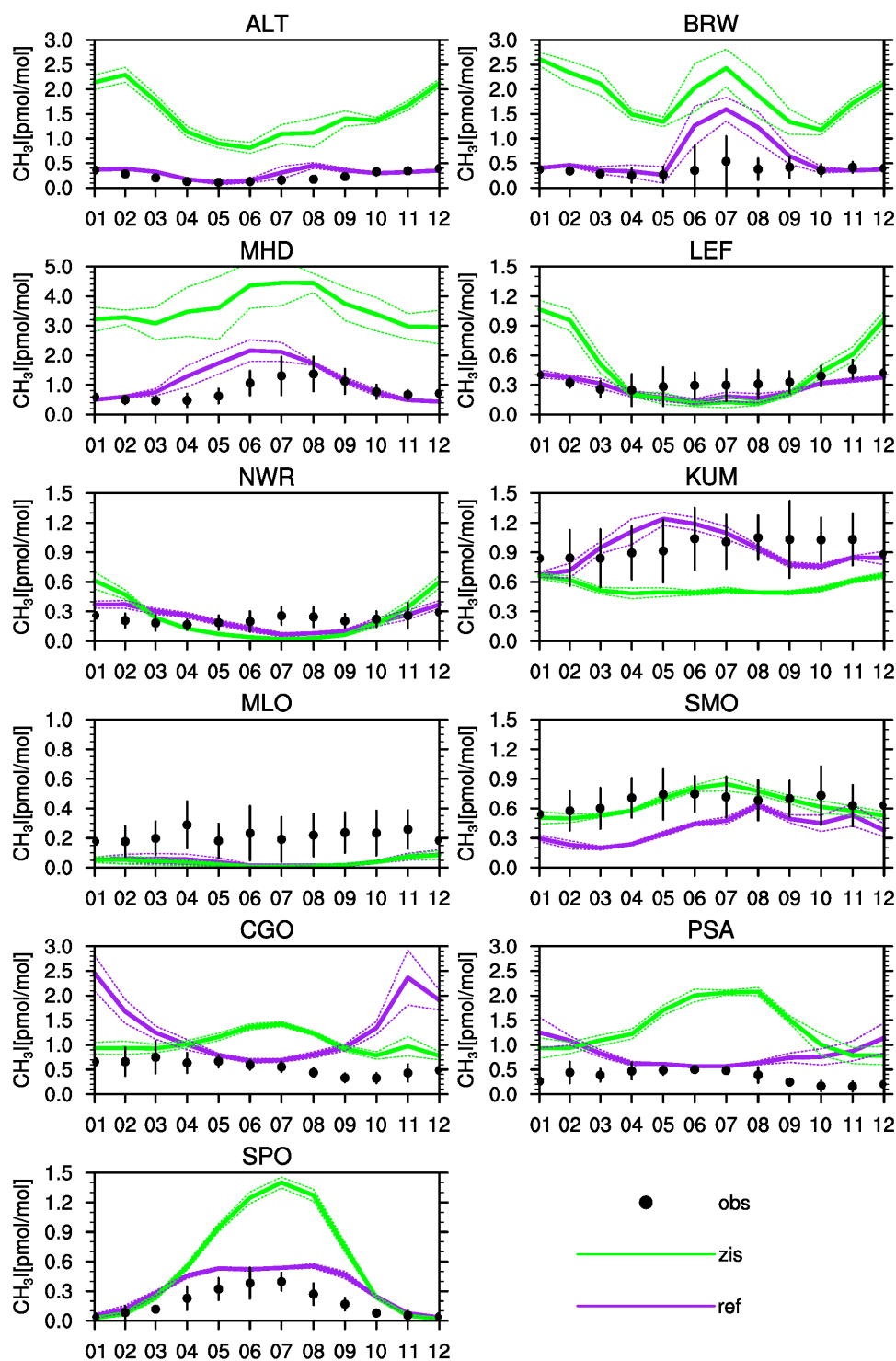


Figure 4.7: Climatology (2006-2011) of monthly mean CH_3I mixing ratios in pmol/mol observed at 11 NOAA/ESRL ground stations (black dots) in comparison to EMAC sensitivity simulations with different input emission inventories (coloured lines). Vertical bars and dashed lines denote \pm standard deviation.

At CGO, the SH midlatitude site, both simulation cannot reproduce the seasonal variations with correlation values of 0.19 in *zis* and 0.00 in *ref*. Both simulations overestimate the observed CH₃I mixing ratios (PE > 100%).

At the SH polar sites PSA *ref* shows elevated mixing ratios during SH summer (December-February) that cannot be seen in the observations. Averaged over both SH polar sites (PSA, SPO) only a CO of 0.05 is achieved with results from *ref*. The seasonal cycle with maximum values in SH winter (June-August) is better simulated in *zis* (CO 0.77). However, both simulations overestimate the observations significantly. MB in *ref* is 0.30 pmol/mol and in *zis* 0.69 pmol/mol which corresponds to PEs of 169% and 267%, respectively.

Averaged over all latitudes *ref* shows a relatively large CO (0.75) and only a small positive MB (0.14 pmol/mol). The correlation for *zis* is 0.65 and the MB amounts 0.63 pmol/mol. However, considering the results for the individual latitude bands it was obvious that with both emission inventories there remain partly large discrepancies to the measured mixing ratios. The model was often not able to reproduce the seasonal pattern of the observations. With the exception of the tropics both simulations overestimated the observed values in all latitudes, particularly in *zis* where the more recent emissions by Ziska et al. (2013) were used. Thus, based on the comparison to the NOAA/ESRL ground-based observations, the “standard” CH₃I emissions by Bell et al. (2002) (applied in *ref*) are chosen for further simulations.

Aircraft Observations of VSLS

To estimate the amount of VSLS entering the stratosphere it is important to evaluate mixing ratios in the free troposphere. Moreover, in several model studies the tropical Western Pacific region has been shown to be an area where relatively high abundances of VSLS occur and rapid transport to higher altitudes makes injection into the stratosphere efficient (e.g. Aschmann et al., 2009; Tegtmeier et al., 2015). However, aircraft observations in the tropical Western Pacific region are still limited. Modelled VSLS surface mixing ratios in this region show significant differences, particularly for CHBr₃. Figure 4.8 shows the CHBr₃ mixing ratios in the lowest model layer in November and December 2011 in the four EMAC simulations *ref*, *zis*, *ord* and *lia* that used each a different VSLS inventory. The large discrepancies between the simulations in this region again highlight the importance to compare the model results with observations in order to choose the most suitable and realistic emission inventory for further EMAC simulations.

The aircraft campaign of the EU project SHIVA (Stratospheric Ozone: Halogen Impacts in a Varying Atmosphere) was located in the tropical Western Pacific region shown in Figure 4.8. It was based at Miri, on Malaysian Borneo and took place in November and December 2011. An overview of the SHIVA activities is given at the project homepage shiva.iup.uni-heidelberg.de. During 14 flights of the DLR research

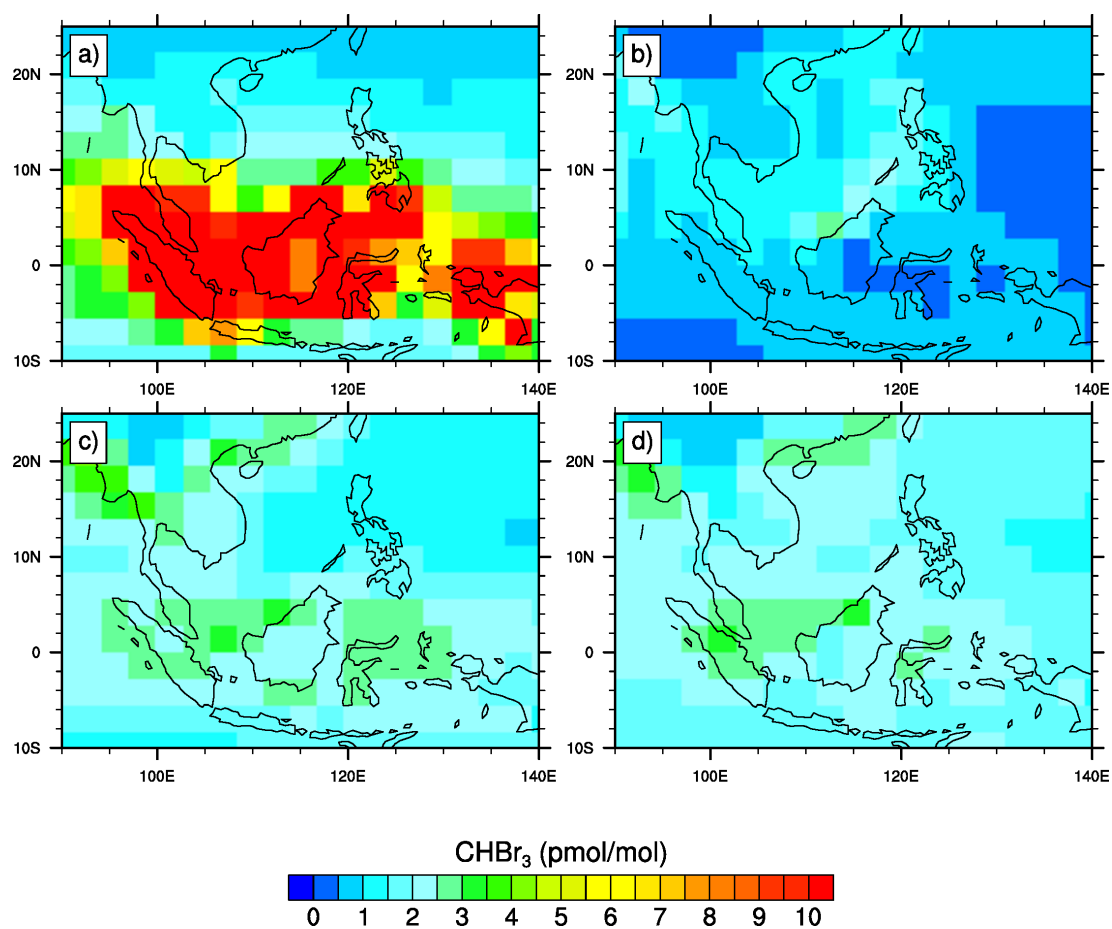


Figure 4.8: November-December mean of $CHBr_3$ surface mixing ratio (pmol/mol) in the tropical West Pacific region for EMAC simulations (a) ref (b) zis (c) ord, and (d) lia.

aircraft Falcon measurements of very-short lived halocarbons and ozone were retrieved up to altitudes of about 200 hPa. VLSL were measured with an in-situ GC/MS system called GHOST-MS (Gas chromatograph for the Observation of Tracers - coupled with a Mass Spectrometer) by a group of the Goethe University of Frankfurt. Another group from the University of East Anglia collected whole air samples (WASP) and analysed them using GC/MS (Sala et al., 2014). Ozone measurements were conducted with a modified Ozone Analysator by a group of the DLR (H. Schlager, pers. communication).

CHBr₃

Figure 4.9 shows CHBr₃ observations from two instruments during 14 SHIVA flights compared to the four EMAC simulations *ref*, *zis*, *ord* and *lia* with different surface emissions for the VLSL CHBr₃, CH₂Br₂ and CH₃I. The EMAC data is sampled on the flight track in a temporal resolution of ~ 12 min. During most of the flights the observations show CHBr₃ mixing ratios of ≤ 2 pmol/mol. In general, the agreement between observations and model is highly dependent on the applied emission inventory. The simulations *ord*, *lia* and *zis* reproduce the order of magnitude and the general pattern over time (and altitude) well. *ref*, on the contrary, overestimates the measured values up to a factor of 6, especially in low altitudes. EMAC reproduces the observed CHBr₃ mixing ratios particularly well when using the Ziska2013 emissions. The bottom-up emissions of the Ziska2013 inventory were derived from surface measurements, also considering data from a measurement campaign that took place in this region (namely the Trans-Brom campaign; Krüger and Quack, 2013). When applying the Ordonez2012 and Liang2010 emissions observed values are overestimated by EMAC. An exception is flight 20111123a where observations show elevated mixing ratios in the planetary boundary layer (PBL) up to almost 4 pmol/mol. Here, higher emissions in *lia* and *ord* capture the observed values better than *zis*. The same is true for flights 20111211a and 20111211b in low altitudes. During the latter two flights convective outflow was sampled explaining still relatively high mixing ratios in ~ 300 hPa. This localised convective effect is not reproduced by the model that uses a parametrization for convection.

The comparison with the aircraft observations shows again, that EMAC significantly overestimates the measurements by several orders of magnitude when using the “reference” CHBr₃ emissions from Warwick et al. (2006). Results from *ord* and *lia* are very similar as the emission strength in the inventories is similarly prescribed (see Figure 3.5(a)). With both, the Ordonez2012 and Liang2010 emissions, EMAC overestimates the observed CHBr₃ values by < 1 pmol/mol in several flights. The agreement between measurements and the simulations *ord* and *lia* is relatively good for flights where the PBL or convective outflow was sampled, thus where elevated mixing ratios occur. The small source strength in the Ziska2013 emissions leads to small discrepancies between *zis* and the observations (> 0.5 pmol/mol). Only in high altitudes and in regions where convective outflow was sampled *zis* underestimates the observed values.

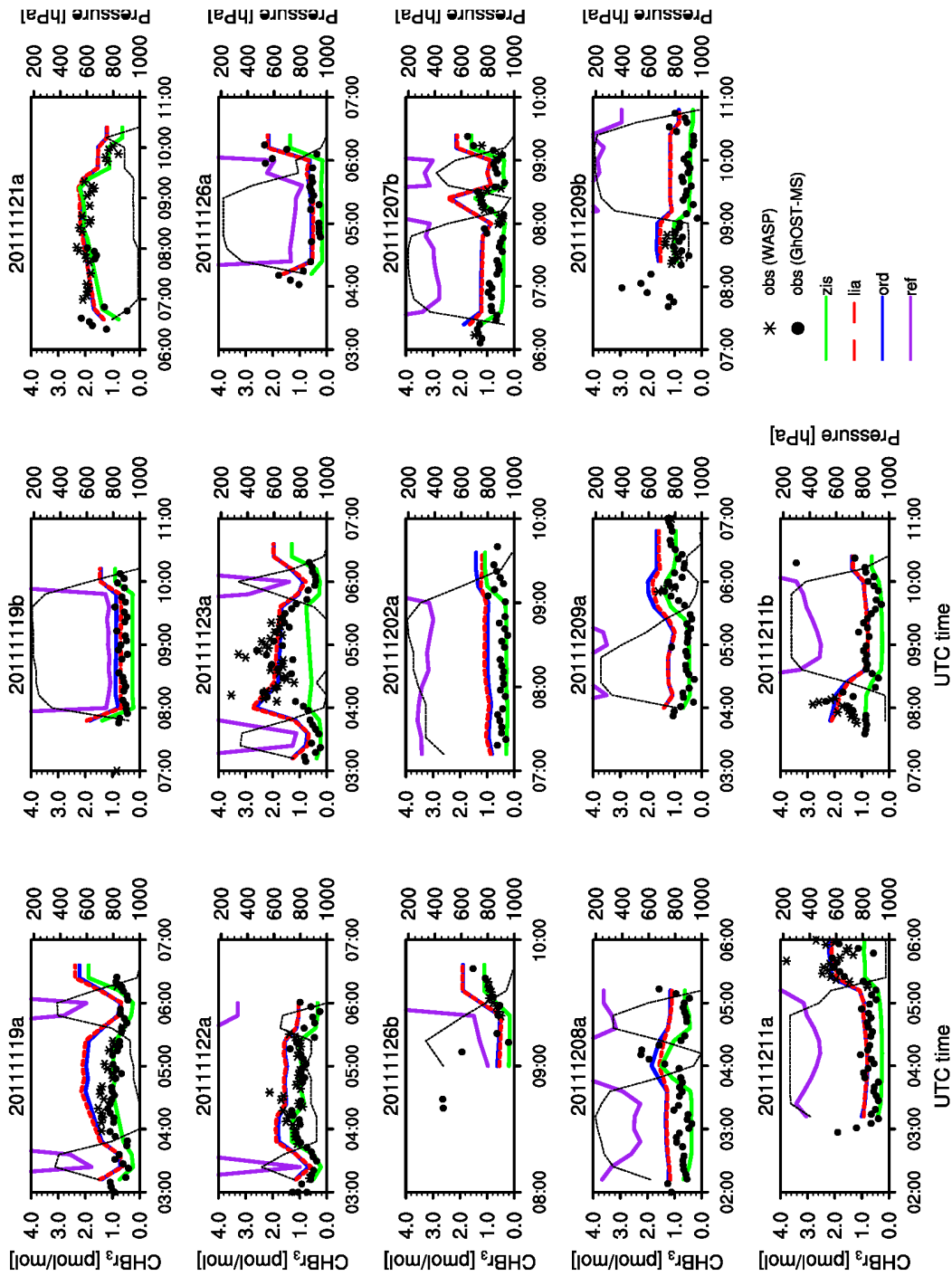


Figure 4.9: Observations of CHBr₃ (in pmol/mol) from 14 flights of the SHIVA campaign in comparison to four EMAC runs sampled on flight track. Black dots denote the observations, coloured lines show the EMAC runs with different VSLs emission inventories (purple: ref; blue: ord; red: lia; green: zis). The black dashed line shows the flight altitude in hPa.

CH₂Br₂

Observed and modelled CH₂Br₂ mixing ratios during 14 SHIVA flights are shown in Figure 4.10. Observed mixing ratios of CH₂Br₂ typically lie in the range (0.5–1.5) pmol/mol and show only a small vertical gradient probably due to the longer lifetime of ~ 120 days. As for CH₂Br₂ the source strengths of the inventories is more constrained (see Table 3.2) the discrepancies between the simulations are smaller than for CHBr₃. When applying the “reference” emissions by Warwick et al. (2006) EMAC overestimates measured values significantly (≥ 0.5 ppt). Simulation *zis* also overestimates the observations during most of the flights although less than *ref* (≤ 0.5 pmol/mol). As for CHBr₃, *lia* and *ord* show very similar results and reproduce measured mixing ratios relatively well. Deviations from measured values occur when mixing ratios are probably influenced by local emissions that are not resolved by the inventories. That is for instance the case for the flights 20111208a and 20111211a where outflow from deep convection was sampled.

The comparison of the CH₂Br₂ observations during the SHIVA flights with the EMAC simulations confirms previous results: The “reference” emissions from Warwick et al. (2006) lead to a significant overestimation of the observed mixing ratios. Here, *lia* and *ord* provided good agreement with the measurements. Simulation *zis* overestimated the measured values which is consistent to a stronger source in the Ziska2013 emissions compared to the Ordonez2012 and Liang2010 emissions (see Table 3.2).

CH₃I

CH₃I is suggested to have only a local lifetime of ~ 7 days (Montzka et al., 2011) and is therefore highly variable in space and time. Observations during the SHIVA flights (Figure 4.11) show a distinct vertical gradient and mixing ratios ≤ 1 pmol/mol. As mentioned before, only two inventories were available for CH₃I. Thus, *ref*, *lia* and *ord* using the “reference” emissions from Bell et al. (2002) all produce the same results.

EMAC is able to reproduce the general pattern of CH₃I with higher surface mixing ratios and decreasing values with increasing altitude. However, with both inventories, the model underestimates the observations up to 0.5 pmol/mol. This seems to be especially the case when convective outflow was sampled (e.g. flights 20111119b, 20111211b) but also in low altitudes (e.g. flights 20111119a, 20111123a). Differences between the simulations are small compared to the discrepancies to the observations. All this indicates that the source strength of the inventories is too small. More observations of CH₃I are necessary to improve the emission inventories and the representation in EMAC. As the new emission inventory in *zis* provides no clear improvement the “standard” emissions by Bell et al. (2002) will be used for further simulations.

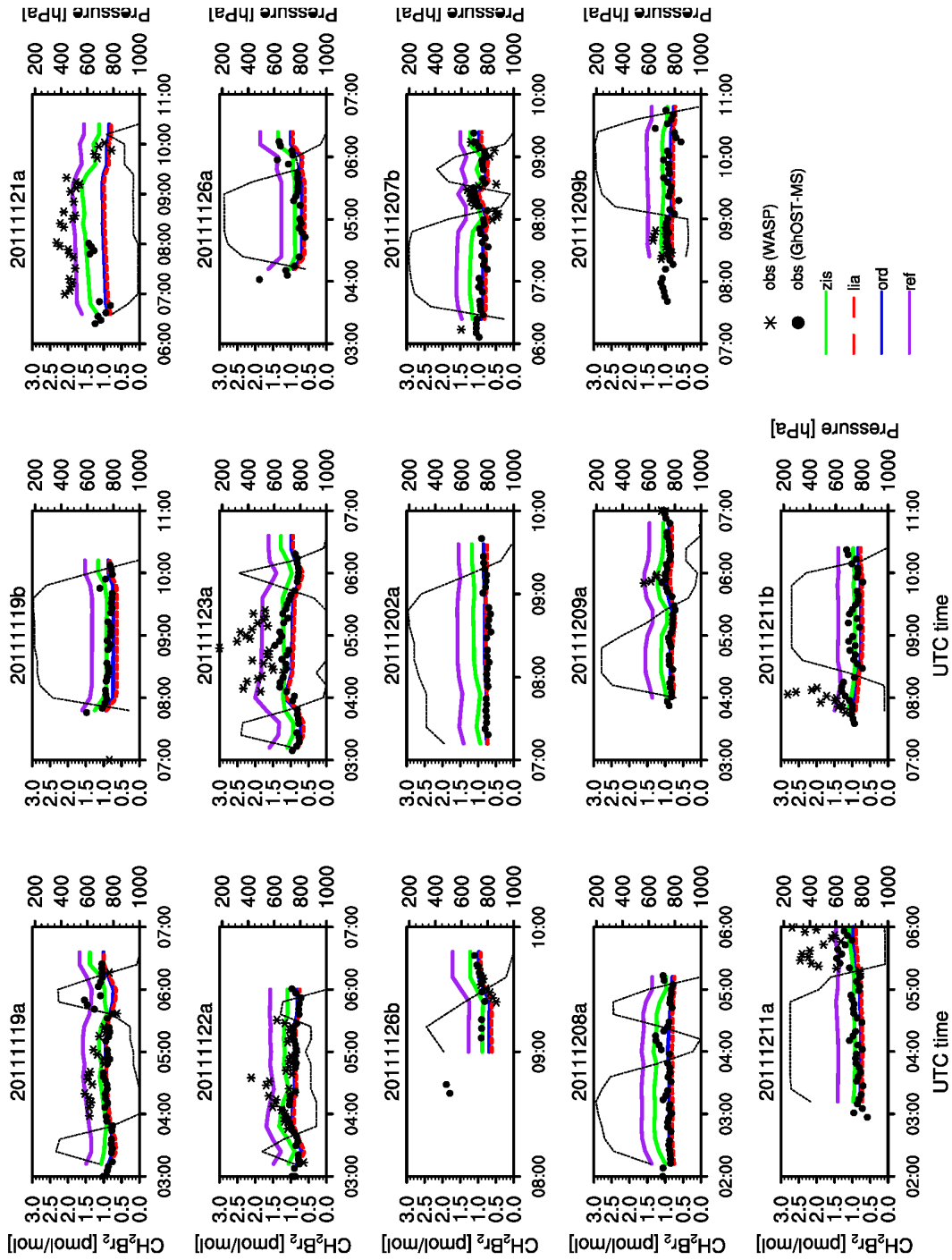
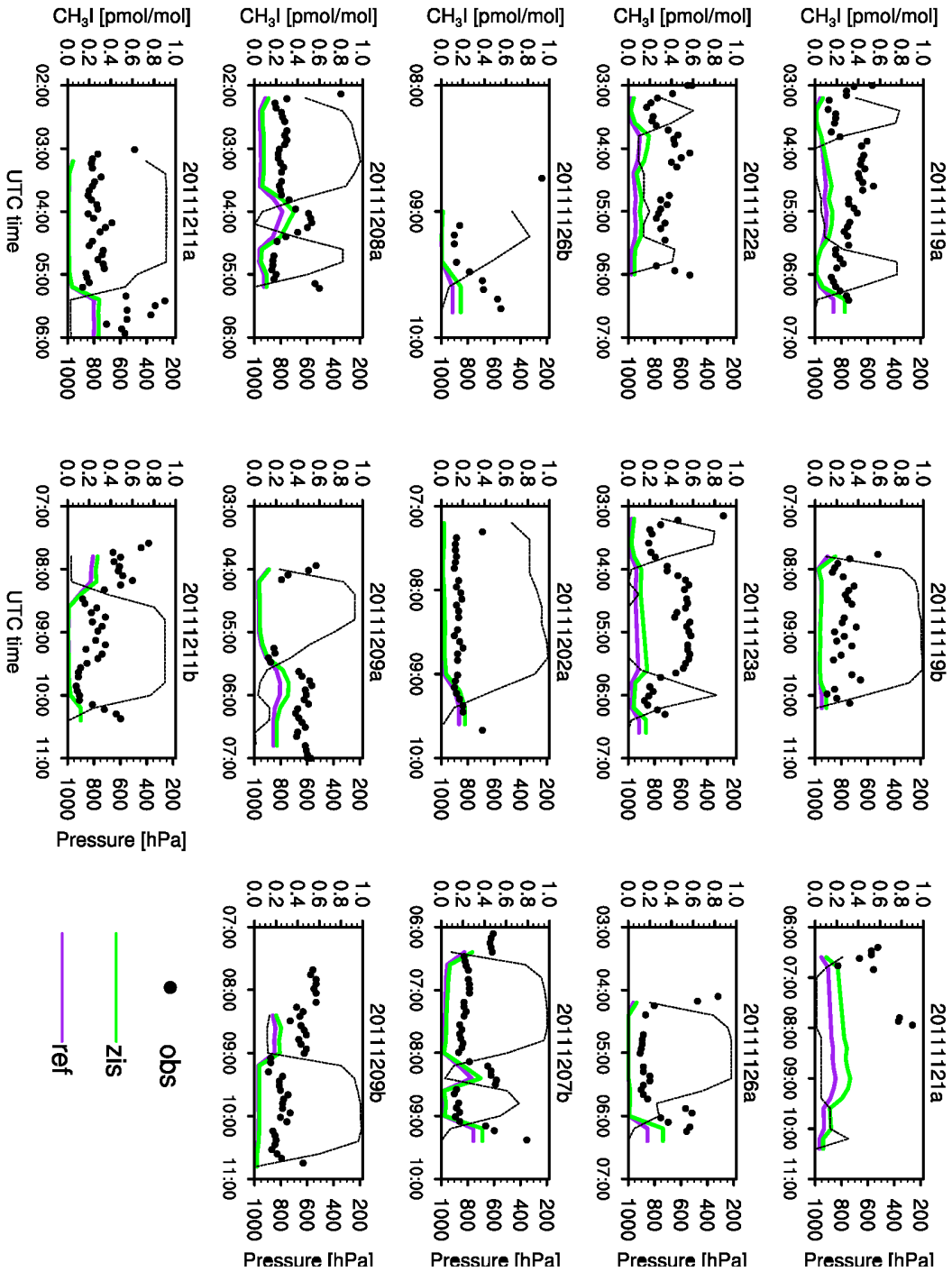


Figure 4.10: As Figure 4.9 but for CH_2Br_2 .

Figure 4.11: As Figure 4.9 but for CH_3I .

O₃

Finally, ozone mixing ratios observed during 14 SHIVA flights are compared to results from the EMAC simulations (Figure 4.12). The differences in VSLS mixing ratios through different emission inventories are not reflected in the ozone mixing ratios. This may be different when comparing the data globally and in stratospheric altitudes (see Section 4.3). In general, the model is able to reproduce the pattern of observed O₃ values relatively well. Modelled values overestimate the observations in all altitudes of the flight track by ~ 20 nmol/mol. Better agreement between the model results and the observations is achieved when convective outflow was sampled (e.g. flight 20111123a).

Vertical Distribution of VSLS

To estimate the amount of VSLS entering the stratosphere it is important to simulate realistic vertical profiles of VSLS. Therefore, data from all SHIVA flights is summarized to vertical profiles in Figures 4.13, 4.14 and 4.15 for CHBr₃, CH₂Br₂ and CH₃I, respectively. For clarity, each simulation is shown in an extra plot in comparison to the observations.

CHBr₃

For CHBr₃ (Figure 4.13) it is apparent that observed values are significantly overestimated when using the previous standard emissions from Warwick et al. (2006). Note the differing x-axis for *ref* (Figure 4.13(a)). Particularly at the surface, *ref* shows mixing ratios that are up to a factor 10 larger than the measurements. Around 200 hPa *ref* still overestimates the observations by a factor of 6. The overestimation of surface emissions in the Warwick2006 inventory leads probably to too much bromine from VSLS entering the stratosphere.

A better representation of the vertical pattern is achieved with *zis* (Fig 4.13(b)). Here, surface mixing ratios are well reproduced. Above ~ 700 hPa *zis* underestimates measured CHBr₃ values by a factor 2. This may be caused by missing or too weak convective events in the model, leading to less upward transport of CHBr₃.

Results from *ord* and *lia* are almost similar (Figures 4.13(c) and 4.13(d)): Near the surface and in higher altitudes observed values are overestimated by a factor of ~ 2 .

CH₂Br₂

The analogous vertical profiles for CH₂Br₂ are shown in Figure 4.14. Again, *ref* overestimates the measured values in all altitudes (4.14(a)). A less distinct overestimation is obtained when applying the Ziska2013 emissions (4.14(b)). The best result is provided by *ord* and *lia* (Figures 4.14(c) and 4.14(d)). Below ~ 700 hPa the model performs with both inventories pretty well. With increasing altitudes a small negative bias (~ 0.1 pmol/mol) can be found for both simulations.

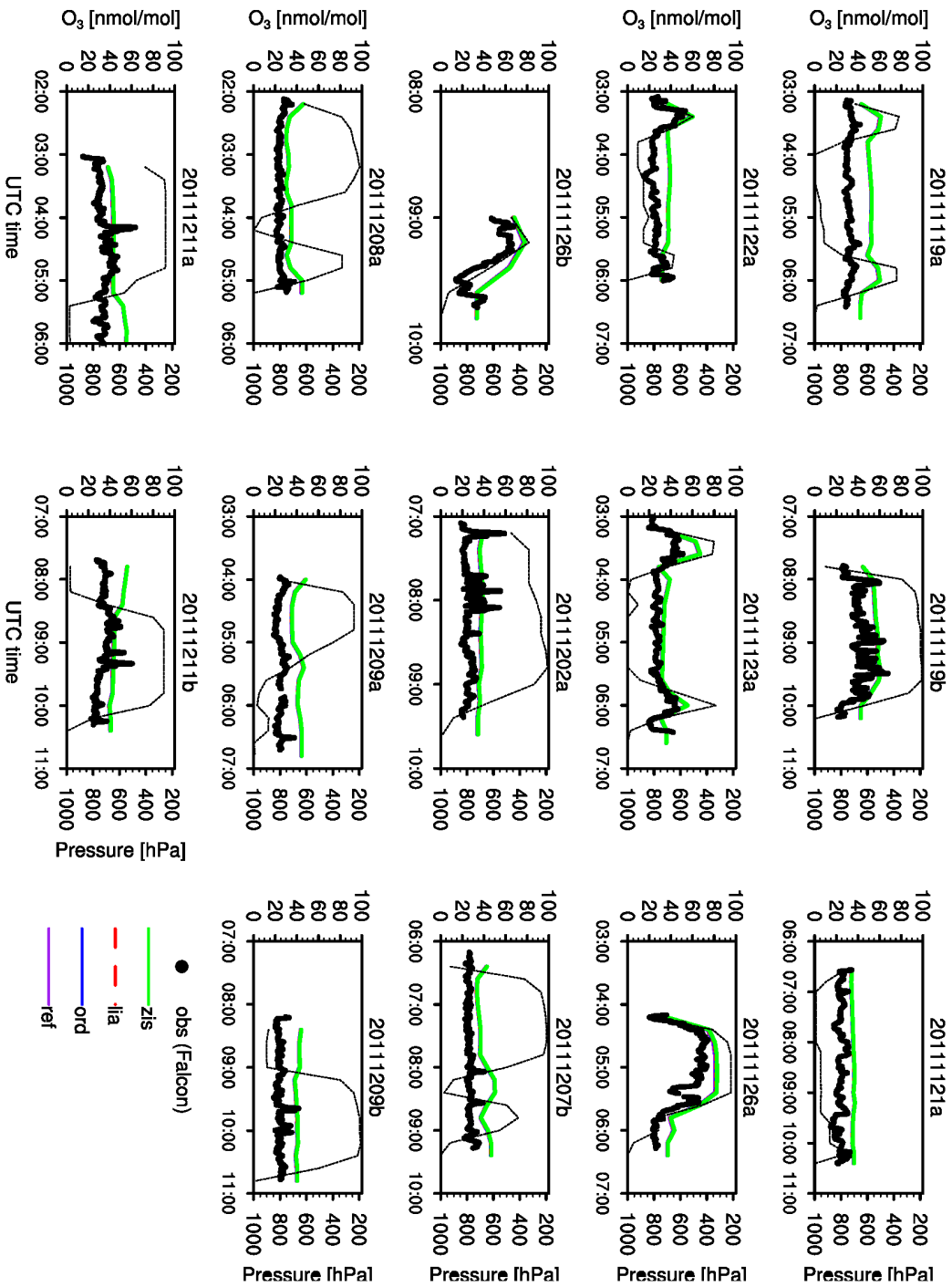


Figure 4.12: As Figure 4.9 but for O_3 (in nmol/mol). Note that only one line is visible as the results of the simulations ref, zis, ord and lia cannot be differentiated.

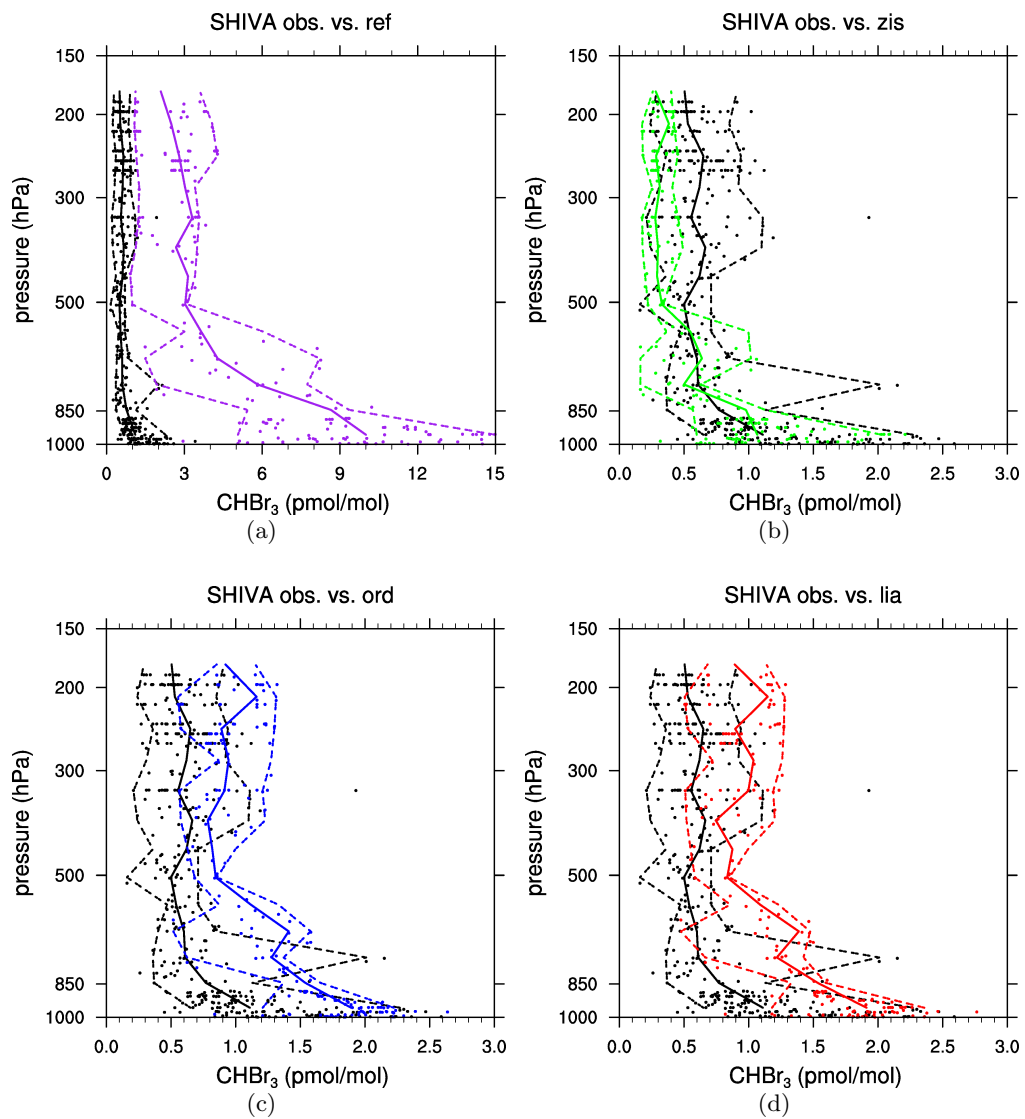
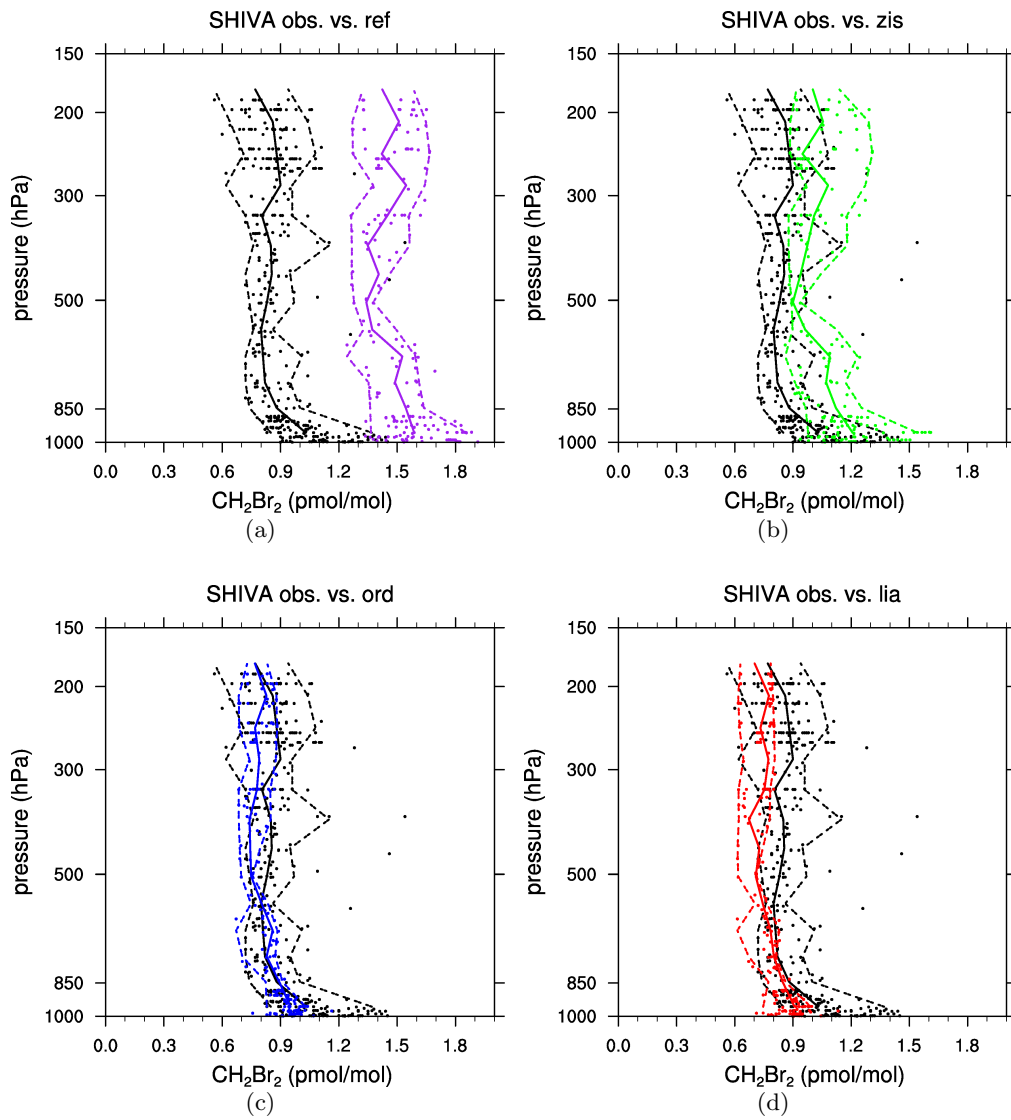


Figure 4.13: $CHBr_3$ (in pmol/mol) observations (black) from 14 flights of the SHIVA campaign in comparison to 4 EMAC runs (colours) with different VSLs emissions: a) ref, b) zis, c) ord and d) lia. The solid lines mark the median of the data binned in 1 km altitude intervals. The dashed lines show the related 5% and 95% percentiles.

Figure 4.14: As Figure 4.9 but for CH_2Br_2 .

CH₃I

Observed mixing ratios of CH₃I lie in the range of ~ 0.5 pmol/mol at the surface and ~ 0.2 pmol/mol in about 200 hPa (Figure 4.15). However, with both available inventories EMAC underestimates the measured values. With Bell2002 emissions *ref* shows a surface mixing ratio of ~ 0.15 pmol/mol and at 200 hPa ~ 0.05 pmol/mol (Figure 4.15(a)). *zis* shows slightly larger surface mixing ratios (~ 0.2 pmol/mol) but apart from that it is relatively similar to *ref* (Figure 4.15(b)).

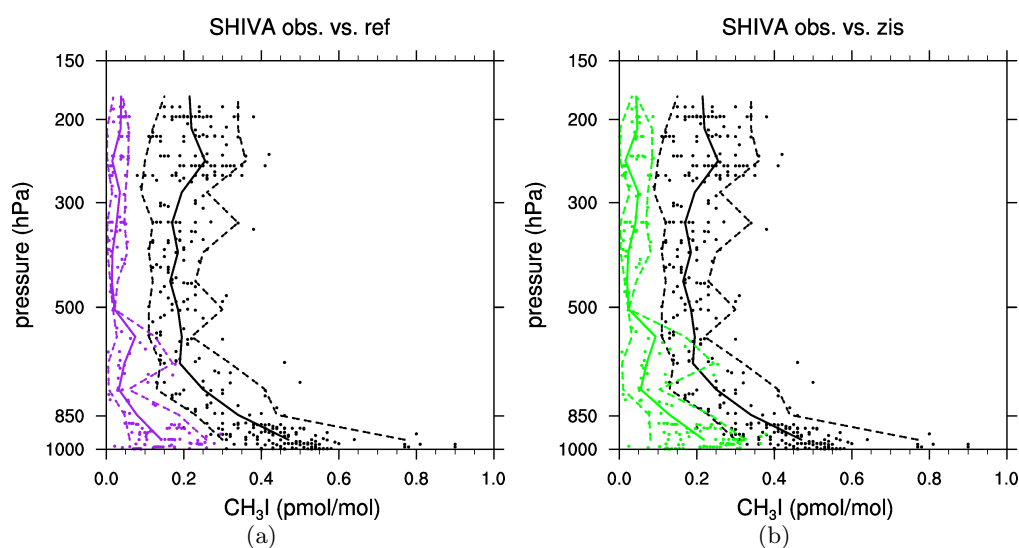


Figure 4.15: As Figure 4.9 but for CH₃I.

4.2.2 Final Conclusion

Four emission inventories for CH₂Br₂ and CHBr₃ and two inventories for CH₃I were applied in a set of transient EMAC simulations and evaluated. Partly large differences in the inventories lead to variable results in the simulations. Results from the simulations were compared to long-term ground-based and airborne observations.

The “reference” emissions by Warwick et al. (2006) in *ref* led to a significant overestimation of measured CHBr₃ values in the tropics and the tropical West Pacific region in particular. In other latitudes CHBr₃ measurements were underestimated. Excluding the mid latitude sites, the seasonal cycle of CHBr₃ could be reproduced relatively good by *ref*. Results for CH₂Br₂ with the “reference” emissions also showed an overestimation of the observed mixing ratios, except for NH mid and polar latitudes. The seasonal cycle of CH₂Br₂ mixing ratios was represented in the model data.

Simulation *zis* used the only bottom-up inventory by Ziska et al. (2013). Except for NH polar latitudes, observed CHBr₃ values were significantly underestimated. In the tropics and in particular in the tropical West Pacific region *zis* provided relatively small discrepancies to measurements of CHBr₃. Observed CH₂Br₂ values were overestimated

by *zis* in the tropics and the SH. The pattern of seasonal variations was less well captured by *zis* as in the other simulations.

The simulations *ord* and *lia* provided similar results because of large similarities in the inventories by Ordóñez et al. (2012) and Liang et al. (2010). Generally, the prescribed seasonality of the Ordonez2012 emissions provided no improved simulation of the seasonal cycle compared to results with aseasonal surface emissions. Compared to CHBr_3 observations both simulations showed an underestimation in extra tropical latitudes. At tropical sites *ord* overestimated the measurements and *lia* showed only small discrepancies. In the West Pacific region CHBr_3 values of both simulations were larger than the observations. Both inventories yield to a relatively good agreement between modelled and measured CH_2Br_2 . Particularly *lia* was able to reproduce the observed values with small deviations from absolute values and a good representation of the seasonal cycle.

Simulation *lia* showed for both VSLs CHBr_3 and CH_2Br_2 in all latitudes and particularly in the tropics a relatively good agreement with the available observations considering absolute values and seasonal variations. Thus, the Liang2010 inventory is selected for further simulations as it provides a more realistic and improved representation of VSLs in EMAC than the previous standard emissions of the reference simulation *ref*.

The comparison of two CH_3I inventories used in EMAC with observations did not provide a clear result with respect to the spatial distribution. With both inventories observed CH_3I values were overestimated by EMAC in all latitudes with the exception of the tropics. There, the simulations *ref* and *zis* underestimated the measurements. The usage of the more recent emissions by Ziska et al. (2013) led to larger discrepancies to ground-based observations. Therefore, the "reference" emissions by Bell et al. (2002) are chosen for further simulations.

It was shown that the representation of the major brominated VSLs CHBr_3 and CH_2Br_2 is significantly improved when using the emissions by Liang et al. (2010) instead of the previously "standard" emissions by Warwick et al. (2006). Nevertheless, a better spatial resolution of the inventories would probably further improve the representation of VSLs in the model. This is only possible through more globally distributed observations to capture strong local variations.

4.3 Stratospheric Sensitivity to Changes in VSLs Surface Emissions

The previous section showed that VSLs emission strength and distribution vary significantly between inventories. The agreement between tropospheric observations and EMAC simulations is highly dependent on the applied emission inventory. It has been shown in several studies that VSLs contribute to the stratospheric bromine loading

and finally to the stratospheric ozone depletion (e.g. Salawitch et al., 2005; Sinnhuber and Meul, 2015). Thus, it must be investigated if a change in surface emissions is also detectable in the stratosphere.

4.3.1 Bromine Loading

Figure 4.16 shows the vertical distribution of the zonally averaged total inorganic bromine Br_y of the reference simulation *ref* and differences to the three sensitivity runs *zis*, *lia* and *ord* with differing VSLS emission inventories. Remember that the four simulations only vary due to differences in the applied CHBr₃, CH₂Br₂ and CH₃I surface emissions. Consistently to the largest source strengths in the Warwick2006 inventory, *ref* shows in all latitudes and altitudes higher values of Br_y than the other simulations. With the new emission inventories, EMAC shows up to ~ 5 pmol/mol less Br_y ($\sim 60\%$) above the tropical tropopause than in *ref*. The Ziska2013 inventory has the smallest source strength for the brominated VSLS and correspondingly the lowest stratospheric Br_y values. *ord* and *lia* produce about 3 pmol/mol (30%) less Br_y than *ref* in ~ 50 hPa. These results are reasonable with regard to the prescribed source strengths of the inventories (see Table 3.2). Nevertheless, it is an important result as it shows that changes in VSLS surface emissions do have a significant effect on the stratospheric bromine loading.

A common approach to quantify the contribution of VSLS to stratospheric Br_y, namely Br_y^{VSLS}, is to determine the sum of source and product gas injection (SGI and PGI) at the tropical cold point tropopause (CPT). SGI is determined by summing the mixing ratios of the VSL source gases at the CPT multiplied by their number of bromine atoms (e.g. for CHBr₃ multiplied by 3). Analogous, PGI is the mixing ratio of product gases at the CPT. The sum of all brominated VSL product gases is defined within the TBUDGET submodule (see Section 3.2) as the variable Br_S.

Figure 4.17 shows the tropical profiles of Br_y^{VSLS} for the four simulations. Shown is also the position of the cold point tropopause where values of SGI and PGI are determined. An overview of the results is given in Table 4.5. Note, Br_y^{VSLS} also includes

Table 4.5: Contribution of VSLS to stratospheric Br_y in pmol/mol. Major VSLS are CHBr₃ and CH₂Br₂, minor VSLS are CH₂ClBr, CHCl₂Br and CHCl₂Br₂.

Simulation	SGI (major VSLS)	SGI (minor VSLS)	PGI	Br _y ^{VSLS}
ref	4.4	0.35	4.1	8.9
zis	2.1	0.35	1.3	3.7
ord	2.5	0.35	2.5	5.3
lia	2.3	0.35	2.3	4.9

the contribution of minor VSLS CH₂ClBr, CHCl₂Br and CHCl₂Br₂ which is for all simulations identical. SGI of the minor VSLS accounts for ~ 0.35 pmol/mol compared to 0.17 (0.08–0.51) pmol/mol derived by observations at the tropical tropopause (Car-

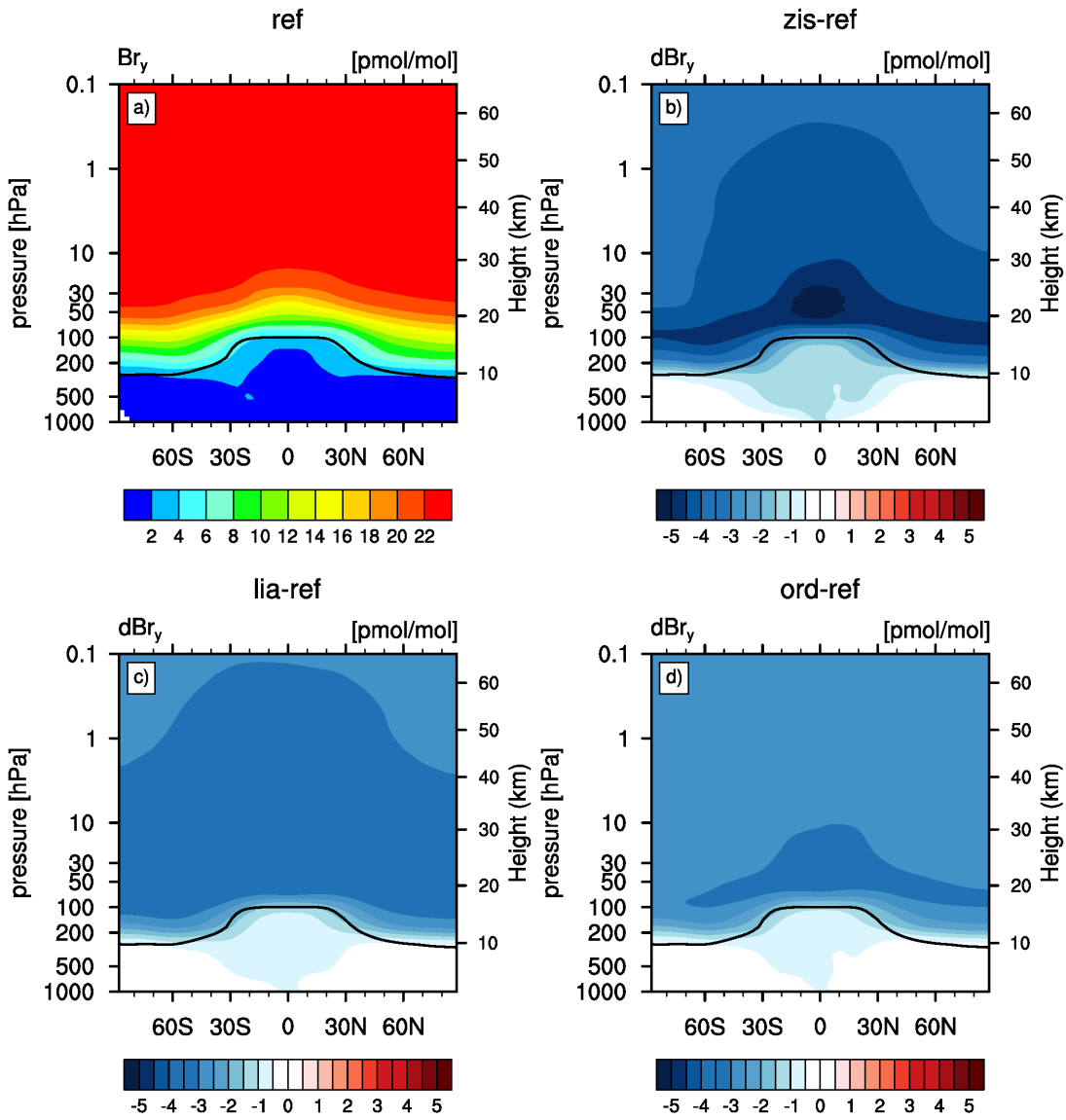


Figure 4.16: Annual mean of zonally averaged total Br_y (in pmol/mol) of ref (a) and differences (in pmol/mol) between reference and sensitivity simulations: b) zis-ref c) lia-ref, and d) ord-ref. The black line denotes the tropopause.

penter et al., 2014). The total contribution from VSLS to Br_y is 8.9 pmol/mol for *ref*, 4.9 pmol/mol for *lia*, 5.3 pmol/mol for *ord* and 3.7 pmol/mol for *zis*. The results of the latter three simulations lie in the Br_y^{VSLS} range of 5 (2–8) pmol/mol reported recently by Carpenter et al. (2014). As *ref* significantly overestimated observed values in the tropics it is likely that contribution from VSLS to Br_y of ≥ 8 pmol/mol is also an overestimation. Hossaini et al. (2013) came to analogous modelled Br_y^{VSLS} results when comparing four similar VSLS emission inventories in their CTM. Apart from the Warwick2006 emissions they used the same emissions as in this study. Above 30 km (~ 10 hPa) they found that Br_y^{VSLS} ranges from 5 to 8 pmol/mol which is in good agreement with ~ 4 to 8 pmol/mol obtained in this study for similar altitudes (see Figure 4.17).

Considering only the major VSLS CHBr₃ and CH₂Br₂ leads to a SGI of (2.1–4.4) pmol/mol with *zis* accounting for the lower and *ref* for the upper limit of the range. Other studies report 1.28 (0.6–2.65) pmol/mol from observations (Carpenter et al., 2014) and 2.0 (1.2–2.5) pmol/mol from a multi-model mean of several chemistry (climate) models (Hossaini et al., 2016). Again, the reference emissions from Warwick et al. (2006) seem to overestimate SGI from the major VSLS, whereas results from *zis* (2.1 pmol/mol), *lia* (2.3 pmol/mol) and *ord* (2.5 pmol/mol) are consistent with the estimates of other studies.

The contribution of PGI to Br_y^{VSLS} in the simulations is approximately as large as the corresponding SGI. Only exception is the simulation *zis*. Here, PGI is significantly smaller than SGI (see Table 4.5). In the region of the tropical tropopause *zis* shows about 4 % more OH (not shown) than *ref*. Possibly this indicates that the reaction of VSLS with OH is limited by small VSLS abundances leading to more available OH and a smaller contribution from PGI.

Previous studies stated the importance of the West Pacific region for transport of VSLS into the stratosphere (e.g. Aschmann et al., 2009). Br_y^{VSLS} for the region where the SHIVA campaign took place (1°N–8°N, 102°E–122°E) is slightly higher with (3.8–9.3) pmol/mol. Sala et al. (2014) report 4.35 ± 0.44 pmol/mol from observations during the SHIVA flights. *ref* significantly overestimates this result probably due to an overestimation of the prescribed surface emissions. Results from *lia* and *ord* are larger (5.1 pmol/mol and 5.6 pmol/mol), from *zis* slightly smaller (3.8 pmol/mol) than the given range (Figure not shown).

In general, the model results for Br_y^{VSLS} are highly dependent on the applied surface emissions. In all simulations further uncertainties arise for instance from the representation of convection, loss through wash-out, degradation of VSLS by photolysis and reaction with OH. The position of the cold-point tropopause where SGI and PGI are usually determined may also differ between model and observations. However, EMAC shows reasonable results for Br_y^{VSLS} when applying emissions from Ziska et al. (2013), Ordóñez et al. (2012) and Liang et al. (2010). It was previously shown (see Section

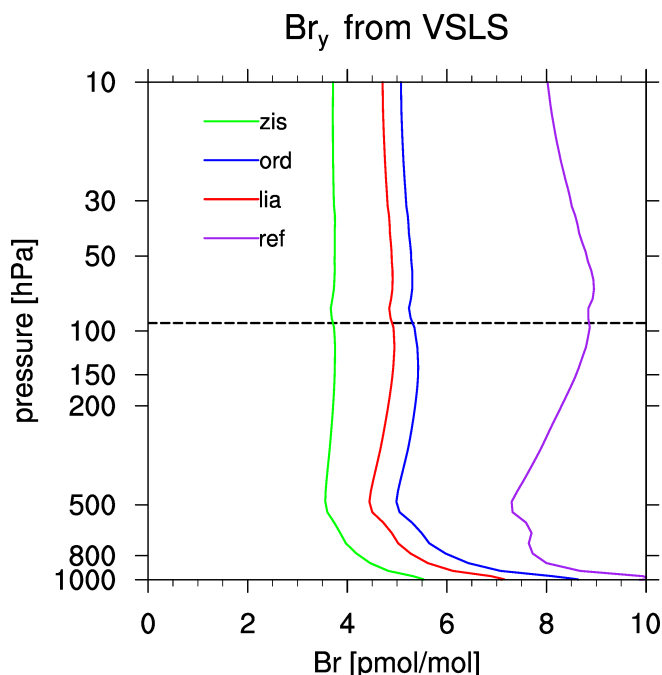


Figure 4.17: Tropical ($\pm 30^\circ$) mean profile of total inorganic bromine from VLSL ($\text{Br}_y^{\text{VLSL}}$; in pmol/mol) for the year 2012. Profiles are shown for the EMAC simulations *ref* (purple), *zis* (green), *ord* (blue) and *lia* (red). The black horizontal line denotes the cold point tropopause in the simulations.

4.2) that the reference emissions by Warwick et al. (2006) lead to a clear overestimation of VLSL measurements. Therefore, *ref* probably also overestimates the injection of bromine into the stratosphere. The other VLSL inventories led to a relative good agreement between model and observations. However, the performance of the model was dependent on the investigated latitude and altitude range. Therefore, the simulations *zis*, *ord* and *lia* are considered for the determination of $\text{Br}_y^{\text{VLSL}}$. Consequently, the contribution of VLSL to the stratospheric bromine burden is suggested to amount to 4.5 ± 0.8 pmol/mol provided that the uncertainty range arises from uncertainties on the surface emissions.

4.3.2 Ozone

In the previous section it was shown that a change in VLSL surface emissions affects the stratospheric bromine loading. Therefore it must be assumed that also the total ozone amount is affected. Compared to *ref* the decrease in Br_y in *zis*, *ord* and *lia* leads to a significant global increase in stratospheric ozone. The increase in ozone is most distinct in the lower polar stratosphere (see Figure 4.18) of up to $0.07 \mu\text{mol/mol}$ ($\sim 7\%$) in *zis* and $0.05 \mu\text{mol/mol}$ ($\sim 5\%$) in *ord* and *lia*.

The largest differences occur in SH spring (SON) over Antarctica (not shown). Here, the maximum ozone increase is obtained in the simulation with the lowest VLSL emis-

sions (*zis*) and is $\sim 13\%$ larger than in *ref*. For the simulations *ord* and *lia* the ozone increase in SH spring amounts to 8% and 9%, respectively. The positive bias of EMAC ozone values in comparison to observations (see Section 4.1) may affect the absolute values of these results but certainly not the quintessence of the results. The Liang2010 emissions were previously selected for further simulations as they provided globally the most reasonable VLSL results compared to observations. Thus, the simulation *lia* probably also produces more realistic ozone values than *ref*.

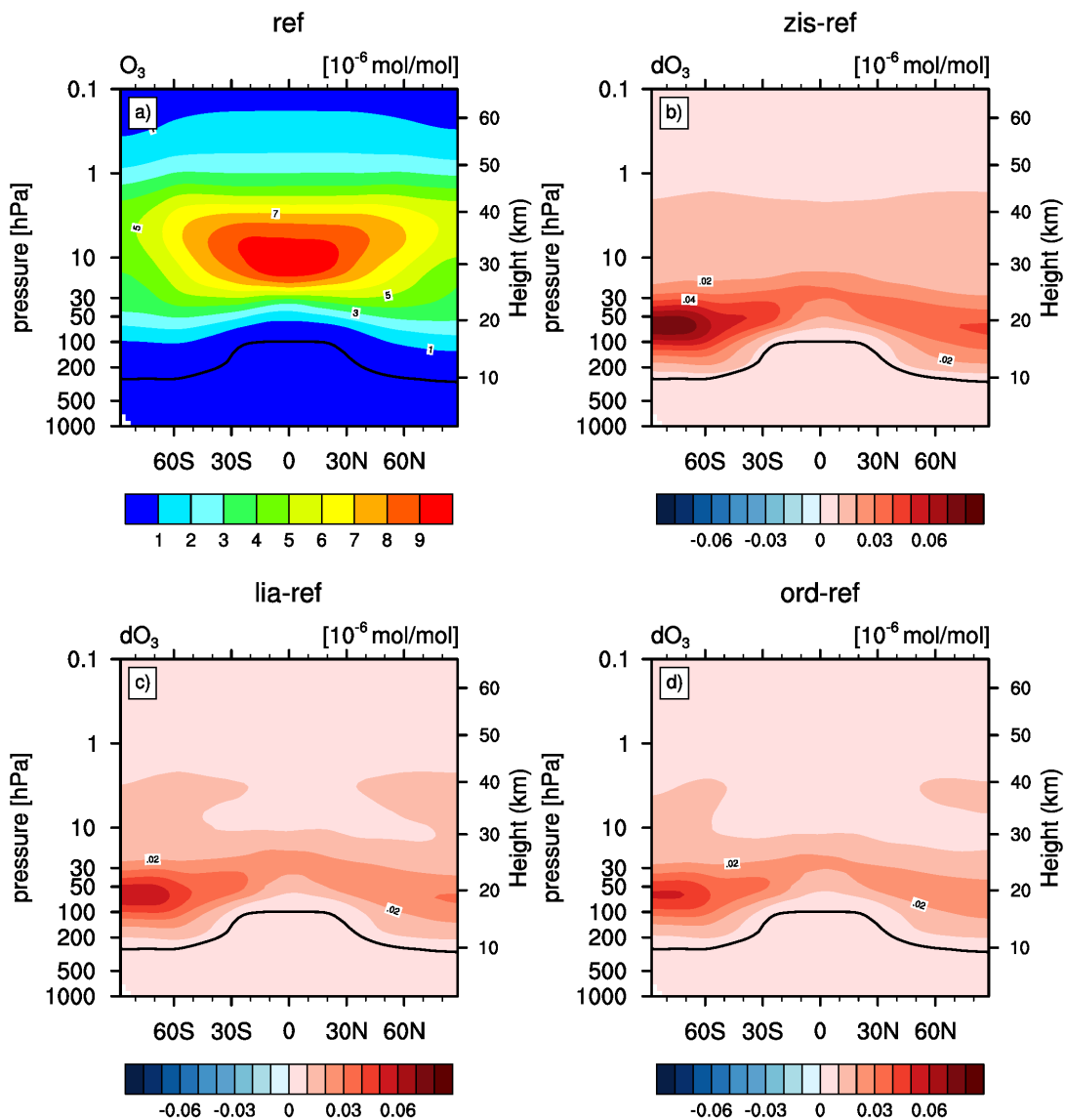


Figure 4.18: As Figure 4.16 but for O_3 .

4.4 Summary

A consistent validation of four VSLs emission inventories applied in EMAC was conducted. The model results were validated with globally distributed observations. The analyses of the VSLs emission inventories has shown: there is not one inventory that is the best inventory for all latitudes and altitudes. This indicates once again that uncertainties concerning the emissions and distribution of VSLs are high and there are still more observations needed. Nonetheless, the comparison of the EMAC simulations with observations showed that the major brominated VSLs CHBr_3 and CH_2Br_2 are better reproduced by the model when using one of the three new emission inventories instead of the "reference" emissions by Warwick et al. (2006).

EMAC significantly overestimate measured CHBr_3 values when using the "reference" emissions, particularly in the tropics, an important region for upward transport of VSLs into the stratosphere. For CHBr_3 *zis* performed particularly well in the tropics but showed partly large discrepancies to observations in other latitude ranges. Moreover, *ord*, *lia* and *ref* agreed better to observed CH_2Br_2 values than *zis*. Taking all latitude ranges and both substances into account *ord* and especially *lia* provided good agreement with measurements. Using the only seasonal varying emissions by Ordóñez et al. (2012) in *ord* showed no added value. Discrepancies to observations were slightly larger in *ord* than in *lia*. For CH_3I no improvement was found when applying the more recent emissions by Ziska et al. (2013).

Thus, for further simulations for the major VSLs CHBr_3 and CH_2Br_2 the emission inventory from Liang et al. (2010) will be applied. As no more recent estimates were available, emissions for the minor VSLs CH_2ClBr , CHCl_2Br and CHCl_2Br_2 are still taken from Warwick et al. (2006). As before, CH_3I emissions will be taken from Bell et al. (2002).

It was shown that altered VSLs surface emissions lead to significant changes in the stratospheric bromine and ozone loading. (3–5) pmol/mol less Br_y was obtained in the stratosphere with the new VSLs inventories in *zis*, *ord* and *lia*. The reduction of bromine (relative to *ref*) causes an increase in stratospheric ozone, especially in the lower stratosphere of polar latitudes. The most distinct increase in O_3 of (8–13) % relative to the reference simulation could be detected on the Southern Hemisphere during spring.

Based on the EMAC sensitivity simulations *zis*, *ord* and *lia* the contribution of VSLs to stratospheric bromine was determined to add up to 4.5 ± 0.8 pmol/mol. The broad range $\text{Br}_y^{\text{VSLs}}$ arises from the uncertainties on VSLs surface emissions but is consistent to recent studies (Carpenter et al., 2014).

EMAC showed with new VSLs emissions reasonable results in comparison to observations and other studies. A significant improvement of the model's performance was obtained when using the emissions from Liang et al. (2010) for CHBr_3 and CH_2Br_2 . With this new "standard" set-up EMAC is well suited for further simulations.

Chapter 5

The Impact of VSLS on Bromine and Ozone Loss

In the last chapter it was shown that a change in VSLS surface emissions significantly affects the stratospheric bromine loading and consequently ozone values. EMAC was shown to represent VSLS mixing ratios reasonably with the VSLS emissions by Liang et al. (2010). The aim of this chapter is now to quantify the contribution of VSLS to the total stratospheric bromine and to determine the stratospheric ozone loss through VSLS under climatic conditions of the year 2000. Data from two time slice simulations will be investigated: *TS2000lia* using VSLS emissions by Liang et al. (2010) and *TS2000zero* without any VSLS emissions. Both simulations represent the year 2000, thus the climate of the recent past. This approach enables to determine the impact of VSLS on the above mentioned quantities.

5.1 Bromine Loading

With the EMAC submodel TBUDGET it is possible to differentiate the brominated product gases (PGs) released from long-lived and very short-lived source gases, named Br_L and Br_S . The sum of Br_L and Br_S is the total inorganic bromine Br_y content. The total bromine is the sum of long-lived and very short-lived source gases (SGs) (each SG is multiplied by its number of bromine atoms) plus the inorganic product gases Br_y . The tropical profile of these substances can be seen in Figure 5.1. Below the cold point tropopause (CPT) (denoted with the dashed black line) the long-lived SG (in grey) are well mixed and add up to ~ 15 pmol/mol. In the stratosphere, the long-lived SGs decrease due to degradation through photolysis. Consequently, the product gases Br_L increase to the same degree with increasing height until ~ 10 hPa. At the CPT long-lived SG contribute 14.9 pmol/mol to total bromine of which 7.7 pmol/mol are provided by methyl bromide (CH_3Br ; not shown). Very Short-Lived (VSL) source gases (green line) underlie a strong vertical gradient because of photochemical loss.

Mixing ratios span a range from ~ 7 pmol/mol at the surface, to ~ 3.5 pmol/mol in 500 hPa, to ~ 2.5 pmol/mol at the cold point tropopause. In altitudes between 500 and 100 hPa a small increase of the VSLs SGs is visible which may be related to convective outflow. This is consistent to observations during the SHIVA campaign where elevated mixing ratios occurred when convective outflow was sampled (see Section 4.2). When VSL source gases are depleted through photochemistry inorganic bromine is released, shown as Br_g (blue line). In contrary to the long-lived halogens, most of the VSLs are already degraded in the troposphere so that inorganic bromine from VSLs (Br_g) makes up the main part of tropospheric Br_y . At the CPT mixing ratios of VSL SGs and PGs amount to 2.5 pmol/mol and 2.8 pmol/mol, respectively, yielding to an injection of 5.3 pmol/mol bromine into the stratosphere. This result is in good agreement with previous results from the nudged transient simulations discussed in Section 4.3 where $\text{Br}_y^{\text{VSLs}}$ was found to amount to 4.5 ± 0.8 pmol/mol. Total bromine shows in the troposphere decreasing values up to 500 hPa which is probably caused by depletion of VSL source gases and wash-out of soluble product gases. Above 500 hPa a small increase of ~ 0.5 pmol/mol can be seen which may be related to elevated VSLs values in convective outflow. In the stratosphere total bromine almost shows no vertical gradient and adds up to 20.2 pmol/mol at the cold point tropopause, of which 14.9 pmol/mol are provided by long-lived brominated compounds and 5.3 pmol/mol by VSLs. The year-to-year variability of all values at the CPT accounts for ± 0.1 pmol/mol.

The contribution of VSL major (CHBr_3 and CH_2Br_2) and minor (CH_2ClBr , CHCl_2Br and CHCl_2Br_2) SGs and PGs to Br_y is summarized in Table 5.1. The major VSLs

Table 5.1: Contribution of VSLs to stratospheric Br_y in pmol/mol. Major VSLs are CHBr_3 and CH_2Br_2 , minor VSLs are CH_2ClBr , CHCl_2Br and CHCl_2Br_2 .

Simulation	SGI (major VSLs)	SGI (minor VSLs)	PGI	$\text{Br}_y^{\text{VSLs}}$
TS2000lia	2.2	0.33	2.8	5.3

CHBr_3 and CH_2Br_2 deliver 2.2 pmol/mol bromine via source gas injection (SGI) into the stratosphere. Due to its longer lifetime SGI of CH_2Br_2 is with 1.2 pmol/mol slightly larger than SGI of CHBr_3 (1.0 pmol/mol; not shown). Additional 0.33 pmol/mol bromine arises from the SGI of minor VSLs. Thus, the total SGI of VSLs amounts to 2.5 pmol/mol and is smaller than the product gas injection (PGI) pathway (2.8 pmol/mol).

The set-up of the simulation *TS2000zero* is equal to *TS2000lia* with the exception that VSLs emissions are set to zero. Differences between the simulations therefore only arise from the consideration of VSLs. Figure 5.2 shows the total bromine (i.e. VSL and long-lived SGs + PGs) in *TS2000lia* (a) and the total bromine provided by VSLs only (b) which is derived by subtracting *TS2000zero* from *TS2000lia*. Near the surface VSLs provide up to 10 pmol/mol ($\sim 40\%$) to the total atmospheric bromine. In the stratosphere at least 4.75 pmol/mol (24%) of the total bromine arises from very

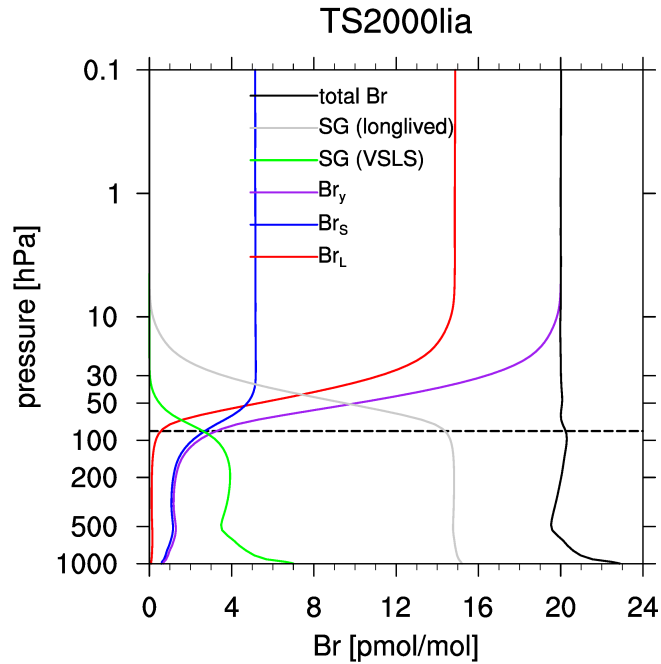


Figure 5.1: Annual mean profile of zonally averaged bromine mixing ratios in the tropics ($\pm 20^\circ$). Shown are long-lived and very short-lived source gases (SG), inorganic bromine (Br_y), total bromine, and the contribution of VSLS product gases (Br_s) and long-lived product gases (Br_L) to Br_y . The dashed horizontal line denotes the position of the cold point tropopause.

short-lived compounds, in the tropical stratosphere up to 5.3 pmol/mol ($\sim 26\%$). The smallest contribution of about 4 pmol/mol (22%) occurs in the free troposphere at 30°N/S . In the next section it will be investigated how this additional bromine from VSLS, that was often neglected in earlier climate studies, affects the stratospheric ozone layer.

5.2 Ozone

Comparing the ozone values of *TS2000lia* and *TS2000zero* allows the quantification of the ozone loss induced by VSLS. The impact of VSLS on ozone occurs predominantly in altitudes below 30 hPa and is largest in the lower stratosphere over the South Pole during the SH spring (September-October). In October stratospheric ozone values over Antarctica are 200 nmol/mol (-14%) smaller when considering VSLS (see Figure 5.3(b)). The annual mean shows about 80 nmol/mol (-3%) less ozone in the south polar stratosphere in the simulation with VSLS emissions. Over the North Pole the impact is significantly smaller. Here, the largest decreases of ~ 50 nmol/mol (-2%) occur in NH spring (March-April; not shown). Thus, VSLS locally destroy up to 14% of the stratospheric ozone.

The seasonal variation of column ozone also shows that the impact of VSLS on ozone is largest in polar latitudes during spring (Figure 5.4). Over the South Pole column

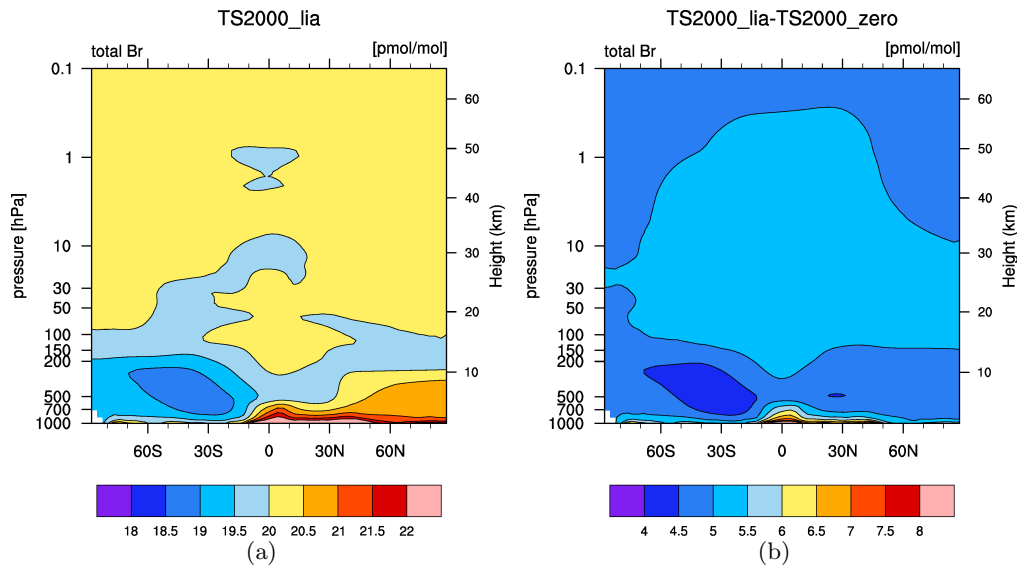


Figure 5.2: Annual mean of zonal total bromine (in pmol/mol) in a) TS2000lia and b) difference between TS2000ref and TS2000zero.

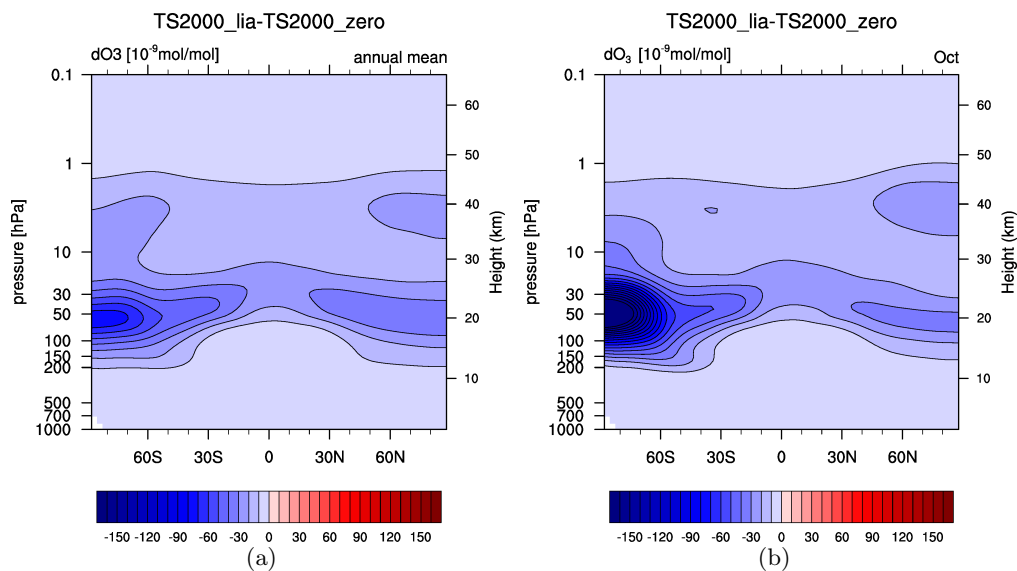


Figure 5.3: Difference in zonal mean ozone mixing ratio (in nmol/mol) between TS2000lia and TS2000zero of a) the annual mean and b) the October mean.

O_3 is reduced by up to ~ 13 DU ($\sim 6\%$) during SON. Due to a larger variability the impact on Arctic O_3 column is less distinct with a maximum decrease in NH spring of ~ 5 DU ($\sim 2\%$). In the mid-latitudes ozone loss through VSLS adds up to 2-5 DU ($(1-2)\%$). The smallest effect occurs in the tropics (-1 DU).

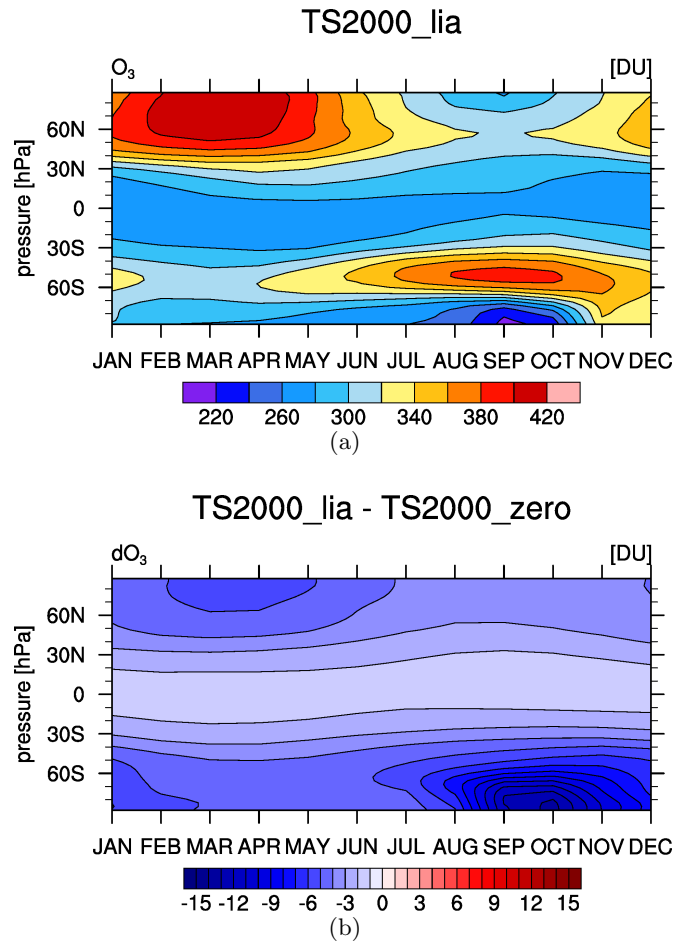


Figure 5.4: Seasonal variation of zonal column O_3 (in DU) a) in TS2000lia and b) difference between TS2000lia and TS2000zero.

The location of the largest impact indicates that Br_y^{VSLS} enhances O_3 loss through the coupled BrO_x – ClO_x cycle in the lower stratosphere (see Section 2.1.1) as already suggested in other studies (Salawitch et al., 2005; Braesicke et al., 2013). Mixing ratios of BrO in this region show almost no seasonal variation (see Figure 5.5). On the contrary, ozone mixing ratios and the well-known ozone hole are strongly dependent on the seasonal cycle of ClO that shows a maximum in September. Thus, bromine from VSLS is most efficient in destroying ozone when mixing ratios of ClO maximize.

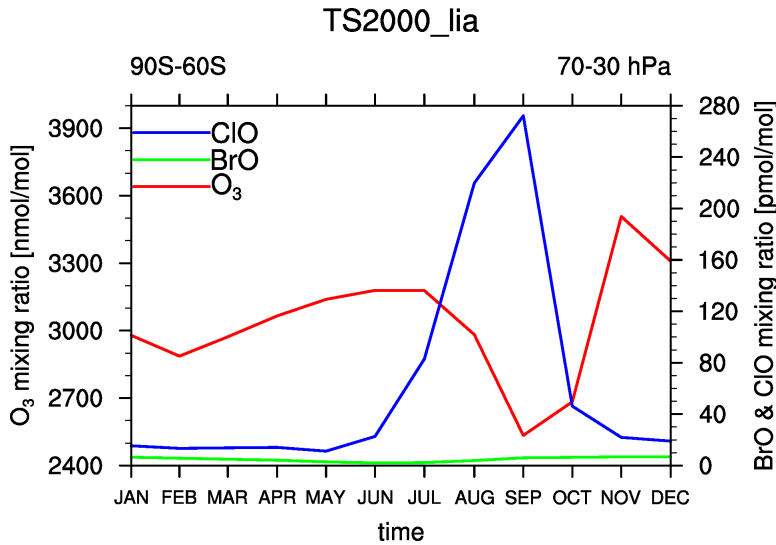


Figure 5.5: Seasonal variation of ozone (in nmol/mol; left y-axis), BrO and ClO (in pmol/mol; right y-axis) for southpolar latitudes in 70-30 hPa.

5.3 Summary

For the year 2000 the reference simulation *TS2000lia* has a mean stratospheric Br_y burden of ~ 20 pmol/mol. This result is in good agreement with observations documented in Carpenter et al. (2014) (see also Figure 1.1). The contribution of VSLs to stratospheric bromine accounts for 5.3 ± 0.1 pmol/mol when using the emissions by Liang et al. (2010). This result lies in the $\text{Br}_y^{\text{VSLs}}$ range of 5 (2–8) pmol/mol reported recently by Carpenter et al. (2014). Source gas injection (SGI) of the major VSLs CHBr_3 and CH_2Br_2 amounts to 2.2 ± 0.1 pmol/mol which is in good agreement with observation based studies that reported 1.28 (0.6–2.65) pmol/mol (Carpenter et al., 2014). Consistently, a multi-model mean of several chemistry (climate) models resulted in 2.0 (1.2–2.5) pmol/mol SGI of the major VSLs (Hossaini et al., 2016). Minor VSLs contribute 0.33 pmol/mol additional bromine via SGI which is in accordance to the 0.17 (0.08–0.51) pmol/mol obtained from observations at the tropical tropopause (Carpenter et al., 2014). Product gas injection contributes additional 2.6 pmol/mol bromine. This result agrees well to recent studies estimating PGI of major and minor VSLs adding up to (1.1–4.3) pmol/mol. Taking the additional bromine from VSLs into account leads to a decrease of the stratospheric ozone amount. In all latitudes less ozone is present in the simulation with VSLs emissions. The largest effect on ozone occurs in SH spring over Antarctica where up to 14% of the total ozone are destroyed by VSLs. In annual average VSLs are accountable for 3% less ozone. The ozone depletion is most effective when active chlorine maximizes and the ClO_x - BrO_x cycle can be most efficient. Ozone loss related to VSLs was also found in other studies (Carpenter et al., 2014). Feng et al. (2007) reported up to 10 DU ozone loss by VSLs in the mid-latitudes, which is larger than the –5 DU in *TS2000lia*. The difference might be a result of the

higher $\text{Br}_y^{\text{VSLs}}$ value (6 pmol/mol) that Feng et al. (2007) assumed in their CTM simulation. Braesicke et al. (2013) found up to 20 % less ozone in the polar regions under 2000 stratospheric conditions in their coupled chemistry-climate simulations which is in relative good agreement with the 14 % found in this study.

Chapter 6

The Impact of Climate Change on VSLs Transport and Chemistry

Increasing greenhouse gas concentrations lead to a significant alteration of the climate system. Climate change is topic of many studies as it is the result of complex interacting dynamical and chemical processes (e.g. IPCC, 2007, 2013). However, to date it is highly uncertain if VSLs emissions will change in a future climate, for instance through higher sea surface temperatures or changes in the ocean's nutrient supply. Therefore, in a first step, it will be investigated here, how climate change affects the transport and chemistry of VSLs when VSLs surface emissions remain unchanged. For this purpose the time slice simulations *TS2000lia* and *TS2100lia*, representing the climate of the years 2000 and 2100, will be analysed. VSLs emissions are equally prescribed in both simulations and for the major VSLs CHBr_3 and CH_2Br_2 taken from Liang et al. (2010).

6.1 Future Changes in Bromine Loading

Differences between the simulations *TS2000lia* and *TS2100* only occur in consequence of changes in the climate system as the same emissions for VSLs are specified.

Analogous to the previous chapter Figure 6.1 shows the tropical profile of the gases that contribute to total bromine in the year 2100. Compared to the year 2000 tropospheric mixing ratios of long-lived bromine source gases (SGs; grey line) are significantly reduced by 7 pmol/mol in 2100. This effect is the result of the phase out of long-lived halogen compounds in the framework of the Montreal Protocol. Above the cold point tropopause (CPT) the long-lived SGs are destructed through photolysis and decrease with increasing height. Simultaneously, the product gases (PGs) from long-lived SGs (named Br_L , red line). VSL source gases show similar mixing ratios as in the *TS2000lia* simulation: a strong tropospheric vertical gradient caused by the photochemical degra-

dation of VLSL. As most of the VLSL is already destructed in the troposphere Br_S (i.e. the product gases from VLSL) provide the bigger fraction of Br_y until ~ 30 hPa. At the CPT VLSL provide 2.4 pmol/mol bromine via SGI and 2.6 pmol/mol bromine via PGI. Thus, the future total contribution of VLSL to stratospheric bromine adds up to 5.0 pmol/mol. This value of $\text{Br}_y^{\text{VLSL}}$ is by 0.3 pmol/mol smaller than in *TS2000lia*. Note that the cold point tropopause (CPT, denoted with the black dashed line) lies ~ 8 hPa higher than in 2000. However, the vertical resolution of EMAC in the tropopause region is of the same order of magnitude as the increase of the CPT height. This means, that the increase of the CPT height is probably statistically not significant. Using the CPT height from the 2000 simulation changes the results for SGI (+0.3 pmol/mol) and PGI (-0.3 pmol/mol) but not the overall result for $\text{Br}_y^{\text{VLSL}}$ in *TS2100lia*. Uncertainties through the inter annual variability amount to 0.1 pmol/mol in both simulations. Thus, the differences of $\text{Br}_y^{\text{VLSL}}$ between the years 2000 and 2100 are only by 0.1 pmol/mol out of the uncertainty range.

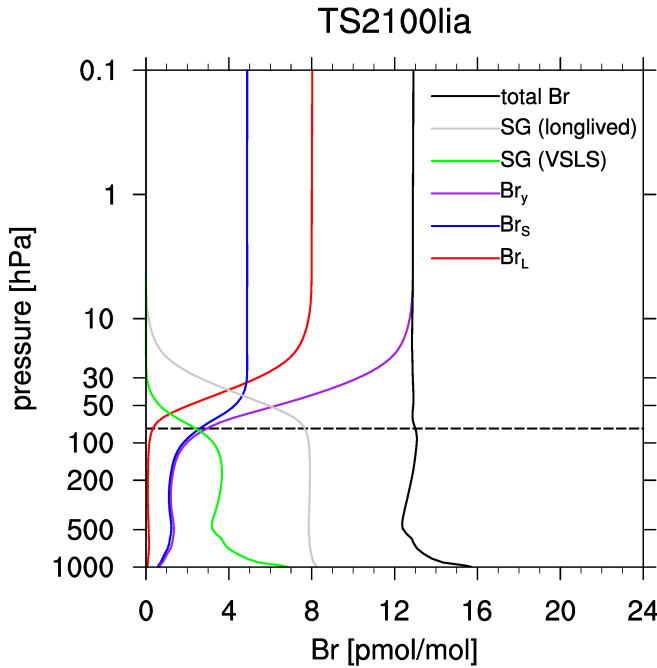


Figure 6.1: Annual mean profile of zonally averaged bromine mixing ratios in the tropics ($\pm 20^\circ$). Shown are long-lived and very short-lived source gases (SG), inorganic bromine (Br_y), total bromine, and the contribution of VLSL product gases (Br_S) and long-lived product gases (Br_L) to Br_y . The dashed horizontal line denotes the position of the cold point tropopause.

A summary of the results at the cold point tropopause for the year 2100 is given in Table 6.1 in comparison to previous results from simulation *TS2000lia*. Both, SGI and PGI injection of VLSL is reduced with respect to the year 2000 leading to a reduction of the total VLSL contribution to stratospheric bromine by 0.3 pmol/mol. SGI of CH_2Br_2 (1.1 pmol/mol) is now only slightly higher than that of CHBr_3 (1.0 pmol/mol). In order to ensure that the reduction of $\text{Br}_y^{\text{VLSL}}$ is not just a tropical phenomena, Figure

Table 6.1: Contribution of VSLS to stratospheric Br_y in pmol/mol in the simulations TS2000lia and TS2100lia. Major VSLS are CHBr_3 and CH_2Br_2 , minor VSLS are CH_2ClBr , CHCl_2Br and CHCl_2Br_2 .

Simulation	SGI (major VSLS)	SGI (minor VSLS)	PGI	$\text{Br}_y^{\text{VSLS}}$
TS2000lia	2.2	0.33	2.8	5.3
TS2100lia	2.1	0.31	2.6	5.0

6.2 shows a latitude-height cross section of $\text{Br}_y^{\text{VSLS}}$ in the year 2000 (Figure 6.2(a)) and the difference to the year 2100 (Figure 6.2(b)). Compared to 2000's conditions

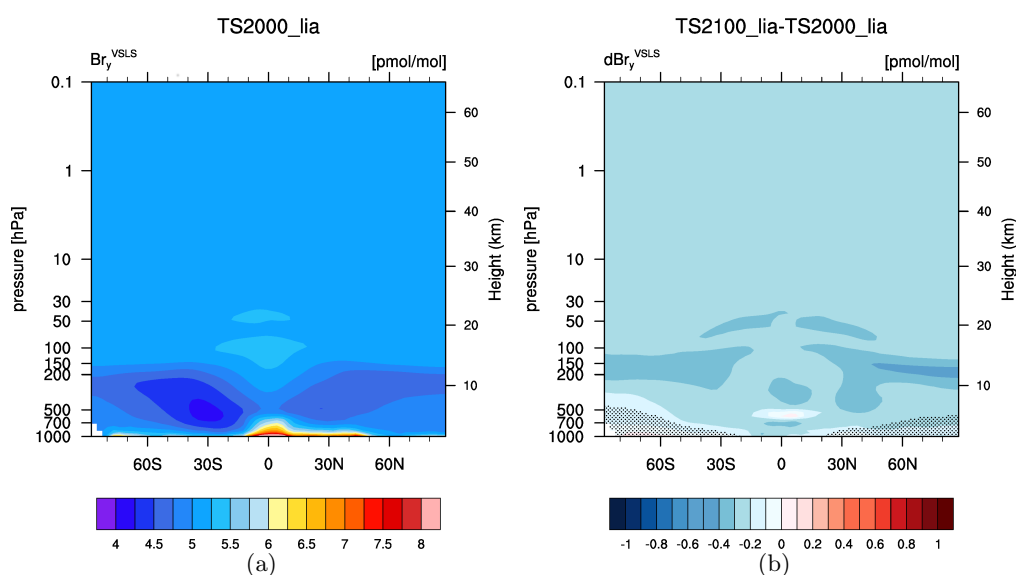


Figure 6.2: Annual mean of zonal bromine from VSLS bromine compounds (in pmol/mol) a) in TS2000lia and b) difference between TS2100lia and TS2000lia. Differences that are not significant according to a t-test (95 % confidence level) are shaded.

stratospheric bromine from VSLS decreases globally by 0.3 pmol/mol, in polar latitudes up to 0.5 pmol/mol. The dipole pattern in the tropics and the minima in the polar stratosphere indicate a change of VSLS transport.

Recent (chemistry-) climate model studies suggest an increased tropical upwelling and an acceleration of the BDC as a result of rising greenhouse gas concentrations (e.g. Butchart et al., 2006; Deckert and Dameris, 2008; Butchart et al., 2010; Oberländer et al., 2013). The vertical transport within the Brewer-Dobson-Circulation (BDC) can be illustrated with the vertical component of the mean stratospheric residual circulation \bar{w}^* . Figure 6.3 shows absolute values of \bar{w}^* in simulation *TS2000lia* (Figure 6.3(a)) and the difference between simulations *TS2100lia* and *TS2000lia* (Figure 6.3(b)). In 2000 the known pattern of the Brewer-Dobson circulation can clearly be seen: upward transport in the tropics and downward transport in the extratropics. The influence of GHG-forced climate change is notable in the right plot. With respect to the year 2000 an increase of the aforementioned pattern is visible: an accelerated tropical up-

ward transport combined with an accelerated downward transport in the extratropics, especially in the mid latitudes. This change in vertical transport also influences the distribution of VSLs that are mainly emitted in the tropics. In fact, the direct injection

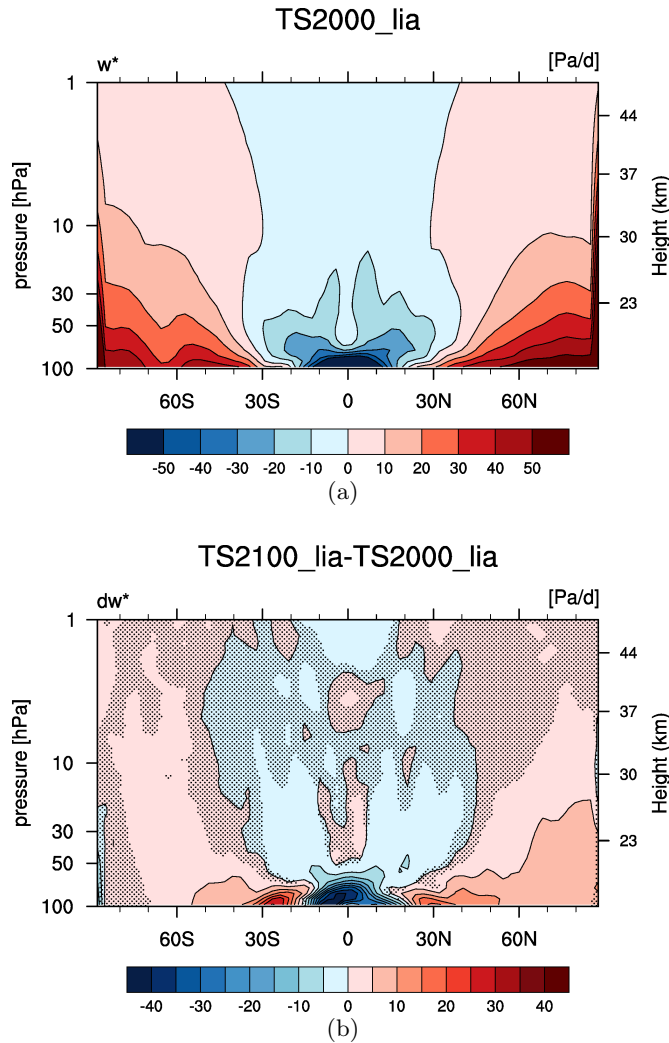


Figure 6.3: Vertical component of the stratospheric residual circulation in Pa/d a) in simulation TS2000lia and b) difference between simulations TS2100lia and TS2000lia. Negative values denote a vertical upward transport whereas positive values denote a downward motion. Differences that are not significant according to a t-test (95 % confidence level) are shaded.

of VSL source gases increases above the tropical tropopause by up to 0.5 pmol/mol in *TS2100lia* compared to the year 2000. At the same time the tropospheric abundance of VSLs decreases by up to 0.4 pmol/mol (see Figure 6.4(a)). The pattern of changed SGI is also shown as a tropical profile (in Figure 6.5(a)). The dashed grey and orange horizontal lines denote the height of the cold point tropopause for the years 2000 and 2100, respectively. Averaged over the tropics, tropospheric mixing ratios of VSLs decrease by ~ 0.3 pmol/mol whereas stratospheric mixing ratios just above the tropopause increase by the same value. The minor reduction of SGs below 500 hPa

may be related to an increase of convective outflow. The largest changes of SGI and PGI in the tropics occur in ~ 70 hPa which is consistent with the position of the largest acceleration of upward motion (Figure 6.3(b)). The pattern for the product gases from

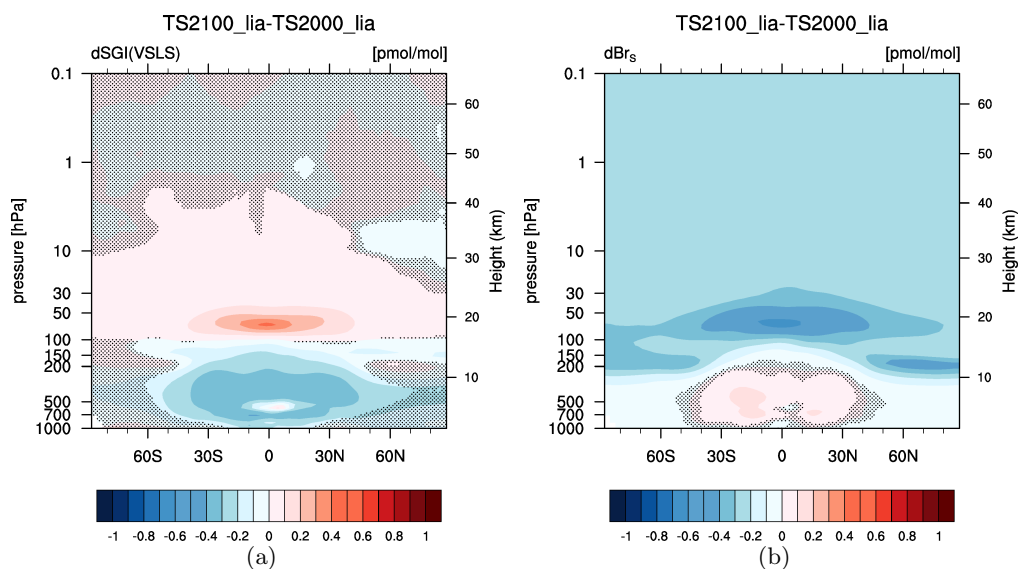


Figure 6.4: Difference (in pmol/mol) of a) zonal mean Source Gas Injection and b) Product Gas Injection from VLSL between TS2100lia and TS2000lia. Differences that are not significant according to a t-test (95 % confidence level) are shaded.

VLSL (Br_S) is opposed (Figure 6.4(b)). The tropospheric abundance of the VSL PGs tends to increase by up to 0.2 pmol/mol. In the stratosphere mixing ratios decrease by up to 0.7 pmol/mol above the tropical tropopause and 0.5 pmol/mol in the polar lower stratosphere.

In addition to dynamical changes VLSL undergo a varied atmospheric chemistry due to climate change. An increase of the tropospheric temperature by up to 6 K (Figure 6.6(b)) yields to raised water vapour that in turn increases the tropospheric OH abundance (Figure 6.6(a)). More available OH and the positive temperature dependence of the reaction rates (Figure 6.6(d)) enhances the VLSL degradation by oxidation in the troposphere. This contributes to a reduction in the tropospheric mixing ratios of the SGs and to a small increase of Br_S (Figure 6.4). The temperature dependence of the reaction with OH leads to reduced reaction rates above the tropopause due to decreasing stratospheric temperatures (see Figure 6.6(d) using the example of $CHBr_3$). This fact probably also contributes to the decrease of VSL product gases in the stratosphere. There are no significant differences between the photolysis reaction rates in *TS2000lia* and *TS2100lia*.

In 2100, stratospheric bromine is reduced by ~ 7 pmol/mol compared to the year 2000. This decrease arises primarily from the phase out of long-lived bromine compounds (see Figure 6.6(c)). The fraction of VSL SGI and PGI is dependent on the position of the cold point tropopause. Hossaini et al. (2012b) reported an increase of

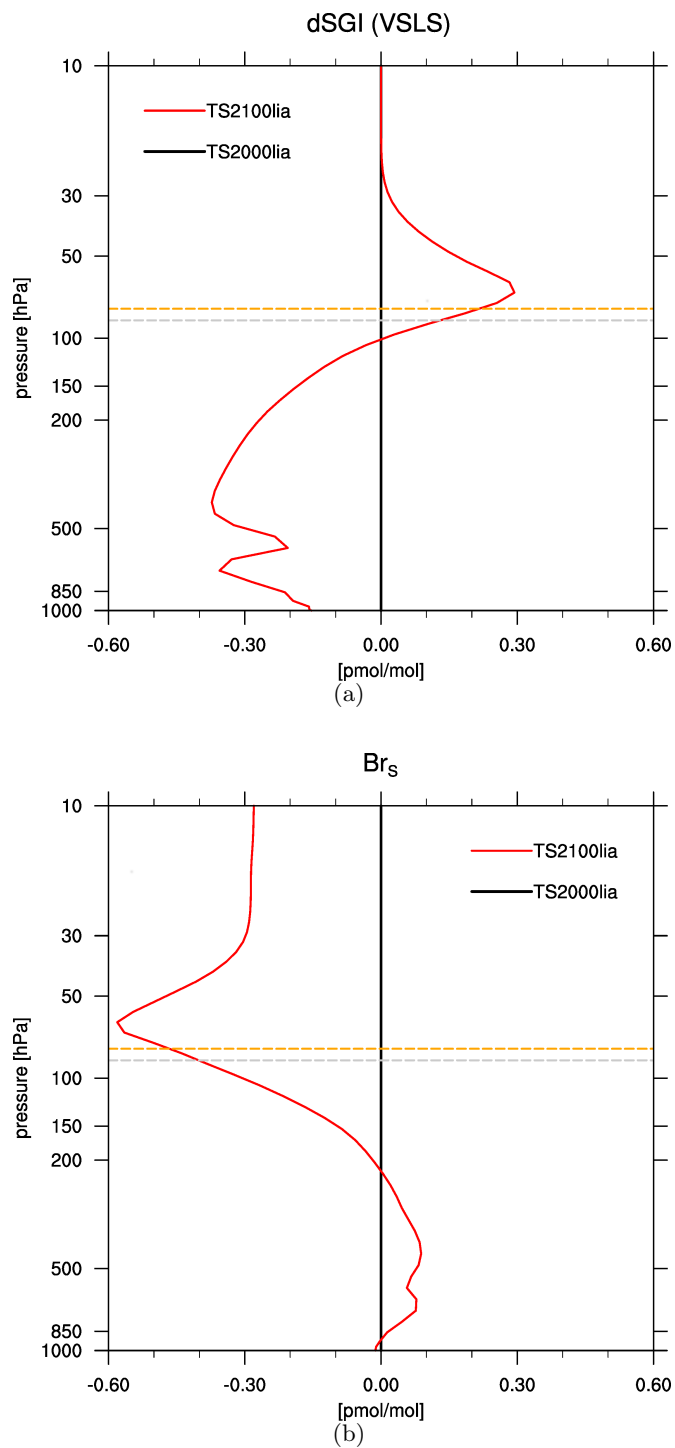


Figure 6.5: Zonal mean change (in pmol/mol) in 2100 with respect to 2000 of a) SGI and b) PGI in the tropics ($\pm 20^\circ$). The horizontal dashed lines denote the cold point tropopause in 2000 (grey) and 2100 (orange).

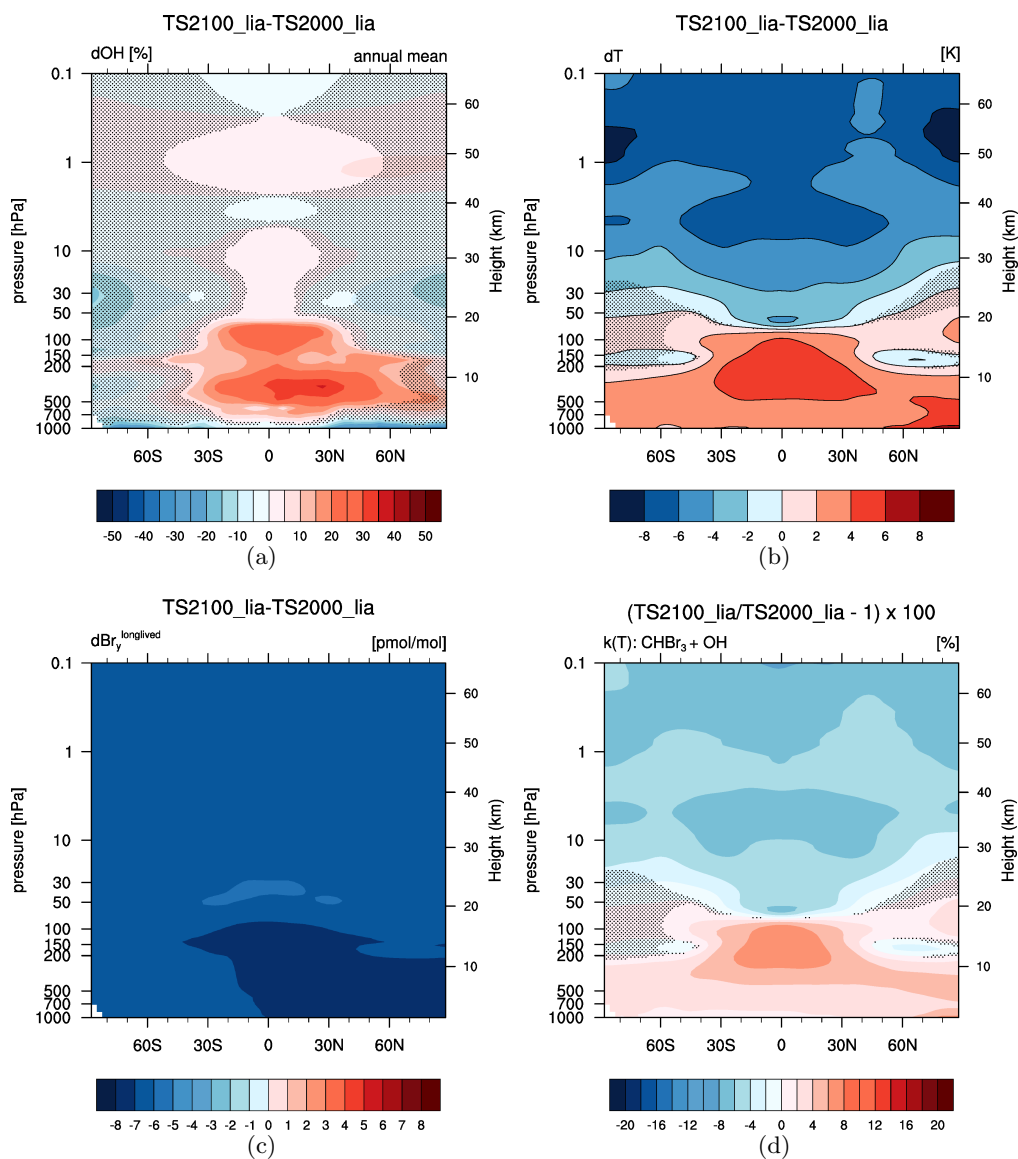


Figure 6.6: Difference of zonal mean a) OH (in %), b) temperature (in K), c) bromine from long-lived source gases (in pmol/mol), and d) reaction rates of $\text{CHBr}_3 + \text{OH}$ (in %) between TS2100lia and TS2000lia. Differences that are not significant according to a t-test (95 % confidence level) are shaded.

SGI by 0.3 pmol/mol until 2100 with respect to the year 2000 when using the greenhouse gas scenario RCP4.5 in their chemistry-climate model instead of the RCP6.0 used in this study. Considering the changed position of the cold point tropopause (CPT) in 2000 and 2100 for the determination of SGI, the increase is not visible in the simulations of this study. However, when using only the position of the CPT of the year 2000 for both simulations yields also in an increase of SGI by 0.3 pmol/mol. Overall, the total contribution of VSLS to the stratospheric bromine is by 0.3 pmol/mol ($\sim 5\%$) smaller than in 2000 amounting to 5.0 pmol/mol in 2100. An enhanced vertical transport through an accelerated Brewer-Dobson-Circulation enables more VSLS to reach the stratosphere before being degraded photochemically. In addition, the colder stratosphere in response to the rising greenhouse gas emissions, decelerates the chemical VSLS depletion reactions. Both processes lead to a reduction of Br_S in the stratosphere. On the other hand, an increase of OH and temperature in the troposphere favors the reaction of VSLS with OH, leading to a small increase of the product gas Br_S in the troposphere.

6.2 Impact of VSLS on Stratospheric Ozone

Previously, it was shown that brominated VSLS contribute to stratospheric ozone loss under 2000's climate conditions, particularly through the coupled BrO_x - ClO_x cycle (see Section 5.2). The phase out of long-lived ozone depleting substances in the framework of the Montreal Protocol leads to a recovery of the future stratospheric ozone layer in most latitudes (Figure 6.7(a)). Stratospheric chlorine Cl_y decreases in all latitudes with respect to 2000's values (Figure 6.7(b)). In the polar lower stratosphere the reduction amounts to ≥ 600 pmol/mol (-70%), in the upper stratosphere ~ 1800 pmol/mol (-70%). Consequently, polar stratospheric ozone values increase by ~ 500 nmol/mol (20%). Above the tropical tropopause a reduction by up to 300 nmol/mol (-35%) of stratospheric ozone is obvious. The increased tropical upwelling and the accelerated Brewer-Dobson-circulation (Figure 6.3(b)) enhance the transport of O_3 from the tropics to higher latitudes yielding to additional O_3 in the polar stratosphere and less ozone in the tropics (Shepherd, 2008).

The VSLS induced ozone loss in the year 2100 can be illustrated when subtracting the no-VSLS simulation *TS2100zero* from the reference simulation *TS2100lia*. Averaged annually, stratospheric ozone is reduced globally by $\sim (20-30)$ nmol/mol through VSLS (see Figure 6.8(a)). The largest O_3 loss occurs in the southpolar stratosphere with 45 nmol/mol (-1%). In 2000 the maximum ozone loss through VSLS appears during spring of the Southern hemisphere (SH), particularly in October (see Section 5.2). In 2100, October ozone values are diminished by up to 114 nmol/mol in the south polar stratosphere (Figure 6.8(b)). Mainly, due to the phase out of long-lived halogens absolute polar ozone values are significantly larger in 2100 than in 2000 (Figure 6.7(a)).

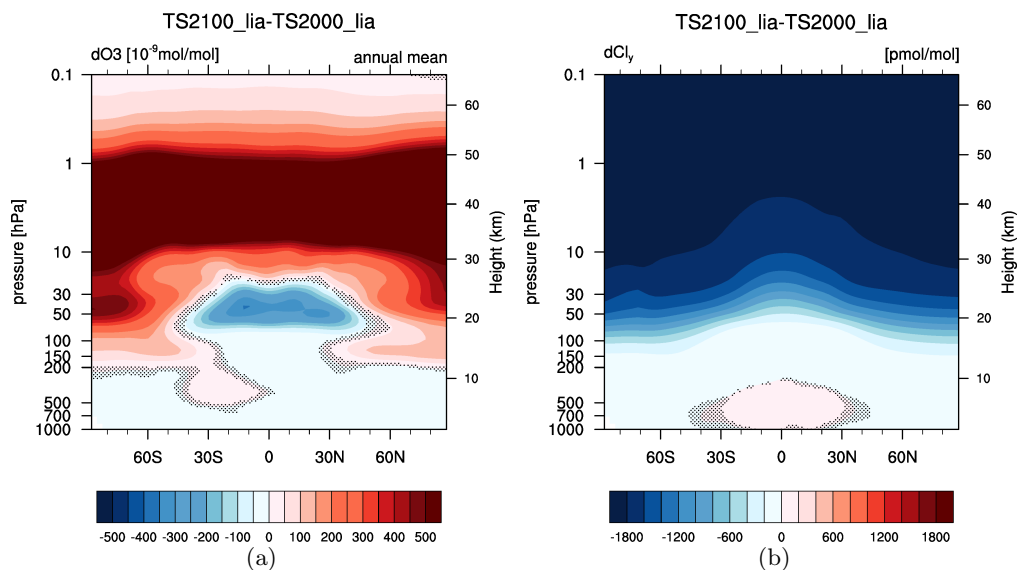


Figure 6.7: Difference in zonal mean a) ozone mixing ratio (in nmol/mol) and b) Cl_y mixing ratio (in pmol/mol) between TS2100lia and TS2000lia. Differences that are not significant according to a t-test (95 % confidence level) are shaded.

Thus, the October ozone loss induced by VSLS corresponds to only $\sim 4\%$ of the total ozone. Additionally, VSLS induced O_3 loss in 2100 underlies a weaker seasonality than in 2000 and generally lies in the range of (2–4)%. Maximum O_3 loss occurs in SH summer (i.e. in December -4.1% of total O_3) and minimum loss in SH winter (in July -2.4%). Again, this confirms that VSLS are most efficient in depleting ozone when the abundance of chlorine is high (e.g. Yang et al., 2014). In the region of the highest ozone loss induced by VSLS (90°S – 60°S , (70–30) hPa) the abundance of active chlorine (ClO) significantly decreases from year 2000 to 2100 (see Figure 6.10). Maximum values of ClO in SH spring are reduced by ~ 180 pmol/mol. Simultaneously, O_3 mixing ratios increase over the whole year, in SH spring by up to 1000 nmol/mol. The ozone hole is no longer visible.

The zonal column ozone indicates also a recovery of the ozone layer in 2100 (Figure 6.9(a)). With respect to 2000’s values the polar ozone column increased by ~ 70 DU (15%) at the Northern hemisphere and 100 DU (30%) at the Southern hemisphere during the corresponding spring months (Figure 6.9(b)). Only in the tropics a decrease by ≤ 10 DU (-3%) is visible that is caused by the accelerated Brewer-Dobson-Circulation and slower ozone producing reaction rates in the stratosphere (e.g. Meul et al., 2016).

The contribution of VSLS to the ozone column loss is obtained by subtracting $TS2100_{zero}$ (no VSLS emissions) from $TS2100_{lia}$ (Figure 6.9(c)). Considering brominated VSLS leads to a global reduction of the O_3 column. About 4 DU ($\leq -1\%$) less ozone is present at the North Pole and up to 7 DU ($\sim 2\%$) near the South Pole during the corresponding spring. In the tropics and mid latitudes the impact is less distinct and adds up to 2 and 3 DU ($\leq 1\%$), respectively.

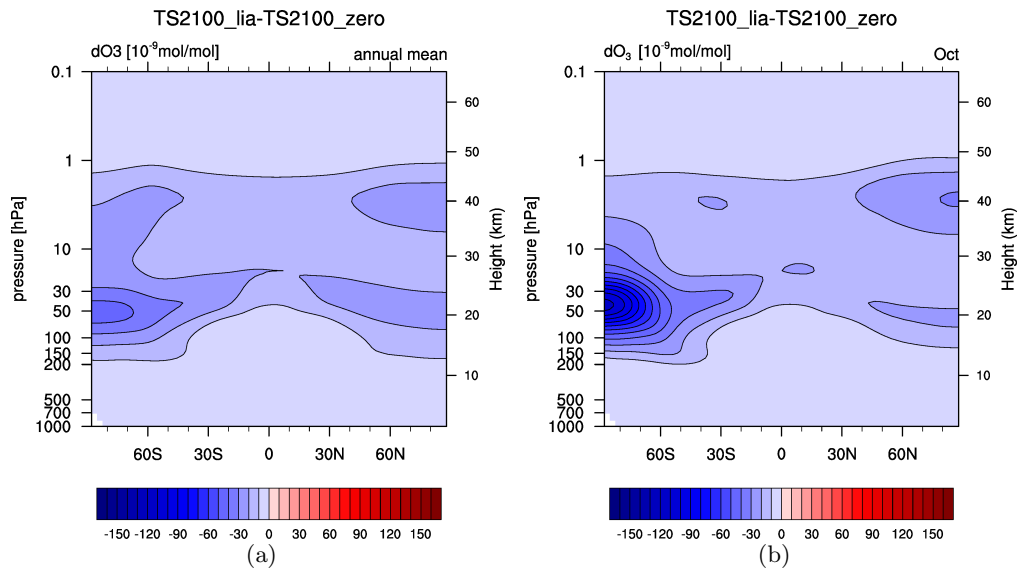


Figure 6.8: Difference in zonal mean ozone mixing ratio (in nmol/mol) between TS2100lia and TS2100zero of a) the annual mean and b) the October mean.

The contribution of VSLS to stratospheric ozone loss is in 2100 significantly smaller than in 2000. While in October 2000 up to 200 nmol/mol (-14%) less ozone is available in the lower Antarctic stratosphere, the equivalent ozone values in 2100 are reduced by at most 114 nmol/mol (-4%). The abundance of bromine from VSLS changes only little (from 5.3 pmol/mol to 5 pmol/mol). Rather the reduction of available chlorine limits the effective chemical depletion of ozone via the coupled $\text{BrO}_x\text{-ClO}_x$ cycle. Yang et al. (2014) conducted chemistry-climate simulations with differing chlorine backgrounds. When increasing the VSLS burden they found a larger ozone destruction under a high chlorine background indicating the importance of the coupled chlorine-bromine reactions.

6.3 Climatic Impact of a Potential VSLS Emission Scenario

Probably the most challenging fact in simulating very short-lived halogens is that only little is known about the sources. It is still highly uncertain how perturbed environmental factors like salinity, wind stress, air and sea surface temperatures and many others might influence the source strengths. It was previously shown that VSLS contribute significantly to the stratospheric bromine burden and also affect the stratospheric ozone layer under recent climate conditions and under a projected future climate when VSLS emissions stay constant. Now it must be investigated how a potential increase of VSLS emissions may alter stratospheric bromine and ozone. Due to the lack of reliable data on the future emission strength of VSLS, VSLS emissions are multiplied by an arbi-

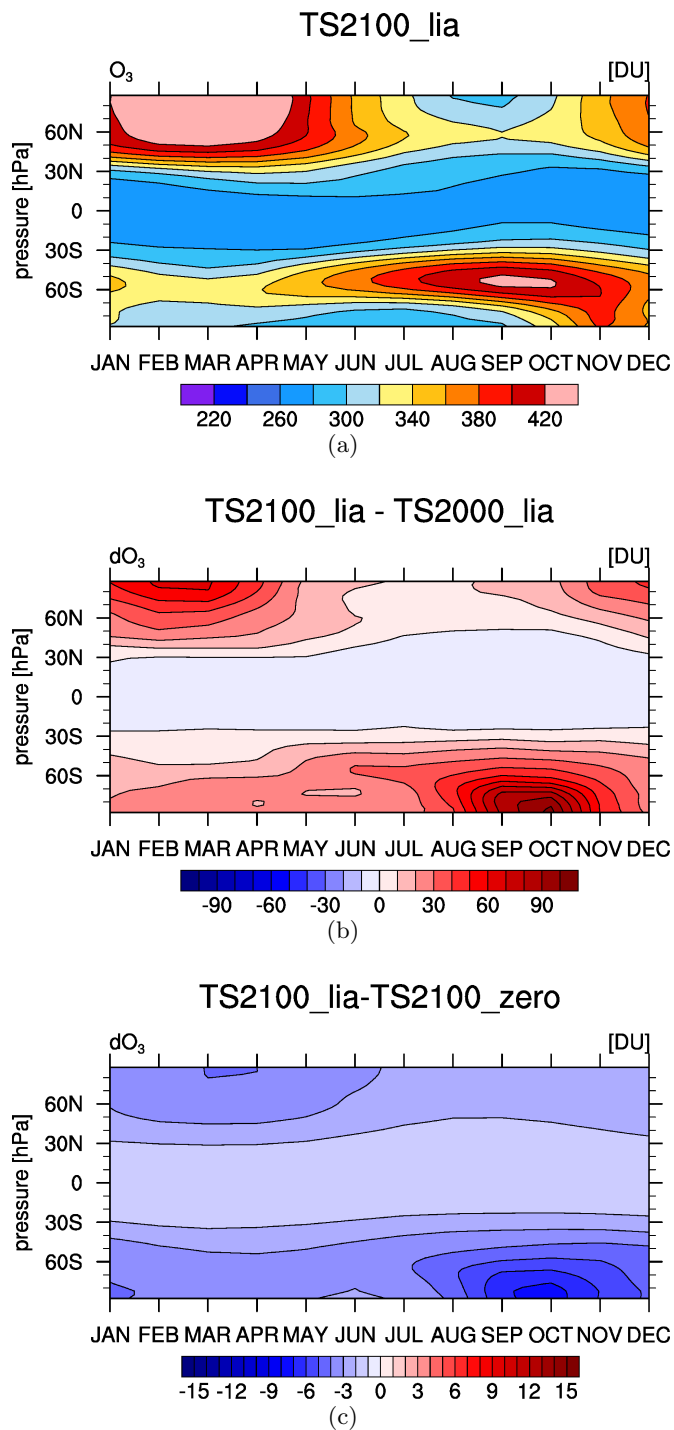


Figure 6.9: Seasonal variation of zonal column O_3 (in DU) a) in TS2100lia b) difference between TS2100lia and TS2000lia and c) difference between TS2100lia and TS2100zero.

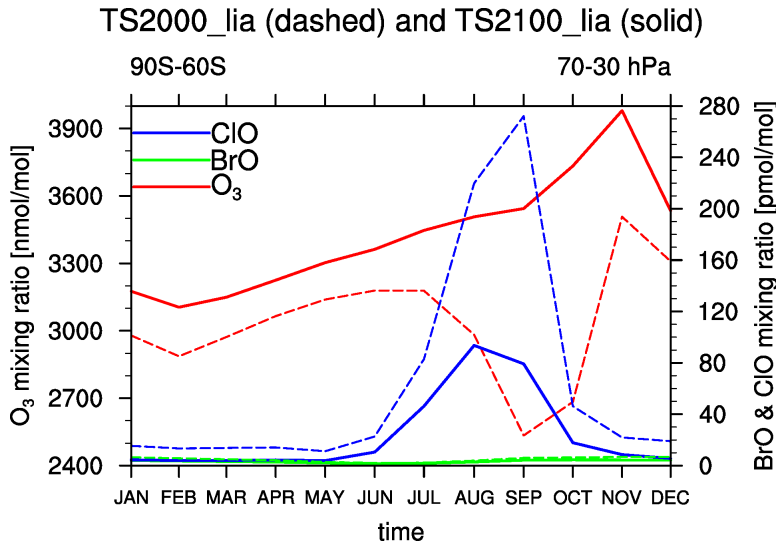
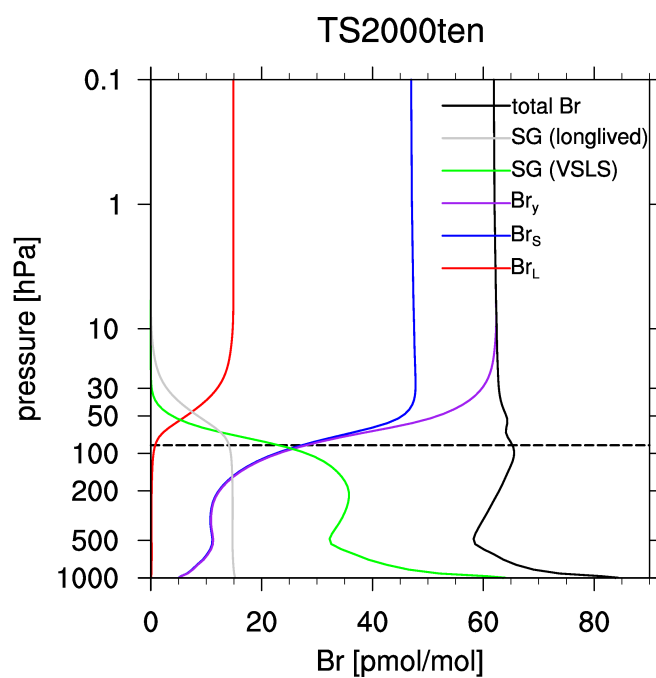


Figure 6.10: Seasonal variation of ozone (in nmol/mol; left y-axis), BrO and ClO (in pmol/mol; right y-axis) for south polar latitudes in 70-30 hPa for the year 2000 (dashed lines) and 2100 (solid lines).

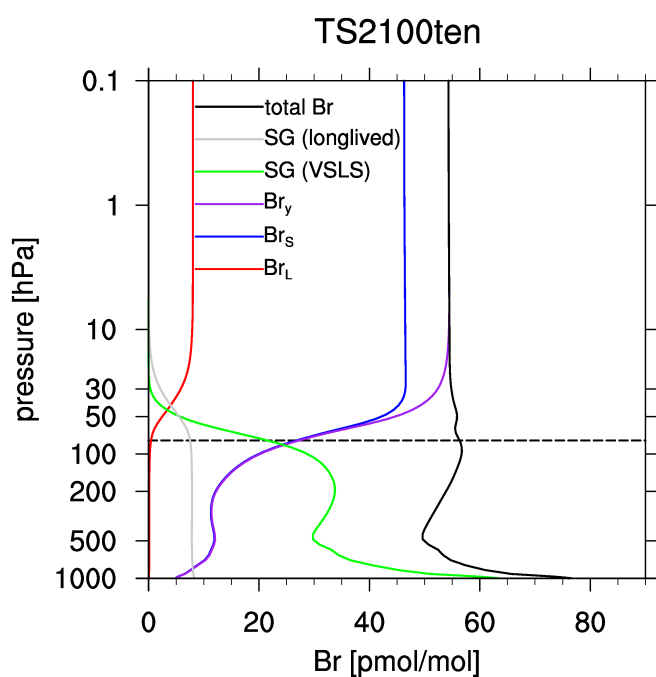
trary factor 10. This approach enables to determine if an increase of surface emission also increases the stratospheric bromine loading and the ozone depletion induced by VSLS. Two simulations with 10xVSLS emissions called *TS2000ten* and *TS2100ten* are compared to the previously discussed simulations.

6.3.1 Bromine Loading

Initially, the tropical profiles of those compounds are shown that contribute to the total atmospheric bromine in 2000 and 2100 (Figure 6.11). When comparing the vertical distribution of bromine compounds in *TS2000ten* (Figure 6.11(a)) to that of *TS2000lia* (Section 5.1, Figure 5.1) it is particularly notable that surface mixing ratios of very short-lived (VSL) source gases (SGs, green line) increased by a factor of almost 10 from 7 pmol/mol to 65 pmol/mol. This result is as expected due to the prescribed emissions. The VSL source gases have a strong tropospheric gradient as they are depleted efficiently in the troposphere by photochemistry. With increasing height, VSL source gases decrease whereas the VSL product gases (called Br_S , blue line) increase. At the Earth's surface Br_S amounts to approximately 5 pmol/mol compared to ~ 1 pmol/mol in the reference simulation *TS2000lia*. The long-lived source gases (grey line) show almost no tropospheric gradient and contribute ~ 15 pmol/mol to the total bromine burden in the troposphere. As VSLS make up the main fraction of the total tropospheric bromine burden (black line) it shows a similar gradient as the VSL source gases. At the surface total bromine adds up to ~ 85 pmol/mol, around the tropopause it amounts to 65 pmol/mol. The values at the tropical cold point tropopause (horizontal black dashed line) are commonly used as a measure to estimate the input of VSLS into the stratosphere. Here, the VSL source gases account for 24.3 ± 1.1 pmol/mol and the VSL prod-



(a)



(b)

Figure 6.11: Annual mean profile of zonally averaged bromine mixing ratios in the tropics ($\pm 20^\circ$) in a) TS2000ten and b) TS2100ten. Shown are long-lived and very short-lived source gases (SG), inorganic bromine (Br_y), total bromine, and the contribution of VLSL product gases (Br_s) and long-lived product gases (Br_L) to Br_y . The dashed horizontal line denotes the position of the cold point tropopause.

uct gases 26.2 ± 0.7 pmol/mol adding up to 50.5 ± 0.9 pmol/mol bromine from VSLS entering the stratosphere. The uncertainty range arises from the year-to-year variability of the results. In the reference simulation *TS2000lia* with 1xVSLS emissions resulted in a contribution of VSLS to total bromine ($\text{Br}_y^{\text{VSLS}}$) of 5.3 ± 0.1 pmol/mol. Thus, the multiplication of the VSLS surface emissions with 10 leads approximately to a tenfold increase of $\text{Br}_y^{\text{VSLS}}$ in the stratosphere.

The tropical profile of the 10xVSLS future simulation *TS2100ten* (Figure 6.11(b)) differs from the corresponding 2000 simulation primarily in the amount of long-lived gases restricted in the Montreal Protocol. While in 2000 tropospheric mixing ratios add up to ~ 15 pmol/mol, in 2100 only ~ 8 pmol/mol bromine is provided by long-lived substances in the troposphere. This is consistent to previous results of the reference simulations *TS2000lia* and *TS2100lia* (see Section 6.1). Moreover, the height of the cold point tropopause (CPT) changes from 86 hPa in 2000 to an altitude of 78 hPa in 2100. As already noted, the position of the CPT alters the absolute values of source gas and product gas injection but not the total injection of VSLS. At the CPT the VSL source gases amount to 23.1 ± 1.3 pmol/mol and Br_S 25.4 ± 0.9 pmol/mol. This value consists of 20.1 pmol/mol bromine by the major VSLS CHBr_3 and CH_2Br_2 . The minor VSLS account for 3.1 pmol/mol (see also Table 6.2). Thus, $\text{Br}_y^{\text{VSLS}}$ adds up to 48.5 ± 0.8 pmol/mol from a total bromine burden of 56.5 ± 0.9 pmol/mol. With respect to *TS2000ten* altogether ~ 9 pmol/mol less bromine is available at the CPT. From this reduction ~ 2 pmol/mol arise from a decreased contribution of VSLS. This is consistent to values in the reference simulations *TS2000lia* and *TS2100lia* where $\text{Br}_y^{\text{VSLS}}$ also decreased from 2000 to 2100 by 0.3 pmol/mol. A summary of the values

Table 6.2: Contribution of VSLS to stratospheric Br_y in pmol/mol in the simulations *TS2000lia*, *TS2100lia* and the corresponding simulations with VSLS emissions increased by a factor of 10 *TS2000ten* and *TS2100ten*. Major VSLS are CHBr_3 and CH_2Br_2 , minor VSLS are CH_2ClBr , CHCl_2Br and CHCl_2Br_2 .

Simulation	SGI (major VSLS)	SGI (minor VSLS)	PGI	$\text{Br}_y^{\text{VSLS}}$
<i>TS2000lia</i>	2.2	0.33	2.8	5.3
<i>TS2000ten</i>	21.2	3.1	26.2	50.5
<i>TS2100lia</i>	2.1	0.31	2.6	5.0
<i>TS2100ten</i>	20.1	3.0	25.4	48.5

at the tropical cold point tropopause for all simulations can be found in Table 6.2.

The global contribution of VSLS to the total bromine amount is obtained when subtracting the no-VSLS simulation *TS2000zero* from the corresponding 10xVSLS simulation *TS2000ten* (Figure 6.12(a)). The tenfold increased surface emissions lead to a very similar distribution as in the reference simulation *TS2000lia* (see Figure 5.2(b)). High mixing ratios near the surface are rapidly diminished with increasing height due to photochemical depletion of the VSLS. In the stratosphere VSLS account for ~ 50 pmol/mol additional bromine compared to the ~ 5 pmol/mol bromine in the reference simulation.

In 2100, the contribution of VSLs to Br_y decreases in the troposphere by up to ~ 2 pmol/mol, in polar regions of the lower stratosphere even by 3 pmol/mol (6%). With increasing altitude the difference to the year-2000 simulations is smaller and amounts to ~ 0.7 pmol/mol (1%). Generally, the same processes are accountable that were already discussed in Section 6.1 and can be related to rising greenhouse gas emissions. An increased tropical upwelling and accelerated Brewer-Dobson-Circulation favor the transport of intact VSL source gases into the stratosphere before being degraded. Moreover, the cooling of the stratosphere leads to slower VSLs-depleting chemical reactions.

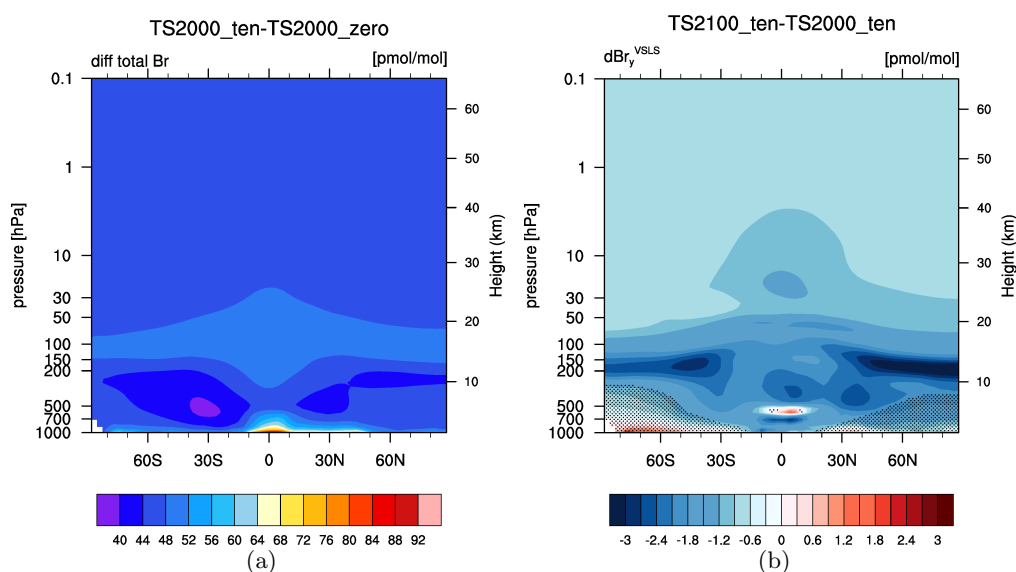


Figure 6.12: a) Contribution of VSLs (in pmol/mol) to zonal total bromine ($\text{TS2000}_{\text{ten}} - \text{TS2000}_{\text{zero}}$) and b) differences in zonal $\text{Br}_y^{\text{VSLs}}$ between $\text{TS2100}_{\text{ten}}$ and $\text{TS2000}_{\text{ten}}$. Differences that are not significant according to a t-test (95 % confidence level) are shaded.

OH mixing ratios in the 10xVSLs and the 0xVSLs simulations differ significantly. Increasing the VSLs emissions leads in both simulation pairs to a decrease of OH around the tropical tropopause by up to 25 % (see Figure 6.13). Apart from that region, an increase of OH mixing ratios is visible, particularly in the polar regions of the upper troposphere and lower stratosphere (up to 55 %).

A tenfold increase of the prescribed surface emissions leads approximately to a tenfold increase of the VSLs injection into the stratosphere. While in the simulations with reference emissions ($\text{TS2000}_{\text{lia}}$ and $\text{TS2100}_{\text{lia}}$) $\text{Br}_y^{\text{VSLs}}$ amounts to 5.3 ± 0.1 pmol/mol in 2000 and 5.0 ± 0.1 pmol/mol in 2100, the corresponding simulations with 10xVSLs surface emissions lead to 50.5 ± 0.9 pmol/mol and 48.5 ± 0.8 pmol/mol bromine from VSLs. Moreover, considering VSLs in the simulations alters the oxidation capacity of the atmosphere through changes in the OH abundance.

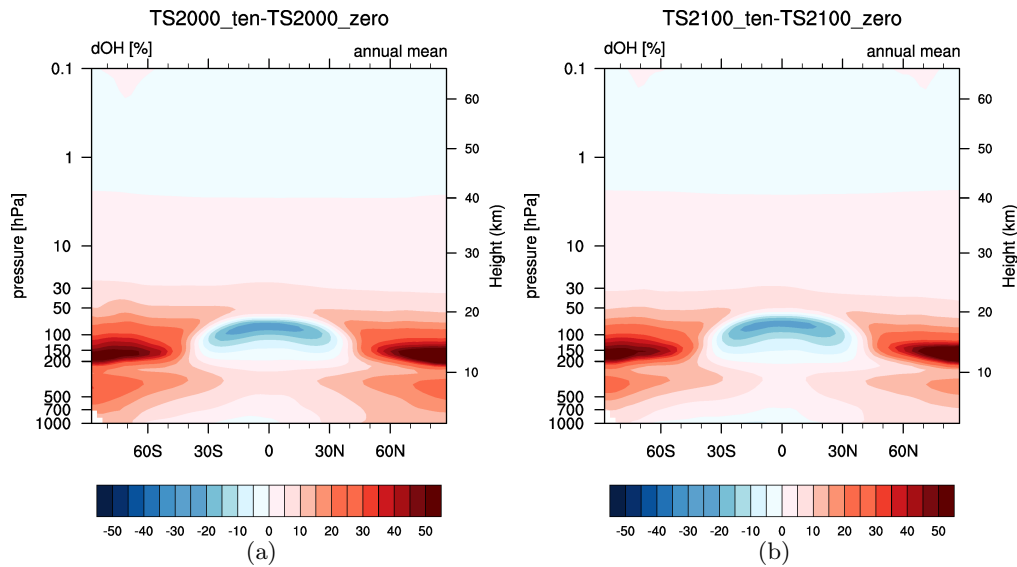


Figure 6.13: a) Zonal mean differences of OH between a) TS2000ten and TS2000zero and b) TS2100ten and TS2000zero. Differences that are not significant according to a t-test (95 % confidence level) are shaded.

6.3.2 Impact on Ozone Loss

The previous section showed that an increase of the VSLS surface emissions comparably increases the injection of bromine into the stratosphere. However, it was also shown that the impact of VSLS on stratospheric ozone is limited by the available atmospheric chlorine. Therefore, it must be investigated if this significant increase of Br_y simultaneously decreases stratospheric ozone values.

Differences between the simulations *TS2000ten* and *TS2000zero* present the contribution of increased VSLS mixing ratios on atmospheric ozone (Figure 6.14). Averaged over all months of the year VSLS lead to reduction of the stratospheric ozone burden. The impact is largest in the south polar stratosphere from the tropopause to ~ 30 hPa. Between 100 hPa and 50 hPa ozone values are reduced by up to 600 nmol/mol (-35%) (Figure 6.14(a)). In October stratospheric ozone is reduced by ~ 1000 nmol/mol (-70%) in the same region (Figure 6.14(b)).

In 2100, halogens from long-lived compounds are significantly reduced (see e.g. Figure 6.7(b)). The influence of VSLS on stratospheric ozone is still visible but considerably smaller. In the south polar stratosphere - the region with the largest ozone depletion - annual O_3 mixing ratios are reduced by ~ 500 nmol/mol. In October ozone values are reduced by ~ 1000 nmol/mol. As absolute ozone values are significantly larger in 2100 than in 2000 in response to the declining halogen loading from long-lived compounds, the relative difference with respect to the no-VSLS simulation here amounts to $\sim -25\%$ for the annual mean and $\sim -40\%$ for the October mean in the south polar stratosphere.

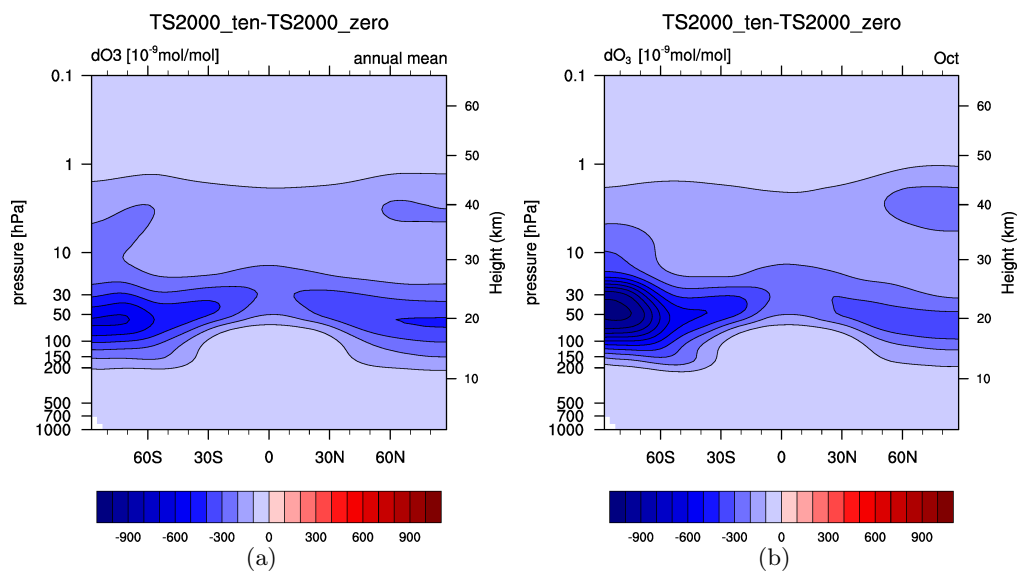


Figure 6.14: Differences in zonal mean ozone mixing ratio (in nmol/mol) between TS2000ten and TS2000zero of the a) annual mean and b) October mean.

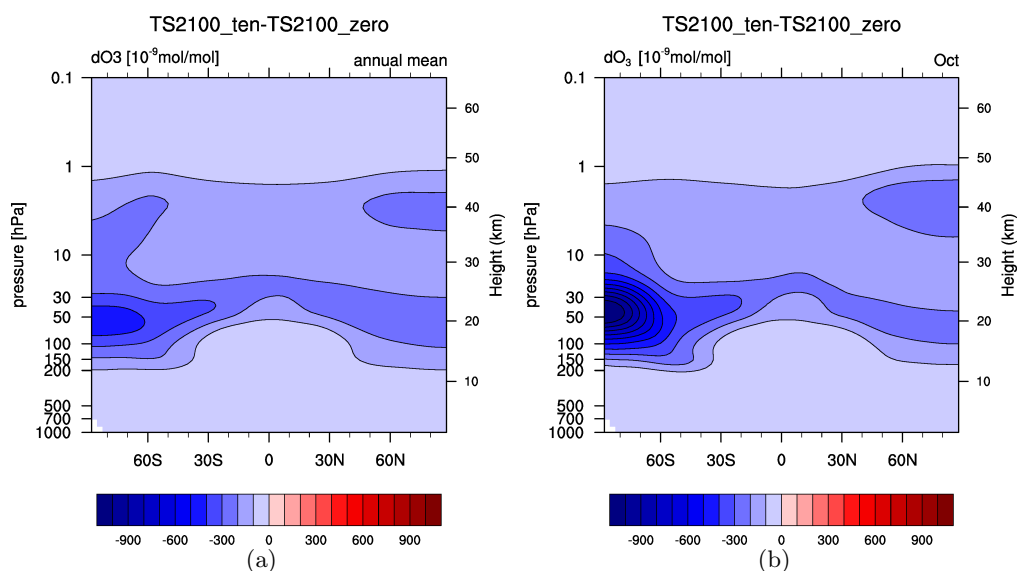


Figure 6.15: Differences in zonal mean ozone mixing ratio (in nmol/mol) between TS2100ten and TS2100zero of the a) annual mean and b) October mean.

As in the reference simulations *TS2000lia* and *TS2100lia* the impact of the VSLS on stratospheric ozone is reduced in 2100. This indicates again that the declining chlorine abundance hampers the effective ozone depletion by brominated VSLS. In the south polar stratosphere, O_3 values of simulation *TS2000ten* are significantly smaller (~ -300 nmol/mol) than in the reference simulation over the whole year (see Figure 6.16). When ClO maximizes in late winter and early spring (July-September) the differences between *TS2000lia* and *TS2000ten* increase. In *TS2000ten* September ozone values are approximately 1100 nmol/mol smaller than the corresponding values in *TS2000lia*. It is notable that values of ClO also differ between the simulations although only the emission of brominated VSLS are varied in the set-up. Possibly the ClO producing ClO_x cycle 1 (see Section 2.1.1) is limited through the high amount of available bromine that reacts with O_3 via the BrO_x cycle. The future seasonal variation of O_3 in the

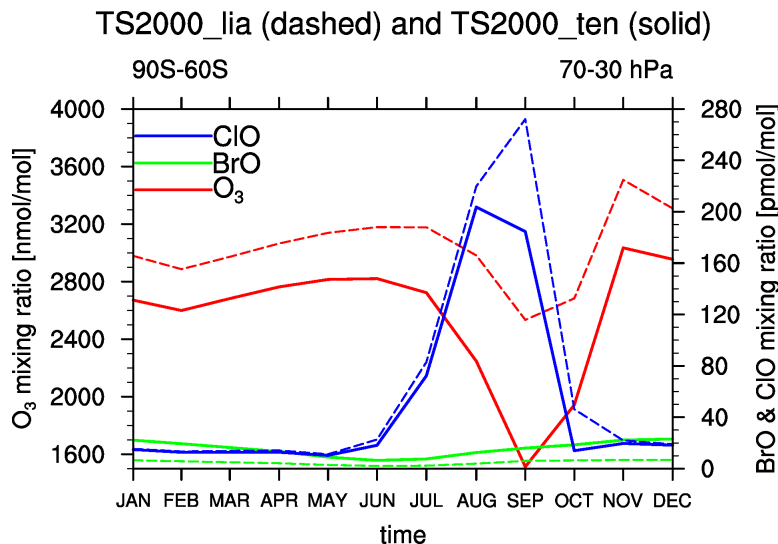


Figure 6.16: Seasonal variation of ozone (in nmol/mol; left y-axis), BrO and ClO (in pmol/mol right y-axis) for southpolar latitudes in 70-30 hPa in *TS2000lia* (dashed lines) and *TS2000ten* (solid lines).

stratosphere over Antarctica shows no obvious ozone hole in the reference simulation (dashed red line in Figure 6.17). With increased VSLS emissions the typical ozone loss in the SH spring months is however obvious with ~ 700 nmol/mol less ozone than in the reference simulation (solid red line). The largest ozone depletion again occurs when ClO maximizes.

A tenfold increase of the VSLS surface emissions enhances the input of bromine into the stratosphere by a factor of approximately 10, both in the year 2000 and 2100. The impact on stratospheric ozone is also intensified. While in the reference simulation *TS2000lia* VSLS locally depleted up to 3% of the total ozone, in *TS2000ten* 35% are depleted in the stratosphere over the South Pole. In October the depletion increased to 70% in *TS2000ten* compared to 14% in the corresponding reference simulation. In response to decreasing chlorine emissions the ozone depletion via the coupled ClO_x -

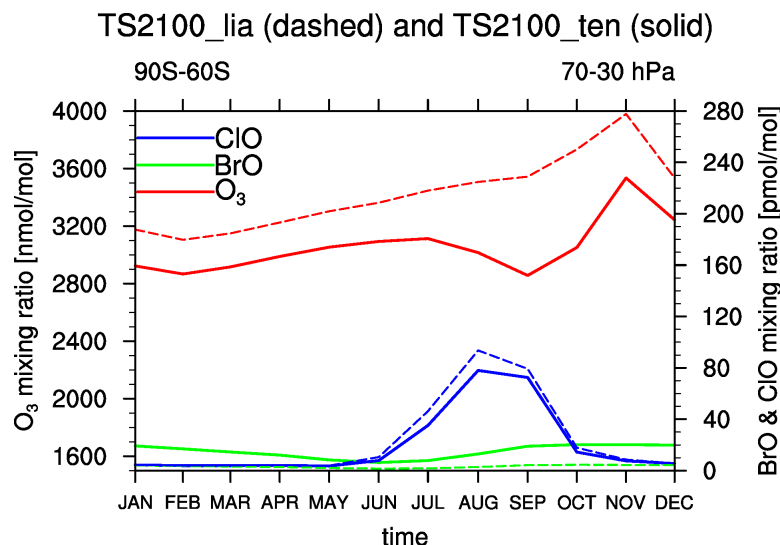


Figure 6.17: Seasonal variation of ozone (in nmol/mol; left y-axis), BrO and ClO (in pmol/mol right y-axis) for south polar latitudes in 70-30 hPa in TS2100lia (dashed lines) and TS2100ten (solid lines).

BrO_x cycle is hampered in 2100. Thus, the impact of VSLS on ozone loss is reduced in *TS2100ten* and amounts to annually averaged 25 % and in October 40 % compared to 1 % and 4 % in *TS2100lia*. These results suggest that a potential increase of VSLS surface emissions probably delays the projected recovery of the ozone layer, particularly on the Southern hemisphere and therefore must be taken into account to reliably simulate future stratospheric ozone values.

6.4 Implication of Changed VSLS Emissions on Radiative Forcing

The simulations performed within this study are all QCTM simulations meaning that dynamics and chemistry do not feedback (see Section 3.3.1 for more details). A chemical perturbation, in this case a change in VSLS surface emissions, alters the chemical quantities but does not feedback on the dynamics or radiation. The following section should give a brief overview of the radiative effect of VSLS.

In all QCTM simulations of the same time period the dynamics and radiation are equally prescribed with the climatological fields of the corresponding coupled preparatory simulation (i.e. *TS2000* and *TS2100*). EMAC calls the climatological fields of radiative quantities in a first call (“rad01”) yielding in equal dynamics in the QCTM simulations. To address the effect of the perturbed emissions on the radiation budget EMAC calls the perturbed radiation quantities - only for diagnostic purposes - a second time. It is important to remember, that the model does not use the perturbed quantities but the climatological fields of the preparatory simulation for further calculations (see also Dietmüller et al., 2016). The difference of the net radiative flux

(= *shortwave flux* + *longwave flux*) between the first (“rad01”) and second (“rad02”) radiation call is here defined as “radiative forcing” (RF). An instantaneous globally and annually averaged radiative forcing is determined at the climatological tropopause.

Apart from the QCTM set-up the simulation *TS2000lia* is conducted identically to the preparatory coupled simulation *TS2000*, thus also using identical VSLS surface emissions. Consequently, the difference rad02-rad01 can be considered as the uncertainty range made by using the QCTM approach, i.e. climatological fields of the radiative quantities instead of instantaneous values. The radiative forcing for *TS2000lia* amounts to -0.03 W/m^2 .

The no-VSLS simulation *TS2000zero* has higher stratospheric ozone mixing ratios than the reference simulation with VSLS (see Section 5.2). The positive ozone perturbation leads to a positive RF of 0.06 W/m^2 with respect to the coupled reference simulation. In other words, considering the $\sim 5 \text{ pmol/mol}$ extra bromine from VSLS induces a negative RF of -0.06 W/m^2 .

The 10xVSLS simulation *TS2000ten* has a negative ozone perturbation due to a higher stratospheric bromine loading (see Section 6.3.2). The radiative forcing with respect to the 1xVSLS coupled simulation *TS2000* is -0.30 W/m^2 .

The 2100 simulations show the same signs. Here, the uncertainty made by using the QCTM set-up account to 0.02 W/m^2 . The simulation with no VSLS emissions *TS2100zero* has a RF of 0.05 W/m^2 consistent to a positive ozone perturbation. The simulation with tenfold increased VSLS emissions yields in a RF of -0.28 W/m^2 .

The values of the 0xVSLS simulations are probably not significant as they are of the same order of magnitude as the uncertainty due to the QCTM approach. However, they are in good agreement with results by Hossaini et al. (2015) who found a radiative effect of brominated VSLS of -0.06 (-0.035 to -0.096) W/m^2 in 2011.

Table 6.3: Radiative forcing at the climatological tropopause with respect to the corresponding coupled reference simulation with 1x VSLS emissions (TS2000 and TS2100). All values are in W/m^2

Simulation	RF
TS2000lia	-0.03
TS2000zero	+0.06
TS2000ten	-0.30
TS2100lia	+0.02
TS2100zero	+0.05
TS2100ten	-0.28

The results (summarized in Table 6.3) indicate the following: VSLS affect the ozone layer in the lower stratosphere and therefore the radiative budget. In contrary to long-lived halogen compounds that are themselves radiatively active greenhouse gases with a warming effect, VSLS only cause a negative RF through ozone loss. The stratospheric ozone loss leads to less absorption of short-wave radiation and consequently

less long-wave radiation in the stratosphere yielding in lower stratospheric temperatures. More shortwave radiation is able to enter the troposphere probably inducing higher tropospheric temperatures (Riese et al., 2012; IPCC, 2013).

6.5 Summary

Chemical and dynamical changes let the years 2000 and 2100 differ significantly from each other. The success of the Montreal Protocol is visible in a decrease of bromine from long-lived compounds by ~ 7 pmol/mol. The total contribution of VSLS to the stratospheric bromine burden decreases from 5.3 ± 0.1 pmol/mol in 2000 to 5.0 ± 0.1 pmol/mol in 2100. The vertical transport of tropical VSL source gases is more accelerated due to an intensified tropical convection and an accelerated Brewer-Dobson circulation. An increase of ~ 0.5 pmol/mol above the tropical tropopause is visible as more VSLS are able to reach higher altitudes before being depleted in the stratosphere. Simultaneously, the tropospheric mixing ratios of VSL source gases decreases by ~ 0.4 pmol/mol in the tropics due to the enhanced vertical transport and elevated OH mixing ratios. The VSL product gases (Br_S) show a small increase (≤ 0.2 pmol/mol) in the tropical troposphere due to more available OH and higher temperatures that accelerate the VSLS depleting reaction with OH. Declining stratospheric temperatures however decelerate VSLS reactions with OH contributing to a reduction of Br_S by up to 0.7 pmol/mol above the tropical tropopause.

A reduced stratospheric halogen content due to the restriction of long-lived compounds yields in a recovery of the ozone layer. The largest ozone depletion due to VSLS is found in the lower stratosphere over Antarctica during spring. The impact of VSLS on ozone decreases from 14 % in 2000 to 4 % in 2100. This decrease is a result declining chlorine values hampering the effective ozone depletion via the coupled BrO_x - ClO_x cycle. The connection of background chlorine values to the VSLS-induced ozone loss was also shown in a study by Yang et al. (2014).

A tenfold increase of the VSLS surface emission leads to an approximately tenfold increase of bromine input into the stratosphere. Consequently, VSLS-induced ozone depletion intensifies to ~ 70 % in 2000 and 40 % in 2100 during spring of the Southern hemisphere.

VSLS have an impact on radiative forcing through their contribution to ozone loss. Considering ~ 5 pmol/mol additional bromine from VSLS in a year 2000 simulation leads to a radiative forcing of -0.06 W/m² compared to a simulation without VSLS emissions. This is consistent to a value of -0.06 (-0.035 to -0.096) W/m² reported by Hossaini et al. (2015). A tenfold increase of the VSLS surface emissions significantly enhances ozone loss and thus the impact on the radiation budget (RF -0.30 pmol/mol in 2000 and -0.28 pmol/mol in 2100).

Chapter 7

Summary and Conclusions

The fate of the stratospheric ozone layer has been topic of many studies and eventually led to global restriction of long-lived ozone depleting halogen compounds in the framework of the Montreal Protocol - "Perhaps the single most successful international agreement" as Kofi Annan once said. Until the early 2000's the stratospheric ozone depletion was attributed to long-lived halogen substances only. Measurements of the stratospheric bromine content however suggested an additional halogen source from very short-lived substances (VSLS) with a lifetime of less than six months. Despite their short lifetime VSLS are able to deliver bromine to the stratosphere and affect the stratospheric ozone layer but they are not regulated in the Montreal Protocol (e.g. Salawitch et al., 2005; Feng et al., 2007; Hossaini et al., 2015; Sinnhuber and Meul, 2015). Brominated VSLS arise predominantly from natural sources and there is still a lack of knowledge on their source strength and distribution. Particularly, it is highly unclear if the emissions might alter in a changing climate or due to increasing farming of seaweed (Ziska et al., 2013; Leedham et al., 2013). It is essential to increase the knowledge on VSLS, their distribution, transport and impact on ozone. Furthermore, it must be assessed how climate change alters the influence of VSLS and what impact a potential increase of VSLS emissions might have in the atmosphere.

The focus of this study was to investigate the impact of naturally emitted VSLS on the stratospheric chemistry and interactions with a changing climate. A new EMAC submodel (TBUDGET) was developed to identify halogen compounds from very short-lived source gases. With the chemistry-climate model EMAC several simulations were performed to increase the current understanding of VSLS. In the following the initially mentioned major questions will be answered and the results of this study summarized.

How well are VSLS represented in the chemistry-climate model EMAC?

The source strength and distribution of VSLS emissions is highly uncertain due to spatially and temporally variable sources and sparse measurements. These uncertainties are reflected in the input emissions required for the modelling of VSLS. In or-

der to simulate realistic VLS emissions with respect to their global distribution and strength, four recent emission inventories for the major VLS bromoform (CHBr_3) and dibromomethane (CH_2Br_2) and two emission inventories for methyl iodide (CH_3I) were applied in a set of four transient EMAC simulations from 2005 to 2012. The model results were evaluated and validated with observations from long-term ground based measurements and air-borne measurements from the SHIVA campaign.

The previous "standard" VLS emissions by Warwick et al. (2006) in the simulation *ref* were shown to significantly overestimate measured CHBr_3 values in the tropics and therefore likely the contribution of VLS to stratospheric bromine. In the extratropics measured CHBr_3 values were often underestimated. The reference simulation *ref* showed also larger CH_2Br_2 values than the observations in most latitudes. The seasonal cycle of both substances could be reproduced relatively good excluding the mid latitude sites.

The bottom-up emissions from Ziska et al. (2013) were applied in simulation *zis*. Except for the polar latitudes of the Northern Hemisphere (NH) CHBr_3 values in *zis* generally underestimated measurements. In the tropics and particularly in the West Pacific region *zis* led only to small discrepancies to CHBr_3 measurements. Observed CH_2Br_2 values were overestimated in *zis*, especially in the tropics and the Southern Hemisphere (SH). The seasonal variation of CHBr_3 and CH_2Br_2 was less well captured than in the other simulations.

The simulations *ord* and *lia* provided similar results due to large conformity in the inventories by Ordóñez et al. (2012) and Liang et al. (2010). Compared to CHBr_3 observations both simulations showed an overestimation in extratropical latitudes. In the tropics *ord* overestimated measured values and *lia* showed only small discrepancies to measurements. In the West Pacific region both simulations overestimated CHBr_3 observations. Observed values of CH_2Br_2 were relatively good captured with both inventories. The seasonal cycle was reproduced relatively good.

For CH_3I two emission inventories were applied to EMAC. The "standard" emissions by Bell et al. (2002) were used in simulation *ref* and the more recent bottom-up emissions by Ziska et al. (2013) were used in *zis*. CH_3I observations were overestimated in the extratropics and underestimated in the tropics in both simulations. The model was not able to reproduce the seasonal variations with either of the inventories. As the discrepancies to observations were larger in *zis* the "standard" emissions by Bell et al. (2002) were selected for further simulations.

Simulation *lia* with CHBr_3 and CH_2Br_2 surface emissions by Liang et al. (2010) showed in all latitudes and particular in the tropics a good representation of the CHBr_3 and CH_2Br_2 considering both, seasonal variations and absolute values. Compared to the reference simulation *ref*, with previous standard emissions by Warwick et al. (2006), the usage of the inventory by Liang et al. (2010) provided a more realistic and improved representation of the major VLS CHBr_3 and CH_2Br_2 in EMAC. The

emissions by Liang et al. (2010) were therefore depicted for further simulations within this study. Moreover, it is highly recommended for future studies with EMAC to apply the emissions by Liang et al. (2010) instead of the emissions by Warwick et al. (2006) in order to simulate a more realistic atmospheric chemistry.

How do emission inventories at the surface influence stratospheric bromine and ozone abundances?

The available emission inventories for the major VLSL CHBr_3 and CH_2Br_2 differ partly substantially. Therefore, it is necessary to investigate if differences at the surface are also reflected in higher altitudes, particularly in the stratosphere. The four transient simulations *ref*, *zis*, *ord* and *lia* with varied VLSL surface emissions showed significant differences in the stratospheric bromine loading. The usage of the more recent emission inventories in *zis*, *ord* and *lia* provided globally (3–5) pmol/mol less stratospheric bromine than in the reference simulation *ref*.

Less available stratospheric bromine resulted in an increase of stratospheric ozone. The largest ozone increase due to varied VLSL surface emissions was detected in the lower stratosphere over Antarctica during spring (September–November) and accounted for up to 13 %.

The contribution of VLSL to the stratospheric bromine burden ($\text{Br}_y^{\text{VLSL}}$) was determined as the abundance of source gases (multiplied by the number of halogen atoms) and product gases at the tropical cold point tropopause. Generally, the model results for $\text{Br}_y^{\text{VLSL}}$ were highly dependent on the applied VLSL surface emissions. Based on results from the simulations that provided good agreement to measurements in the tropics (*zis*, *ord* and *lia*) the contribution of VLSL to stratospheric bromine amounted to 4.5 ± 0.8 pmol/mol. The uncertainty range arises from uncertainties on VLSL surface emissions. Overall, the value of $\text{Br}_y^{\text{VLSL}}$ in this study agrees well with the 5 (2–8) pmol/mol reported recently in Carpenter et al. (2014).

How big is stratospheric ozone loss by VLSL?

A pair of time-slice simulations was conducted in order to determine the impact of VLSL on stratospheric ozone under climatic conditions of the year 2000. Simulation *TS2000lia* used the VLSL emissions by Liang et al. (2010) that were previously shown to provide reasonable results in EMAC in comparison to observations and other model studies. In simulation *TS2000zero* no VLSL emissions were applied.

Considering additional 5.3 ± 0.1 pmol/mol stratospheric bromine from VLSL causes a global stratospheric ozone loss which is largest in the polar regions. The impact of VLSL on ozone was found to be largest during spring in the south polar lower stratosphere and amounts to –14 % of the total ozone which is in relative good agreement with the –20 % reported by Braesicke et al. (2013) and Sinnhuber and Meul (2015). In annual average the impact is with –3 % less distinct. The column ozone is reduced

by up to 13 DU over Antarctica during spring. The effect on the Northern Hemisphere during spring is with ~ 5 DU smaller due to a larger variability and mixing with air from lower latitudes.

The location and timing of the largest impact of VSLS on ozone indicates that the inclusion of $\text{Br}_y^{\text{VSLS}}$ enhances the coupled $\text{BrO}_x\text{-ClO}_x$ cycle as already suggested in other studies (Salawitch et al., 2005; Braesicke et al., 2013; Yang et al., 2014; Sinnhuber and Meul, 2015). When active chlorine maximizes in spring bromine from VSLS is most efficient in destroying ozone.

VSLS were shown to significantly contribute to stratospheric ozone loss, particularly in the polar stratosphere. This results indicates that the consideration of VSLS in chemistry-climate simulations enables a more realistic simulation of atmospheric ozone mixing ratios and is therefore highly recommended.

What impact does climate change have on the chemistry and distribution of VSLS?

Constant Emissions

The increasing emission of greenhouse gases changes the chemical composition and dynamical quantities in the atmosphere yielding in a climate change. As the evolution of VSLS emissions under changed climate conditions is highly uncertain a first pair of time-slice simulations was conducted with unchanged VSLS emissions for the years 2000 (*TS2000lia*) and 2100 (*TS2100lia*) was investigated in combination with the corresponding no-VSLS sensitivity simulations (*TS2000zero* and *TS2100zero*).

In comparison to values in 2000 the stratospheric bromine burden is in 2100 significantly diminished by ~ 7 pmol/mol predominantly due to the phase-out of long-lived halogen compounds. The total contribution of VSLS to stratospheric bromine amounts to 5.3 ± 0.1 pmol/mol in 2000 and 5.0 ± 0.1 pmol/mol in 2100. In 2100, the acceleration of the Brewer-Dobson-Circulation enhances the vertical transport in the tropics enabling more VSLS to reach the stratosphere before being degraded to product gases. Lower stratospheric temperatures due to increasing greenhouse gas concentrations decelerate the chemical depletion of VSLS. Both processes lead to a reduction of very short-lived (VSL) product gases (Br_g) and an increase of VSL source gases in the stratosphere. An increase of hydroxyl (OH) and higher temperatures in the troposphere favor the reaction of VSLS with OH leading to a decrease of VSL source gases and an increase of product gases with respect to the year 2000.

The contribution of VSLS to stratospheric ozone loss is in 2100 significantly smaller. In 2000 the maximum ozone depletion induced by VSLS occurred in October in the south polar stratosphere with -200 nmol/mol (-14%). The equivalent ozone values in 2100 are reduced by -114 nmol/mol corresponding to -4% . Column ozone is reduced by up to 7 DU (2%) near the South Pole during spring. In the Northern hemisphere the largest ozone loss due to VSLS occurs near the North Pole with -4 DU (-1%).

As already mentioned, the abundance of bromine from VSLs changes only little from 5.3 ± 0.1 pmol/mol in 2000 to 5.0 ± 0.1 pmol/mol in 2100. Rather less available stratospheric chlorine ($\sim -70\%$) - due to the phase-out of long-lived ozone depleting substances - limits the efficient depletion of ozone via the coupled $\text{BrO}_x\text{-ClO}_x$ cycle. This result is consistent to a study by Yang et al. (2014) who found a larger impact of VSLs on ozone under a high chlorine background.

Increased Emissions

As the future evolution of VSLs emission is highly uncertain a pair of time-slice simulations was performed with enhanced emissions in order to investigate if a potential increase of VSLs surface emissions is also visible in a similarly increase of bromine and decrease of ozone in the stratosphere. VSLs emissions were multiplied by a factor of 10 which is an arbitrary value and used in the simulations *TS2000ten* and *TS2100ten*.

A tenfold increase of the VSLs surface emissions leads to an increased contribution of VSLs to stratospheric bromine. In simulation *TS2000ten* 50.5 ± 0.9 pmol/mol bromine arise from VSLs which corresponds to approximately a tenfold increase with respect to the reference simulation *TS2000lia*. In simulation *TS2100ten* VSLs contribute 48.5 ± 0.8 pmol/mol to stratospheric bromine. The reduced amount of bromine from VSLs in 2100 was already found in the reference simulations. It is a result of an enhanced vertical transport of source gases in the tropics, a colder stratosphere hampering the chemical degradation of VSLs into product gases and changes in the OH abundance.

The simulations with increased VSLs emissions show qualitatively similar results as the reference simulations. In 2000 the impact of VSLs on ozone loss is significantly larger due to a high chlorine background that enables the ozone depletion via the coupled $\text{BrO}_x\text{-ClO}_x$ cycle. In 2000 up to (1000 nmol/mol (-70%) of the total ozone are depleted by VSLs in the stratosphere over Antarctica during October. In *TS2100ten* the impact of VSLs is reduced through less available chlorine and amounts to -1000 nmol/mol corresponding to -40% of the total ozone in the south polar stratosphere during spring.

Enhanced VSLs emissions increases stratospheric bromine. Furthermore, a perturbation of the surface emissions is also able to influence the oxidation capacity of the atmosphere which is relevant for other compounds as well. Although the impact of VSLs on ozone is limited by chlorine the simulations with increased VSLs emissions showed that VSLs have the potential to substantially affect the stratospheric ozone layer and therefore must be taken into account in future studies.

Conclusions and Outlook

The results of this study have shown that VSLs significantly affect the stratospheric bromine and ozone burden and must therefore be considered in future studies. Ozone depletion induced by VSLs was shown to decrease due to declining chlorine mixing

ratios. However, it was also shown that increased VSLS emissions have the potential to considerably enhance ozone depletion both, under a high and low chlorine background. As the majority of brominated VSLS arises from natural sources the regulation of those substances is not possible. Therefore, it is highly recommended to carry on the regulation of long-lived chlorine compounds and restrict the short-lived substitution compounds as less available stratospheric chlorine limits the efficacy of VSLS induced ozone depletion. It is also reasonable to monitor VSLS emissions to develop adaption strategies in sufficient time in the case of a significant emission increase. Moreover, the results of this study highlight the importance of a realistic representation of VSLS surface emissions as they significantly contribute to stratospheric bromine and thus ozone depletion. More observations are needed to improve the knowledge on present and future VSLS emissions in order to adapt emission inventories and the representation in chemistry-climate models.

In this study, the chemistry-climate model was run in QCTM (Quasi Chemistry Transport Model) mode so that chemical perturbations (i.e. altered surface emissions) did not feedback on the dynamics. This approach enabled to achieve significant results after shorter simulation times as the signal of VSLS perturbations is relatively small. It was also shown that VSLS affect the radiative budget of the atmosphere due to their impact on stratospheric ozone. To assess the feedback of varied VSLS emissions on the dynamics this study could be repeated in a fully coupled run-mode, similarly to the study by Braesicke et al. (2013). For the simulation of the future climate this study used the greenhouse gas scenario RCP6.0. Depending on the future emissions scenario RCP8.5 is probably the more realistic scenario and might alter the results of this study. Due to the phase-out of long-lived halogen compounds the usage of anthropogenic (mainly chlorinated) VSLS has been increasing in recent years (WMO, 2014). The effect of those substances in the stratosphere must therefore also be investigated.

List of Figures

1.1	Changes in total stratospheric Br _y	3
2.1	Vertical distribution of catalytic cycles	13
2.2	Brewer-Dobson Circulation and Ozone distribution	14
2.3	Chemical conditions Over Antarctica	17
2.4	Variation in EESC and modelled average total column ozone changes . .	18
3.1	The MESSy architecture	26
3.2	The MESSy Submodel TBUDGET	30
3.3	CHBr ₃ Emission Map	34
3.4	CH ₂ Br ₂ Emission Map	35
3.5	CHBr ₃ , CH ₂ Br ₂ and CH ₃ I Emission vs. Latitude	35
4.1	Zonally averaged temperature of ERAI, RC1-base-07 and RC1SD-base-10	41
4.2	Climatology of Ozone Column	42
4.3	Zonally averaged ozone of SWOOSH, RC1-base-07 and RC1SD-base-10	43
4.4	NOAA/ESRL sampling sites	45
4.5	CHBr ₃ NOAA/ESRL vs EMAC sensitivity simulations	47
4.6	CH ₂ Br ₂ NOAA/ESRL vs EMAC sensitivity simulations	50
4.7	CH ₃ I NOAA/ESRL vs EMAC sensitivity simulations	53
4.8	CHBr ₃ surface mixing ratio in West Pacific Region	55
4.9	SHIVA CHBr ₃ observations vs. EMAC sensitivity simulations	57
4.10	SHIVA CH ₂ Br ₂ observations vs. EMAC sensitivity simulations	59
4.11	SHIVA CH ₃ I observations vs. EMAC sensitivity simulations	60
4.12	SHIVA Ozone observations vs EMAC sensitivity simulations	62
4.13	SHIVA CHBr ₃ profile	63
4.14	SHIVA CH ₂ Br ₂ profile	64
4.15	SHIVA CH ₃ I profile	65
4.16	Br _y in EMAC sensitivity simulations	68
4.17	Profile of Br _y ^{VSLs} in EMAC sensitivity simulations	70
4.18	O ₃ in EMAC sensitivity simulations	71

5.1	Profile of bromine in TS2000lia	75
5.2	Zonal total bromine in TS2000lia and difference to TS2000zero	76
5.3	Difference in zonal mean ozone mixing ratio between TS2000lia and TS2000zero	76
5.4	Seasonal variation of zonal column O ₃ in TS2000lia and difference to TS2000zero	77
5.5	Seasonal variation of south polar ozone, chlorine and bromine	78
6.1	Profile of bromine in TS2100lia	82
6.2	Zonal bromine from VSL bromine compounds in TS2000lia and differ- ence between TS2100lia and TS2000lia	83
6.3	Vertical component of the residual circulation	84
6.4	Zonal mean change of SGI and PGI in TS2100lia	85
6.5	Zonal mean change of tropical SGI and PGI in TS2100lia	86
6.6	Differences between TS2100lia and TS2000lia in zonal mean tempera- ture, OH, bromine from long-lived SGs and reaction rates	87
6.7	Difference in zonal ozone and chlorine between TS2100ref and TS2000ref	89
6.8	Difference in zonal mean ozone mixing ratio between TS2100lia and TS2100zero	90
6.9	Seasonal variation of zonal column O ₃ in TS2100lia and difference to TS2100ref and TS2100zero	91
6.10	Seasonal variation of south polar ozone, chlorine and bromine in 2100 .	92
6.11	Profile of bromine in 10xVSL simulations	93
6.12	Contribution of VSL to total bromine in 10xVSL simulations	95
6.13	Differences in OH between 0x and 10xVSL simulations	96
6.14	Difference in zonal mean ozone mixing ratio between TS2000ten and TS2000zero	97
6.15	Difference in zonal mean ozone mixing ratio between TS2100ten and TS2100zero	97
6.16	Seasonal variation of south polar ozone, chlorine and bromine in TS2000ten	98
6.17	Seasonal variation of south polar ozone, chlorine and bromine in TS2100ten	99

List of Tables

2.1	VLSL observations	21
3.1	MESSy submodels	28
3.2	Global Source Strength of CHBr_3 and CH_2Br_2	34
3.3	Overview of EMAC Simulations	38
4.1	NOAA/ESRL sampling sites	45
4.2	NOAA-EMAC CHBr_3 error metrics	49
4.3	NOAA-EMAC CH_2Br_2 error metrics	52
4.4	NOAA-EMAC CH_3I error metrics	52
4.5	Contribution to stratospheric Br_y with different surface emissions	67
5.1	Contribution to stratospheric Br_y I	74
6.1	Contribution to stratospheric Br_y II	83
6.2	Contribution to stratospheric Br_y III	94
6.3	Radiative Forcing of Changed VLSL Emissions	100

References

- Aschmann, J. and Sinnhuber, B.-M. (2013). Contribution of very short-lived substances to stratospheric bromine loading: uncertainties and constraints. *Atmospheric Chemistry and Physics*, 13(3):1203–1219.
- Aschmann, J., Sinnhuber, B.-M., Atlas, E., and Schauffler, S. (2009). Modeling the transport of very short-lived substances into the tropical upper troposphere and lower stratosphere. *Atmospheric Chemistry and Physics*, 9(23):9237–9247.
- Aschmann, J., Sinnhuber, B.-M., Chipperfield, M. P., and Hossaini, R. (2011). Impact of deep convection and dehydration on bromine loading in the upper troposphere and lower stratosphere. *Atmospheric Chemistry and Physics*, 11(6):2671–2687.
- Ashfold, M. J., Harris, N. R. P., Atlas, E. L., Manning, A. J., and Pyle, J. A. (2012). Transport of short-lived species into the Tropical Tropopause Layer. *Atmospheric Chemistry and Physics*, 12(14):6309–6322.
- Austin, J., Scinocca, J., Plummer, D., Oman, L., Waugh, D., Akiyoshi, H., Bekki, S., Braesicke, P., Butchart, N., Chipperfield, M., et al. (2010a). Decline and recovery of total column ozone using a multimodel time series analysis. *Journal of Geophysical Research: Atmospheres (1984–2012)*, 115(D3).
- Austin, J., Struthers, H., Scinocca, J., Plummer, D., Akiyoshi, H., Baumgaertner, A., Bekki, S., Bodeker, G., Braesicke, P., Brühl, C., et al. (2010b). Chemistry-climate model simulations of spring Antarctic ozone. *Journal of Geophysical Research: Atmospheres (1984–2012)*, 115(D3).
- Bates, D. R. and Nicolet, M. (1950). The photochemistry of atmospheric water vapor. *Journal of Geophysical Research*, 55(3):301–327.
- Bell, N., Hsu, L., Jacob, D. J., Schultz, M. G., Blake, D. R., Butler, J. H., King, D. B., Lobert, J. M., and Maier-reimer, E. (2002). Methyl iodide: Atmospheric budget and use as a tracer of marine convection in global models. *J. Geophys. Res.*, 107:200–2.
- Blake, N. J., Blake, D. R., Swanson, A. L., Atlas, E., Flocke, F., and Rowland, F. S. (2003). Latitudinal, vertical, and seasonal variations of C1-C4 alkyl nitrates in the

- troposphere over the Pacific Ocean during PEM-Tropics A and B: Oceanic and continental sources. *Journal of Geophysical Research: Atmospheres*, 108(D2).
- Bondu, S., Cocquempot, B., Deslandes, E., and Morin, P. (2008). Effects of salt and light stress on the release of volatile halogenated organic compounds by *Solieria chordalis*: a laboratory incubation study. *Botanica Marina*, 51(6):485–492.
- Braesicke, P., Keeble, J., Yang, X., Stiller, G., Kellmann, S., Abraham, N., Archibald, A., Telford, P., and Pyle, J. (2013). Circulation anomalies in the Southern Hemisphere and ozone changes. *Atmospheric Chemistry and Physics*, 13(21):10677–10688.
- Brewer, A. W. (1949). Evidence for a world circulation provided by the measurements of helium and water vapour distribution in the stratosphere. *Quarterly Journal of the Royal Meteorological Society*, 75(326):351–363.
- Brinkop, S., Dameris, M., Jöckel, P., Garny, H., Lossow, S., and Stiller, G. (2016). The millennium water vapour drop in chemistry–climate model simulations. *Atmospheric Chemistry and Physics*, 16(13):8125–8140.
- Butchart, N., Cionni, I., Eyring, V., Shepherd, T., Waugh, D., Akiyoshi, H., Austin, J., Brühl, C., Chipperfield, M., Cordero, E., et al. (2010). Chemistry-climate model simulations of twenty-first century stratospheric climate and circulation changes. *Journal of Climate*, 23(20):5349–5374.
- Butchart, N., Scaife, A., Bourqui, M., de Grandpre, J., Hare, S., Kettleborough, J., Langematz, U., Manzini, E., Sassi, F., Shibata, K., Shindell, D., and Sigmond, M. (2006). Simulations of anthropogenic change in the strength of the Brewer-Dobson circulation. *Climate Dynamics*, 27:727–741.
- Butler, J. H., Bell, T. G., Hall, B. D., Quack, B., Carpenter, L. J., and Williams, J. (2010). Technical Note: Ensuring consistent, global measurements of very short-lived halocarbon gases in the ocean and atmosphere. *Atmospheric Chemistry and Physics*, 10(2):327–330.
- Butler, J. H., King, D. B., Lobert, J. M., Montzka, S. A., Yvon-Lewis, S. A., Hall, B. D., Warwick, N. J., Mondeel, D. J., Aydin, M., and Elkins, J. W. (2007). Oceanic distributions and emissions of short-lived halocarbons. *Global Biogeochemical Cycles*, 21(1).
- Butz, A., Bösch, H., Camy-Peyret, C., Chipperfield, M. P., Dorf, M., Kreycky, S., Kritten, L., Prados-Román, C., Schwärzle, J., and Pfeilsticker, K. (2009). Constraints on inorganic gaseous iodine in the tropical upper troposphere and stratosphere inferred from balloon-borne solar occultation observations. *Atmospheric Chemistry and Physics*, 9(18):7229–7242.

- Carpenter, L. and Liss, P. (2000). On temperate sources of bromoform and other reactive organic bromine gases. *Journal of Geophysical Research: Atmospheres (1984–2012)*, 105(D16):20539–20547.
- Carpenter, L., Liss, P., and Penkett, S. (2003). Marine organohalogens in the atmosphere over the Atlantic and Southern Oceans. *Journal of Geophysical Research: Atmospheres (1984–2012)*, 108(D9).
- Carpenter, L., Wevill, D., O’Doherty, S., Spain, G., and Simmonds, P. (2005). Atmospheric bromoform at Mace Head, Ireland: seasonality and evidence for a peatland source. *Atmospheric Chemistry and Physics*, 5(11):2927–2934.
- Carpenter, L. J. (2003). Iodine in the marine boundary layer. *Chemical reviews*, 103(12):4953–4962.
- Carpenter, L. J., Reimann, S., Burkholder, J. B., Clerbaux, C., Hall, B. D., Hossaini, R., Laube, J. C., and Yvon-Lewis, S. A. (2014). Update on ozone-depleting substances (ODSs) and other gases of interest to the Montreal protocol, Chapter 1 in Scientific Assessment of Ozone Depletion: 2014, Global Ozone Research and Monitoring Project–Report No.55. *World Meteorological Organization, Geneva, Switzerland*.
- Chapman, S. (1930). A theory of upper atmosphere ozone. *Royal Meteorological Society*, pages 103–125.
- Charney, J. and Drazin, P. (1961). Propagation of planetary-scale disturbances from the lower into the upper atmosphere. *Journal of Geophysical Research*, 66(1):83–109.
- Chuck, A. L., Turner, S. M., and Liss, P. S. (2005). Oceanic distributions and air-sea fluxes of biogenic halocarbons in the open ocean. *Journal of Geophysical Research: Oceans (1978–2012)*, 110(C10).
- Collins, W., Bellouin, N., Doutriaux-Boucher, M., Gedney, N., Halloran, P., Hinton, T., Hughes, J., Jones, C., Joshi, M., Liddicoat, S., et al. (2011). Development and evaluation of an Earth-system model–HadGEM2. *Geoscientific Model Development*, 4(4):1051–1075.
- Crutzen, P. (1970). The influence of nitrogen oxides on the atmospheric ozone content. *Quarterly Journal of the Royal Meteorological Society*, 96(408):320–325.
- Dameris, M., Godin-Beekmann, S., Bekki, S., Perlwitz, J., Alexander, S., Braesicke, P., Chipperfield, M. P., de Laat, A. J., Orsolini, Y. J., Rex, M., et al. (2014). Update on Polar Ozone: Past, Present, and Future, Chapter 3 in Scientific Assessment of Ozone Depletion: 2014, Global Ozone Research and Monitoring Project–Report No. 55. *World Meteorological Organization, Geneva, Switzerland*.

- Dameris, M., Peter, T., Schmidt, U., and Zellner, R. (2007). Das Ozonloch und seine Ursachen. *Chemie in unserer Zeit*, 3:152–168.
- Damian, V., Sandu, A., Damian, M., Potra, F., and Carmichael, G. R. (2002). The kinetic preprocessor KPP—a software environment for solving chemical kinetics. *Computers & Chemical Engineering*, 26(11):1567–1579.
- Daniel, J. S., Solomon, S., and Albritton, D. L. (1995). On the evaluation of halocarbon radiative forcing and global warming potentials. *Journal of Geophysical Research: Atmospheres*, 100(D1):1271–1285.
- Davis, S. M., Rosenlof, K. H., Hassler, B., Hurst, D. F., Read, W. G., Vömel, H., Selkirk, H., Fujiwara, M., and Damadeo, R. (2016). The Stratospheric Water and Ozone Satellite Homogenized (SWOOSH) database: A long-term database for climate studies. *Earth System Science Data Discussions*, 2016:1–59.
- Deckert, R. and Dameris, M. (2008). Higher tropical SSTs strengthen the tropical upwelling via deep convection. *Geophysical Research Letters*, 35(10).
- Deckert, R., Jöckel, P., Grewe, V., Gottschaldt, K.-D., and Hoor, P. (2011). A quasi chemistry-transport model mode for EMAC. *Geoscientific Model Development*, 4(1):195–206.
- Dee, D., Uppala, S., Simmons, A., Berrisford, P., Poli, P., Kobayashi, S., Andrae, U., Balmaseda, M., Balsamo, G., Bauer, P., et al. (2011). The ERA-Interim reanalysis: Configuration and performance of the data assimilation system. *Quarterly Journal of the Royal Meteorological Society*, 137(656):553–597.
- Dessens, O., Zeng, G., Warwick, N., and Pyle, J. (2009). Short-lived bromine compounds in the lower stratosphere; impact of climate change on ozone. *Atmospheric Science Letters*, 10(3):201–206.
- Dietmüller, S., Jöckel, P., Tost, H., Kunze, M., Gellhorn, C., Brinkop, S., Frömming, C., Ponater, M., Steil, B., Lauer, A., and Hendricks, J. (2016). A new radiation infrastructure for the Modular Earth Submodel System (MESSy, based on version 2.51). *Geoscientific Model Development Discussions*, 2016:1–21.
- Dlugokencky, E. J., Nisbet, E. G., Fisher, R., and Lowry, D. (2011). Global atmospheric methane: budget, changes and dangers. *Philosophical Transactions of the Royal Society of London A: Mathematical, Physical and Engineering Sciences*, 369(1943):2058–2072.
- Dobson, G. (1956). Origin and distribution of the polyatomic molecules in the atmosphere. *Proceedings of the Royal Society of London. Series A, Mathematical and Physical Sciences*, pages 187–193.

- Eichinger, R., Jöckel, P., Brinkop, S., Werner, M., and Lossow, S. (2015). Simulation of the isotopic composition of stratospheric water vapour—Part 1: Description and evaluation of the EMAC model. *Atmospheric Chemistry and Physics*, 15(10):5537–5555.
- Eyring, V., Arblaster, J. M., Cionni, I., Sedlacek, J., Perlwitz, J., Young, P. J., Bekki, S., Bergmann, D., Cameron-Smith, P., Collins, W. J., Faluvegi, G., Gottschaldt, K.-D., Horowitz, L. W., Kinnison, D. E., Lamarque, J.-F., Marsh, D. R., Saint-Martin, D., Shindell, D. T., Sudo, K., Szopa, S., and Watanabe, S. (2013a). Long-term ozone changes and associated climate impacts in CMIP5 simulations. *Journal of Geophysical Research: Atmospheres*, 118(10):5029–5060.
- Eyring, V., Cionni, I., Bodeker, G., Charlton-Perez, A., Kinnison, D., Scinocca, J., Waugh, D., Akiyoshi, H., Bekki, S., Chipperfield, M., Dameris, M., Dhomse, S., Frith, S., Garny, H., Gettelman, A., Kubin, A., Langematz, U., Mancini, E., Marchand, M., Nakamura, T., Oman, L., Pawson, S., Pitari, G., Plummer, D., Rozanov, E., Shepherd, T., Shibata, K., Tian, W., Braesicke, P., Hardiman, S., Lamarque, J., Morgenstern, O., Pyle, J., Smale, D., and Yamashita, Y. (2010). Multi-model assessment of stratospheric ozone return dates and ozone recovery in CCMVal-2 models. *Atmospheric Chemistry and Physics*, 10(19):9451–9472.
- Eyring, V., Lamarque, J.-F., Hess, P., Arfeuille, F., Bowman, K., Chipperfield, M. P., Duncan, B., Fiore, A., Gettelman, A., Giorgetta, M. A., et al. (2013b). Overview of igac/sparc chemistry-climate model initiative (ccmi) community simulations in support of upcoming ozone and climate assessments. *Sparc Newsletter*, 40(Januar):48–66.
- Farman, J., Gardiner, B., and Shanklin, J. (1985). Large losses of total ozone in Antarctica reveal seasonal ClO_x/NO_x interaction. *Nature*, 315:207–210.
- Feng, W., Chipperfield, M., Dorf, M., Pfeilsticker, K., and Ricaud, P. (2007). Mid-latitude ozone changes: studies with a 3-D CTM forced by ERA-40 analyses. *Atmospheric Chemistry and Physics*, 7(9):2357–2369.
- Fueglistaler, S., Dessler, A. E., Dunkerton, T. J., Folkins, I., Fu, Q., and Mote, P. W. (2009). Tropical tropopause layer. *Reviews of Geophysics*, 47(1). RG1004.
- Garcia, R. and Randel, W. (2008). Acceleration of the Brewer-Dobson circulation due to increases in greenhouse gases. *Journal of the Atmospheric Sciences*, 65(8):2731–2739.
- Gettelman, A., Lauritzen, P., Park, M., and Kay, J. (2009). Processes regulating short-lived species in the tropical tropopause layer. *Journal of Geophysical Research: Atmospheres*, 114(D13).

- Grewe, V. (2006). The origin of ozone. *Atmospheric Chemistry and Physics*, 6(6):1495–1511.
- Grewe, V., Brunner, D., Dameris, M., Grenfell, J., Hein, R., Shindell, D., and Staehelin, J. (2001). Origin and variability of upper tropospheric nitrogen oxides and ozone at northern mid-latitudes. *Atmospheric Environment*, 35(20):3421 – 3433.
- Haigh, J. and Pyle, J. (1979). A twodimensional calculation including atmospheric carbon dioxide and stratospheric ozone. *Nature*, 279:222–224.
- Hines, C. O. (1997a). Doppler-spread parameterization of gravity-wave momentum deposition in the middle atmosphere. Part 1: Basic formulation. *Journal of Atmospheric and Solar-Terrestrial Physics*, 59(4):371 – 386.
- Hines, C. O. (1997b). Doppler-spread parameterization of gravity-wave momentum deposition in the middle atmosphere. Part 2: Broad and quasi monochromatic spectra, and implementation. *Journal of Atmospheric and Solar-Terrestrial Physics*, 59(4):387 – 400.
- Hossaini, R., Chipperfield, M., Dhomse, S., Ordonez, C., Saiz-Lopez, A., Abraham, N., Archibald, A., Braesicke, P., Telford, P., Warwick, N., et al. (2012a). Modelling future changes to the stratospheric source gas injection of biogenic bromocarbons. *Geophysical Research Letters*, 39(20).
- Hossaini, R., Chipperfield, M., Montzka, S., Rap, A., Dhomse, S., and Feng, W. (2015). Efficiency of short-lived halogens at influencing climate through depletion of stratospheric ozone. *Nature Geoscience*.
- Hossaini, R., Chipperfield, M. P., Dhomse, S., Ordóñez, C., Saiz-Lopez, A., Abraham, N. L., Archibald, A., Braesicke, P., Telford, P., Warwick, N., Yang, X., and Pyle, J. (2012b). Modelling future changes to the stratospheric source gas injection of biogenic bromocarbons. *Geophysical Research Letters*, 39(20). L20813.
- Hossaini, R., Mantle, H., Chipperfield, M. P., Montzka, S. A., Hamer, P., Ziska, F., Quack, B., Krüger, K., Tegtmeier, S., Atlas, E., Sala, S., Engel, A., Bönisch, H., Keber, T., Oram, D., Mills, G., Ordóñez, C., Saiz-Lopez, A., Warwick, N., Liang, Q., Feng, W., Moore, F., Miller, B. R., Marécal, V., Richards, N. A. D., Dorf, M., and Pfeilsticker, K. (2013). Evaluating global emission inventories of biogenic bromocarbons. *Atmospheric Chemistry and Physics*, 13(23):11819–11838.
- Hossaini, R., Patra, P. K., Leeson, A. A., Krysztofiak, G., Abraham, N. L., Andrews, S. J., Archibald, A. T., Aschmann, J., Atlas, E. L., Belikov, D. A., Bönisch, H., Butler, R., Carpenter, L. J., Dhomse, S., Dorf, M., Engel, A., Feng, L., Feng, W., Fuhlbrügge, S., Griffiths, P. T., Harris, N. R. P., Hommel, R., Keber, T., Krüger, K., Lennartz, S. T., Maksyutov, S., Mantle, H., Mills, G. P., Miller, B., Montzka,

- S. A., Moore, F., Navarro, M. A., Oram, D. E., Palmer, P. I., Pfeilsticker, K., Pyle, J. A., Quack, B., Robinson, A. D., Saikawa, E., Saiz-Lopez, A., Sala, S., Sinnhuber, B.-M., Taguchi, S., Tegtmeier, S., Lidster, R. T., Wilson, C., and Ziska, F. (2016). A multi-model intercomparison of halogenated very short-lived substances (TransCom-VSLS): linking oceanic emissions and tropospheric transport for a reconciled estimate of the stratospheric source gas injection of bromine. *Atmospheric Chemistry and Physics Discussions*, 2016:1–49.
- IPCC (2007). *Climate Change 2007 The Physical Science Basis. Contribution of Working Group I to the Fourth Assessment Report of the Intergovernmental Panel on Climate Change*. Cambridge University Press.
- IPCC (2013). *Climate Change 2013: The Physical Science Basis. Contribution of Working Group I to the Fifth Assessment Report of the Intergovernmental Panel on Climate Change*. Cambridge University Press, Cambridge, United Kingdom and New York, NY, USA.
- Jöckel, P., Kerkweg, A., Buchholz-Dietsch, J., Tost, H., Sander, R., and Pozzer, A. (2008). Technical Note: Coupling of chemical processes with the Modular Earth Submodel System (MESSy) submodel TRACER. *Atmospheric Chemistry and Physics*, 8(6):1677–1687.
- Jöckel, P., Kerkweg, A., Pozzer, A., Sander, R., Tost, H., Riede, H., Baumgärtner, A., Gromov, S., and Kern, B. (2010). Development cycle 2 of the Modular Earth Submodel System (MESSy2). *Geoscientific Model Development*, 3(2):717–752.
- Jöckel, P., Sander, R., Kerkweg, A., Tost, H., and Lelieveld, J. (2005). Technical Note: The Modular Earth Submodel System (MESSy) - a new approach towards Earth System Modeling. *Atmospheric Chemistry and Physics*, 5(2):433–444.
- Jöckel, P., Tost, H., Pozzer, A., Brühl, C., Buchholz, J., Ganzeveld, L., Hoor, P., Kerkweg, A., Lawrence, M., Sander, R., Steil, B., Stiller, G., Tanarhte, M., Taraborrelli, D., van Aardenne, J., and Lelieveld, J. (2006). The atmospheric chemistry general circulation model ECHAM5/MESSy1: consistent simulation of ozone from the surface to the mesosphere. *Atmospheric Chemistry and Physics*, 6(12):5067–5104.
- Jöckel, P., Tost, H., Pozzer, A., Kunze, M., Kirner, O., Brenninkmeijer, C. A. M., Brinkop, S., Cai, D. S., Dyroff, C., Eckstein, J., Frank, F., Garny, H., Gottschaldt, K.-D., Graf, P., Grewe, V., Kerkweg, A., Kern, B., Matthes, S., Mertens, M., Meul, S., Neumaier, M., Nützel, M., Oberländer-Hayn, S., Ruhnke, R., Runde, T., Sander, R., Scharffe, D., and Zahn, A. (2016). Earth System Chemistry integrated Modelling (ESCiMo) with the Modular Earth Submodel System (MESSy) version 2.51. *Geoscientific Model Development*, 9(3):1153–1200.

- Johnston, H. (1971). Reduction of Stratospheric Ozone by Nitrogen Oxide Catalysts from Supersonic Transport Exhaust. *Science*, 173(3996):517–522.
- Kerkweg, A., Buchholz, J., Ganzeveld, L., Pozzer, A., Tost, H., and Jöckel, P. (2006a). Technical Note: An implementation of the dry removal processes DRY DEPosition and SEDimentation in the Modular Earth Submodel System (MESSy). *Atmospheric Chemistry and Physics*, 6(12):4617–4632.
- Kerkweg, A., Jöckel, P., Warwick, N., Gebhardt, S., Brenninkmeijer, C. A. M., and Lelieveld, J. (2008). Consistent simulation of bromine chemistry from the marine boundary layer to the stratosphere - Part 2: Bromocarbons. *Atmospheric Chemistry and Physics*, 8(19):5919–5939.
- Kerkweg, A., Sander, R., Tost, H., and Jöckel, P. (2006b). Technical note: Implementation of prescribed (OFFLEM), calculated (ONLEM), and pseudo-emissions (TNUDGE) of chemical species in the Modular Earth Submodel System (MESSy). *Atmospheric Chemistry and Physics*, 6(11):3603–3609.
- Kern, B. (2013). *Chemical interaction between ocean and atmosphere*. PhD thesis, Johannes Gutenberg-Universität.
- Ko, M., Poulet, G., Blake, D., Boucher, O., Burkholder, J., Chin, M., Cox, R., George, C., Graf, H., Holton, J., et al. (2003). Very short-lived halogen and sulfur substances, Chapter 2 in Scientific Assessment of Ozone Depletion: 2002, Global Ozone Research and Monitoring Project–Report No. 47. *World Meteorological Organization, Geneva, Switzerland*.
- Krüger, K. and Quack, B. (2013). Introduction to special issue: the TransBrom Sonne expedition in the tropical West Pacific. *Atmospheric Chemistry and Physics*, 13(18):9439–9446.
- Landgraf, J. and Crutzen, P. (1998). An Efficient Method for Online Calculations of Photolysis and Heating Rates. *Journal of the Atmospheric Sciences*, 55:863–878.
- Lary, D. and Toumi, R. (1997). Halogen-catalyzed methane oxidation. *Journal of Geophysical Research: Atmospheres*, 102:23–421.
- Lary, D. J., Chipperfield, M. P., Toumi, R., and Lenton, T. (1996). Heterogeneous atmospheric bromine chemistry. *Journal of Geophysical Research: Atmospheres*, 101(D1):1489–1504.
- Laternus, F., Wiencke, C., and Klöser, H. (1996). Antarctic macroalgae-sources of volatile halogenated organic compounds. *Marine environmental research*, 41(2):169–181.

- Law, K., Sturges, W., Blake, D., Blake, N., Burkholder, J., Butler, J., Cox, R., Haynes, P., Ko, M., Kreher, K., et al. (2007). Halogenated Very Short-Lived Substances, Chapter 2 in: Scientific Assessment of Ozone Depletion: 2006, Global Ozone Research and Monitoring Project–Report No. 50. *World Meteorological Organization, Geneva, Switzerland*, 572.
- Lee-Taylor, J. and Redeker, K. (2005). Reevaluation of global emissions from rice paddies of methyl iodide and other species. *Geophysical Research Letters*, 32(15).
- Leedham, E., Hughes, C., Keng, F., Phang, S.-M., Malin, G., and Sturges, W. (2013). Emission of atmospherically significant halocarbons by naturally occurring and farmed tropical macroalgae. *Biogeosciences*, 10(6):3615–3633.
- Lelieveld, J., Brühl, C., Jöckel, P., Steil, B., Crutzen, P. J., Fischer, H., Giorgetta, M. A., Hoor, P., Lawrence, M. G., Sausen, R., and Tost, H. (2007). Stratospheric dryness: model simulations and satellite observations. *Atmospheric Chemistry and Physics*, 7(5):1313–1332.
- Liang, Q., Atlas, E., Blake, D., Dorf, M., Pfeilsticker, K., and Schauffler, S. (2014). Convective transport of very short lived bromocarbons to the stratosphere. *Atmospheric Chemistry and Physics*, 14(11):5781–5792.
- Liang, Q., Stolarski, R., Kawa, S., Nielsen, J., Douglass, A., Rodriguez, J., Blake, D., Atlas, E., and Ott, L. (2010). Finding the missing stratospheric Br_y: a global modeling study of CHBr₃ and CH₂Br₂. *Atmospheric Chemistry and Physics*, 10(5):2269–2286.
- Löffler, M., Brinkop, S., and Jöckel, P. (2016). Impact of major volcanic eruptions on stratospheric water vapour. *Atmospheric Chemistry and Physics*, 16(10):6547–6562.
- Loyola, D. G. and Coldewey-Egbers, M. (2012). Multi-sensor data merging with stacked neural networks for the creation of satellite long-term climate data records. *EURASIP Journal on Advances in Signal Processing*, 2012(1):1–10.
- Loyola, D. G., Coldewey-Egbers, R. M., Dameris, M., Garny, H., Stenke, A., Roozendael, M. V., Lerot, C., Balis, D., and Koukouli, M. (2009). Global long-term monitoring of the ozone layer - a prerequisite for predictions. *International Journal of Remote Sensing*, 30(15-16):4295–4318.
- Manzini, E. and McFarlane, N. A. (1998). The effect of varying the source spectrum of a gravity wave parameterization in a middle atmosphere general circulation model. *Journal of Geophysical Research: Atmospheres*, 103(D24):31523–31539.
- Martin, G., Bellouin, N., Collins, W., Culverwell, I., Halloran, P., Hardiman, S., Hinton, T., Jones, C., McDonald, R., McLaren, A., et al. (2011). The HadGEM2 family of

- met office unified model climate configurations. *Geoscientific Model Development Discussions*, 4:765–841.
- Mata, L., Gaspar, H., and Santos, R. (2012). Carbon/nutrient balance in relation to biomass production and halogenated compound content in the red alga *asparagopsis taxiformis* (bonnemaisoniaceae) 1. *Journal of Phycology*, 48(1):248–253.
- McCormick, M. P., Steele, H. M., Hamill, P., Chu, W. P., and Swissler, T. J. (1982). Polar stratospheric cloud sightings by SAM II. *Journal of the Atmospheric Sciences*, 39(6):1387–1397.
- McLandress, C. and Shepherd, T. G. (2009). Simulated anthropogenic changes in the Brewer-Dobson circulation, including its extension to high latitudes. *Journal of Climate*, 22(6):1516–1540.
- Meinshausen, M., Smith, S. J., Calvin, K., Daniel, J. S., Kainuma, M., Lamarque, J., Matsumoto, K., Montzka, S., Raper, S., Riahi, K., et al. (2011). The RCP greenhouse gas concentrations and their extensions from 1765 to 2300. *Climatic change*, 109(1-2):213–241.
- Meul, S., Dameris, M., Langematz, U., Abalichin, J., Kerschbaumer, A., Kubin, A., and Oberländer-Hayn, S. (2016). Impact of rising greenhouse gas concentrations on future tropical ozone and UV exposure. *Geophysical Research Letters*.
- Miller, J. B., Lehman, S. J., Montzka, S. A., Sweeney, C., Miller, B. R., Karion, A., Wolak, C., Dlugokencky, E. J., Southon, J., Turnbull, J. C., et al. (2012). Linking emissions of fossil fuel CO₂ and other anthropogenic trace gases using atmospheric ¹⁴CO₂. *Journal of Geophysical Research: Atmospheres (1984–2012)*, 117(D8).
- Molina, M. J. and Rowland, F. S. (1974). Stratospheric sink for chlorofluoromethanes: Chlorine atom catalyzed destruction of ozone. *Nature*, 249(5460):820–812.
- Montzka, S., Reimann, S., O’Doherty, S., Engel, A., Krüger, K., and Sturges, W. (2011). Ozone-depleting substances (ODSs) and related chemicals, Chapter 1 in: Scientific Assessment of Ozone Depletion: 2010, Global Ozone Research and Monitoring Project –Report No. 52. *World Meteorological Organization, Geneva, Switzerland*.
- Montzka, S. A., Butler, J. H., Hall, B. D., Mondeel, D. J., and Elkins, J. W. (2003). A decline in tropospheric organic bromine. *Geophysical Research Letters*, 30(15).
- Newman, P. A., Daniel, J. S., Waugh, D. W., and Nash, E. R. (2007). A new formulation of equivalent effective stratospheric chlorine (EESC). *Atmospheric Chemistry and Physics*, 7(17):4537–4552.

- Oberländer, S., Langematz, U., and Meul, S. (2013). Unraveling impact factors for future changes in the Brewer-Dobson circulation. *Journal of Geophysical Research: Atmospheres*, 118(18).
- O'Brien, L., Harris, N., Robinson, A., Gostlow, B., Warwick, N., Yang, X., and Pyle, J. (2009). Bromocarbons in the tropical marine boundary layer at the Cape Verde Observatory—measurements and modelling. *Atmos. Chem. Phys*, 9(22):9083–9099.
- Oman, L., Plummer, D., Waugh, D., Austin, J., Scinocca, J., Douglass, A., Salawitch, R., Canty, T., Akiyoshi, H., Bekki, S., et al. (2010). Multimodel assessment of the factors driving stratospheric ozone evolution over the 21st century. *Journal of Geophysical Research: Atmospheres (1984–2012)*, 115(D24).
- Ooki, A. and Yokouchi, Y. (2011). Dichloromethane in the Indian Ocean: Evidence for in-situ production in seawater. *Marine Chemistry*, 124(1):119–124.
- Ordóñez, C., Lamarque, J.-F., Tilmes, S., Kinnison, D. E., Atlas, E. L., Blake, D. R., Sousa Santos, G., Brasseur, G., and Saiz-Lopez, A. (2012). Bromine and iodine chemistry in a global chemistry-climate model: description and evaluation of very short-lived oceanic sources. *Atmospheric Chemistry and Physics*, 12(3):1423–1447.
- Pawson, S., Steinbrecht, W., Charlton-Perez, A., Fujiwara, M., Karpechko, A., Petropavlovskikh, I., Urban, J., and Weber, M. (2014). Update on Global Ozone: Past, Present, and Future, Chapter 2 in Scientific Assessment of Ozone Depletion: 2014, Global Ozone Research and Monitoring Project—Report No. 55. *World Meteorological Organization, Geneva, Switzerland*.
- Peter, T. (1996). *Formation mechanisms of polar stratospheric clouds*. Pergamon Press, New York.
- Pozzer, A., Jöckel, P., Sander, R., Williams, J., Ganzeveld, L., and Lelieveld, J. (2006). Technical Note: The MESSy-submodel AIRSEA calculating the air-sea exchange of chemical species. *Atmospheric Chemistry and Physics*, 6(12):5435–5444.
- Pyle, J. A., Ashfold, M. J., Harris, N. R. P., Robinson, A. D., Warwick, N. J., Carver, G. D., Gostlow, B., O'Brien, L. M., Manning, A. J., Phang, S. M., Yong, S. E., Leong, K. P., Ung, E. H., and Ong, S. (2011). Bromoform in the tropical boundary layer of the Maritime Continent during OP3. *Atmospheric Chemistry and Physics*, 11(2):529–542.
- Quack, B., Atlas, E., Petrick, G., Stroud, V., Schauffler, S., and Wallace, D. W. (2004). Oceanic bromoform sources for the tropical atmosphere. *Geophysical research letters*, 31(23).

- Quack, B., Atlas, E., Petrick, G., and Wallace, D. W. (2007). Bromoform and dibromomethane above the Mauritanian upwelling: Atmospheric distributions and oceanic emissions. *Journal of Geophysical Research: Atmospheres (1984–2012)*, 112(D9).
- Quack, B. and Wallace, D. (2003). Air-sea flux of bromoform: Controls, rates, and implications. *Global Biogeochemical Cycles*, 17(1).
- Randel, W., Shine, K., Austin, J., Barnett, J., Claud, C., Gillett, N., Keckhut, P., Langematz, U., Lin, R., Long, C., Mears, C., Miller, A., Nash, J., Seidel, D., Thompson, D., Wu, F., and Yoden, S. (2009). An update of observed stratospheric temperature trends. *Journal of Geophysical Research*.
- Ravishankara, A., Daniel, J. S., and Portmann, R. W. (2009). Nitrous oxide (N₂O): the dominant ozone-depleting substance emitted in the 21st century. *science*, 326(5949):123–125.
- Riese, M., Ploeger, F., Rap, A., Vogel, B., Konopka, P., Dameris, M., and Forster, P. (2012). Impact of uncertainties in atmospheric mixing on simulated UTLS composition and related radiative effects. *Journal of Geophysical Research: Atmospheres*, 117(D16). D16305.
- Righi, M., Eyring, V., Gottschaldt, K.-D., Klinger, C., Frank, F., Jöckel, P., and Cionni, I. (2015). Quantitative evaluation of ozone and selected climate parameters in a set of EMAC simulations. *Geoscientific Model Development*, 8(3):733–768.
- Roeckner, E., Bäuml, G., Bonaventura, L., Brokopf, R., Esch, M., Giorgetta, M., Hagemann, S., Kirchner, I., Kornbluh, L., Manzini, E., Rhodin, A., Schlese, U., Schulzweida, U., and Tompkins, A. (2003). *The atmospheric general circulation model ECHAM5: Part 1. Model description*, volume 349. Max-Planck-Institut für Meteorologie.
- Roeckner, E., Brokopf, R., Esch, M., Giorgetta, M., Hagemann, S., Kornbluh, L., Manzini, E., Schlese, U., and Schukzweida, U. (2006). Sensitivity of simulated climate to horizontal and vertical resolution in the ECHAM5 atmosphere model. *Journal of Climate*, 19(16):3771–3791.
- Rosenfield, J. E., Douglass, A. R., and Considine, D. B. (2002). The impact of increasing carbon dioxide on ozone recovery. *Journal of Geophysical Research: Atmospheres (1984–2012)*, 107(D6):ACH-7.
- Rowland, F. S. and Molina, M. J. (1975). Chlorofluoromethanes in the environment. *Reviews of Geophysics*, 13(1):1–35.
- Sala, S., Bönisch, H., Keber, T., Oram, D. E., Mills, G., and Engel, A. (2014). Deriving an atmospheric budget of total organic bromine using airborne in situ measurements

- from the western pacific area during shiva. *Atmospheric Chemistry and Physics*, 14(13):6903–6923.
- Salawitch, R. J., Weisenstein, D. K., Kovalenko, L. J., Sioris, C. E., Wennberg, P. O., Chance, K., Ko, M. K. W., and McLinden, C. A. (2005). Sensitivity of ozone to bromine in the lower stratosphere. *Geophysical Research Letters*, 32(5). L05811.
- Sander, R., Kerkweg, A., Jöckel, P., and Lelieveld, J. (2005). Technical note: The new comprehensive atmospheric chemistry module MECCA. *Atmospheric Chemistry and Physics*, 5(2):445–450.
- Sandu, A. and Sander, R. (2006). Technical note: Simulating chemical systems in Fortran90 and Matlab with the Kinetic PreProcessor KPP-2.1. *Atmospheric Chemistry and Physics*, 6(1):187–195.
- Sandu, A., Verwer, J., Blom, J., Spee, E., Carmichael, G., and Potra, F. (1997). Benchmarking stiff ode solvers for atmospheric chemistry problems II: Rosenbrock solvers. *Atmospheric Environment*, 31(20):3459–3472.
- Seinfeld, J. H. and Pandis, S. N. (2006). *Atmospheric Chemistry and Physics*. Wiley.
- Shaw, T. A. and Shepherd, T. G. (2008). Atmospheric science: Raising the roof. *Nature Geoscience*, 1(1):12–13.
- Shepherd, T. G. (2008). Dynamics, stratospheric ozone, and climate change. *Atmosphere-Ocean*, 46(1):117–138.
- Simmonds, P., Derwent, R., Manning, A., O’Doherty, S., and Spain, G. (2010). Natural chloroform emissions from the blanket peat bogs in the vicinity of Mace Head, Ireland over a 14-year period. *Atmospheric Environment*, 44(10):1284–1291.
- Simpson, I. J., Blake, N. J., Blake, D. R., Meinardi, S., Andersen, M. P. S., and Rowland, F. S. (2007). Strong evidence for negligible methyl chloroform (CH_3CCl_3) emissions from biomass burning. *Geophysical Research Letters*, 34(10).
- Sinnhuber, B.-M. and Meul, S. (2015). Simulating the impact of emissions of brominated very short lived substances on past stratospheric ozone trends. *Geophysical Research Letters*, 42(7):2449–2456.
- Sinnhuber, B.-M., Sheode, N., Sinnhuber, M., Chipperfield, M. P., and Feng, W. (2009). The contribution of anthropogenic bromine emissions to past stratospheric ozone trends: a modelling study. *Atmospheric Chemistry and Physics*, 9(8):2863–2871.
- Solomon, S. (1999). Stratospheric ozone depletion: A review of concepts and history. *Reviews of Geophysics*, 37(3):275–316.

- Solomon, S., Garcia, R., Rowland, F., and Wuebbles, D. (1986). On the depletion of Antarctic ozone. *Nature*, 321:755–758.
- Stolarski, R. S. and Cicerone, R. J. (1974). Stratospheric Chlorine: a Possible Sink for Ozone. *Canadian Journal of Chemistry*, 52(8):1610–1615.
- Sturges, W. T., McIntyre, H. P., Penkett, S. A., Chappellaz, J., Barnola, J.-M., Mulvaney, R., Atlas, E., and Stroud, V. (2001). Methyl bromide, other brominated methanes, and methyl iodide in polar firn air. *Journal of Geophysical Research: Atmospheres*, 106(D2):1595–1606.
- Tegtmeier, S., Krüger, K., Quack, B., Atlas, E., Blake, D. R., Bönisch, H., Engel, A., Hepach, H., Hossaini, R., Navarro, M., et al. (2013). The contribution of oceanic methyl iodide to stratospheric iodine. *Atmospheric Chemistry and Physics*, 13(23):11869–11886.
- Tegtmeier, S., Ziska, F., Pisso, I., Quack, B., Velders, G. J. M., Yang, X., and Krüger, K. (2015). Oceanic bromoform emissions weighted by their ozone depletion potential. *Atmospheric Chemistry and Physics*, 15(23):13647–13663.
- Tiedtke, M. (1989). A Comprehensive Mass Flux Scheme for Cumulus Parameterization in Large-Scale Models. *Monthly Weather Review*, 117(8):1779–1800.
- Toon, O. B. and Tolbert, M. A. (1995). Spectroscopic evidence against nitric acid trihydrate in polar stratospheric clouds. *Nature*.
- Tost, H. (2006). *Global Modelling of Cloud, Convection and Precipitation Influences on Trace Gases and Aerosols*. PhD thesis, Rheinische Friedrich-Wilhelms-Universität Bonn.
- Tost, H., Jöckel, P., Kerkweg, A., Sander, R., and Lelieveld, J. (2006a). Technical note: A new comprehensive SCAVenging submodel for global atmospheric chemistry modelling. *Atmospheric Chemistry and Physics*, 6(3):565–574.
- Tost, H., Jöckel, P., and Lelieveld, J. (2006b). Influence of different convection parameterisations in a GCM. *Atmospheric Chemistry and Physics*, 6(12):5475–5493.
- Tost, H., Jöckel, P., and Lelieveld, J. (2007). Lightning and convection parameterisations – uncertainties in global modelling. *Atmospheric Chemistry and Physics*, 7(17):4553–4568.
- Walker, G. (2007). *An Ocean Of Air: A Natural History Of The Atmosphere*. Bloomsbury UK.
- Warwick, N., Pyle, J., Carver, G., Yang, X., Savage, N., O’Connor, F., and Cox, R. (2006). Global modeling of biogenic bromocarbons. *Journal of Geophysical Research: Atmospheres (1984–2012)*, 111(D24).

- WMO (2007). Scientific Assessment of Ozone Depletion: 2006. Technical report, WMO Global Ozone Research and Monitoring Project Report No. 50, Geneva, Switzerland.
- WMO (2011). Scientific Assessment of Ozone Depletion: 2010. Technical report, WMO Global Ozone Research and Monitoring Project Report No. 52, Geneva, Switzerland.
- WMO (2014). Scientific Assessment of Ozone Depletion: 2013. Technical report, WMO Global Ozone Research and Monitoring Project Report No. 55, Geneva, Switzerland.
- Wofsy, S. C., McElroy, M. B., and Yung, Y. L. (1975). The chemistry of atmospheric bromine. *Geophysical Research Letters*, 2(6):215–218.
- Worton, D., Sturges, W., Schwander, J., Mulvaney, R., Barnola, J.-M., and Chappellaz, J. (2006). 20th century trends and budget implications of chloroform and related tri- and dihalomethanes inferred from firn air. *Atmospheric Chemistry and Physics*, 6(10):2847–2863.
- Xue, L., Wang, T., Simpson, I. J., Ding, A., Gao, J., Blake, D. R., Wang, X., Wang, W., Lei, H., and Jin, D. (2011). Vertical distributions of non-methane hydrocarbons and halocarbons in the lower troposphere over northeast China. *Atmospheric Environment*, 45(36):6501–6509.
- Yang, X., Abraham, N., Archibald, A., Braesicke, P., Keeble, J., Telford, P., Warwick, N., and Pyle, J. (2014). How sensitive is the recovery of stratospheric ozone to changes in concentrations of very short-lived bromocarbons? *Atmospheric Chemistry and Physics*, 14(19):10431–10438.
- Yokouchi, Y., Barrie, L., Toom, D., and Akimoto, H. (1996). The seasonal variation of selected natural and anthropogenic halocarbons in the Arctic troposphere. *Atmospheric Environment*, 30(10):1723–1727.
- Yokouchi, Y., Hasebe, F., Fujiwara, M., Takashima, H., Shiotani, M., Nishi, N., Kanaya, Y., Hashimoto, S., Fraser, P., Toom-Saunty, D., et al. (2005). Correlations and emission ratios among bromoform, dibromochloromethane, and dibromomethane in the atmosphere. *Journal of Geophysical Research: Atmospheres (1984–2012)*, 110(D23).
- Youn, D., Patten, K., Wuebbles, D., Lee, H., and So, C.-W. (2010). Potential impact of iodinated replacement compounds CF_3I and CH_3I on atmospheric ozone: a three-dimensional modeling study. *Atmospheric Chemistry and Physics*, 10(20):10129–10144.
- Yung, Y. L., Pinto, J. P., Watson, R. T., and Sander, S. P. (1980). Atmospheric Bromine and Ozone Perturbations in the Lower Stratosphere. *Journal of the Atmospheric Sciences*, 37:215–218.

Ziska, F. (2014). *Global halocarbon emissions for the recent past and future*. PhD thesis, Christian-Albrechts Universität Kiel.

Ziska, F., Quack, B., Abrahamsson, K., Archer, S., Atlas, E., Bell, T., Butler, J., Carpenter, L., Jones, C., Harris, N., et al. (2013). Global sea-to-air flux climatology for bromoform, dibromomethane and methyl iodide. *Atmospheric Chemistry and Physics*, 13(17):8915–8934.

Danksagung

An erster Stelle möchte ich meinem Doktorvater und Betreuer Prof. Dr. Martin Dameris für jegliche Unterstützung während meiner Zeit am DLR danken. Die Möglichkeit, jederzeit Fragen stellen zu können oder bei Diskussionsbedarf vorbeizukommen sowie motivierende Worte haben mir bei der Erstellung dieser Arbeit sehr geholfen.

Bei Prof. Dr. Markus Rapp und Prof. Dr. Robert Sausen möchte ich für die Möglichkeit bedanken, meine Arbeit am Institut Physik der Atmosphäre anfertigen zu können.

Prof. Dr. Bernhard Mayer danke ich für die Zweitbegutachtung meiner Arbeit.

Auch für die Möglichkeit, bei der SHIVA-Kampagne vor Ort teilzunehmen, möchte ich mich ganz herzlich bei Prof. Dr. Martin Dameris, Prof. Dr. Ulrich Schumann und Dr. Hans Schlager bedanken.

Dr. Hella Garny und Prof. Dr. Volker Grewe danke ich für die Hilfe bei der Erstellung von TBUDGET.

Dr. Patrick Jöckel danke ich für die Einarbeitung in das Modell, geduldige gemeinsame Fehlersuche bei Problemen und die große Unterstützung bei der Implementierung von meinem Submodell.

Meinen Kollegen aus der Abteilung 1 danke ich für die angenehme Atmosphäre und Hilfestellung bei inhaltlichen und technischen Fragen. Dabei waren mir besonders hilfreich: Dr. Lisa Bock, Dr. Sabine Brinkop, Dr. Katrin Dahlmann, Dr. Simone Dietmüller, Dr. Bastian Kern, Dr. Mariano Mertens, Dr. Mattia Righi und Dr. Hiroshi Yamashita.

Dr. Duy Cai danke ich ganz besonders für aufmunternde Worte, fachliche Diskussionen und die uneingeschränkte Hilfsbereitschaft bei jeglichen Problemen.

Zu guter Letzt geht noch ein großes Dankeschön an meine Eltern, meinen Bruder, Christian, Lenni und den ganzen Rest der Familie, die nie aufgehört haben, an ein (positives) Ende meiner Promotionszeit zu glauben.